UNIVERSITY OF CALIFORNIA, SAN DIEGO

The Role of BMP4 and Oxygen in Trophoblast Lineage Specification and Differentiation

A dissertation submitted in partial satisfaction of the requirements for the degree Doctor of Philosophy

in

Biomedical Sciences

by

Anna Kearny Wakeland

Committee in Charge:

Professor Mana M. Parast, Chair
Professor Sylvia Evans
Professor Robert Oshima
Professor Frank Powell
Professor Shunichi Shimasaki

2015

The Dissertation of Anna Kearny Wakeland is approved, and it is acceptable in quality and form for publication on microfilm and electronically:

_____

_____

_____

_____

_____

Chair

University of California, San Diego

2015

DEDICATION

In recognition of their unwavering love and support, I dedicate my dissertation to my best friend and love of my life, Israel Castillo, and to my loving family; my mother, Adelia Kearny, my father, John Wakeland, and my brother, Stephen Wakeland. They all have stood by me every step of the way throughout my graduate studies, and have always been there to listen to me and provide encouragement, humor, empathy, guidance and love.

TABLE OF CONTENTS

LIST OF ABBREVIATIONS

CTB	Cytotrophoblast
STB	Syncytiotrophoblast
EVT	Extravillous Trophoblast
TE	Trophectoderm
ICM	Inner Cell Mass
ExM	Extraembryonic Mesoderm
ExEn	Extraembryonic Endoderm
ExEc	Extraembryonic Ectoderm
mTSC	Mouse Trophoblast Stem Cell
TGC	Trophoblast Giant Cell
BMP4	Bone Morphogenetic Protein 4
hESC	Human Embryonic Stem Cell
ECM	Extracellular Matrix
HIF	Hypoxia-Inducible Factor
ARNT	Aryl Hydrocarbon Receptor Nuclear Translocator
HLA-G	Major Histocompatibility Complex, Class I, G
MMP2	Matrix Metalloproteinase 2
hCG	Human Chorionic Gonadotrophin
PCA	Principal Component Analysis

LIST OF FIGURES

LIST OF TABLES

ACKNOWLEDGEMENTS

First and foremost, I would like to acknowledge and thank Professor Mana M. Parast for her continued support throughout my graduate studies. Her mentorship has been invaluable to both my research and to myself as a scientist. I would also like to acknowledge the members, both past and current, of the Parast Lab for their constant help, advice, and input, including Dr. Yingchun Li, Dr. Matteo Moretto-Zita, Dr. Francesca Soncin, Dr. Mariko Horii, Kanaga Arul Nambi Rajan, Pooja Iyer, Sandra Leon-Garcia, Katharine Nelson, Fabian Flores, and Nastaran Afari. In addition, I would like to acknowledge Planned Parenthood of the Pacific Southwest for providing samples for this study.

Chapter 3, in part, contains material that appears in Development 2013. Li Yingchun, Moretto-Zita Matteo, Soncin Francesca, Wakeland Anna, Wolfe Lynlee, Leon-Garcia Sandra, Pandian Raj, Pizzo Donald, Cui Li, Nazor Kristopher, Loring Jeanne F, Crum Christopher P., Laurent Louise C., Parast Mana M. The Company of Biologists Ltd. 2014. The dissertation author was co-investigator and co-second author of this paper.

VITA

2005-2010	Student Intern, Sandia National Laboratories
2009-2010	Undergraduate Research Assistant, University of New Mexico
2010	Bachelor of Science, Biochemistry, University of New Mexico
2012-2013	Teaching Assistant, Salk Institute Mobile Science Lab
2015	Doctor of Philosophy, Biomedical Sciences, University of California, San Diego

PUBLICATIONS

Li, Y, Moretto-Zita, M, Soncin, F, **Wakeland, A**, Wolfe, L, Leon-Garcia, S, Pandian, R, Pizzo, D, Cui, L, Nazor, K, Loring, J F, Crum, C P., Laurent L C., Parast M M. "BMP4-directed trophoblast differentiation of human embryonic stem cells is mediated through a ΔNp63+ cytotrophoblast stem cell state", *Development*, vol.140, 2013.

ABSTRACT OF THE DISSERTATION

The Role of BMP4 and Oxygen in Trophoblast Lineage Specification and Differentiation

by

Anna Kearny Wakeland

Doctor of Philosophy in Biomedical Sciences

University of California, San Diego, 2015

Professor Mana M. Parast, Chair

Trophoblasts, the placental epithelial cells, provide the main structural and functional component of the placenta. They arise from the trophectoderm, the first lineage to be specified during embryogenesis. Trophectoderm lineage specification and the bulk of placental growth occur under low oxygen tension. *In vivo,* trophoblast precursor cells, known as cytotrophoblasts (CTB), proliferate under physiologic hypoxia and differentiate into invasive extravillous trophoblast (EVT). With increased oxygen tension, CTB differentiate into villous syncytiotrophoblast (STB). One major mechanism

by which hypoxia regulates cell signaling is through hypoxia-inducible factor (HIF). Under hypoxia, the HIF complex is stabilized and acts as a transcription factor to mediate cellular responses to lower oxygen tension. Transgenic mice unable to form an intact HIF complex show abnormal trophoblast differentiation and placental function and die in mid-gestation. However, the role of HIF complex formation in human trophoblast differentiation has yet to be determined.

For my dissertation, I explored how BMP4 signaling and oxygen tension affect trophoblast lineage specification and differentiation, and whether the effects are HIF-dependent. Using mouse trophoblast stem cells (mTSC), primary human trophoblast cells, and BMP4-treated human embryonic stem cells (hESC) as model systems, I found that, in mTSC, BMP4 inhibits differentiation into the trophoblast giant cell lineage, while in human, BMP4 decreases proliferation of CTB in explants and induces both initial trophoblast lineage specification and further differentiation in hESC. I also discovered that hypoxia promotes differentiation into EVT, and that this process is dependent on an intact HIF complex, in both primary cells and hESC. These results establish oxygen tension and HIF as a major regulator of trophoblast lineage-specific differentiation, but also confirm the utility of BMP4-treated hESC as a model which correctly recapitulates these processes in vitro. These data suggest that pluripotent stem cells may be useful in modeling human pregnancy complications such as recurrent miscarriage, preeclampsia, and intrauterine growth restriction, all of which have their roots in abnormal EVT differentiation and function.

Chapter 1

Introduction

1.1 Placentation: mouse and human

The placenta is a transient but crucial organ that sustains the fetus throughout pregnancy. It implants on the uterine wall and connects to the fetus through the umbilical cord. The placenta provides an immunologically protected environment, an interface for nutrient and gas exchange and removal of fetal waste products, and also secretes hormones and growth factors. The placenta is made up of epithelial cells, known as trophoblasts, and extraembryonic mesoderm-derived stromal and vascular tissues. The trophoblasts arise from the outer layer of the blastocyst, known as the trophectoderm (TE), which is the first lineage to be specified in the early embryo, and surrounds the inner cell mass (ICM) (Figure 1.1) (Rossant and Cross, 2001). The ICM gives rise to the fetus, but also contributes to extraembryonic structures, including the allantois (extraembryonic mesoderm, ExM) and yolk sac (extraembryonic endoderm, ExEn) (Figure 1.1) (Rossant and Cross, 2001).

In mice, the portion of the TE in direct contact with the ICM is known as the polar TE; cells in this region maintain their proliferative capacity and form the extraembryonic ectoderm (ExEc), which later gives rise to all trophoblast subtypes. The ExEc expands to form the chorionic membrane. Around day 8.5 of mouse development, chorioallantoic fusion begins, whereby the ExM-derived allantois attaches to the ExEc-derived chorion and creates folds in the chorionic membrane (Rossant and Cross, 2001). Under these folds are stromal cells and blood vessels of the allantois, which carry fetal blood. The folds invaginate and undergo extensive branching to create the densely packed labyrinth. The gene encoding the transcription factor Gcm1 is expressed early in chorioallantoic fusion and is required for initiation of fusion (Anson-Cartwright et al., 2000). The labyrinth is composed of

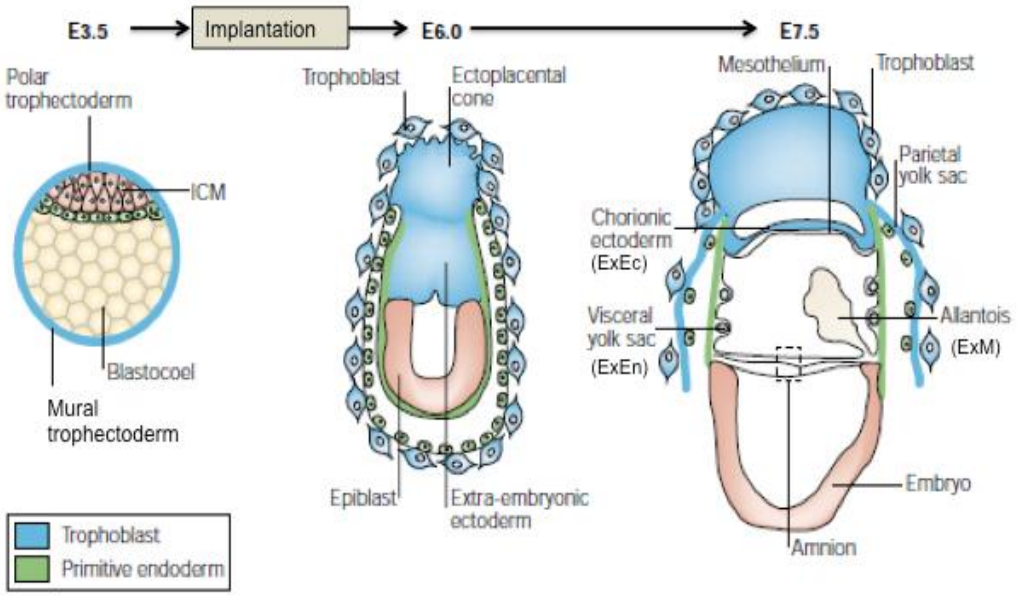

Figure 1.1. Diagram of Early Mouse Embryo Development.
Early development of the mouse embryo from embryonic day (E) 3.5-7.5 showing the extra-embryonic lineages and the components of the placenta. Figure from Rossant and Cross 2001

two layers of multinucleated syncytiotrophoblast (STB) in contact with maternal blood (Figure 1.2) (Soncin 2015). A layer of spongiotrophoblast cells, which are compact non-syncytial cells derived from the ectoplacental cone, supports the labyrinth. Spongiotrophoblast cells also secrete hormones and angiogenic factors (Vuorela 1997). On top of the spongiotrophoblast layer, and abutting the uterine lining (decidua), is the layer of invasive trophoblast giant cells (TGC). TGC are terminally differentiated, invasive cells, formed by endoreduplicating their DNA, which results in polyploidy. There are two waves of TGC formation; primary TGC derive from the mural TE (Figure 1.1) and invade the maternal decidua to form the initial site of attachment. Secondary TGC derive from the polar TE and differentiate first into spongiotrophoblast and then into TGC. These invasive cells further penetrate the decidua to remodel the mother's spiral arteries in order to provide the growing fetus with a steady blood supply (Fryer and Simon, 2006; Soncin et al., 2015).

In the human placenta, chorionic villi form the equivalent structures to the mouse labyrinthine layer (Figure 1.3). The core of the placental villi contains mesenchymal cells and fetal blood vessels that are directly connected to the fetal circulation via the umbilical cord (Figure 1.4). At day 13 post-conception, primary villi, which are composed mostly of mononuclear cytotrophoblast (CTB), start forming finger-like outgrowths into the interstitial space and begin developing into villous "trees." At day 20, they become secondary villi when the allantoic mesenchyme (derived from ExM) invades the core of the villi, and vasculogenesis begins. Tertiary villi are formed when the first fetoplacental capillaries become evident within the villous mesenchyme (Kingdom et al., 2000).

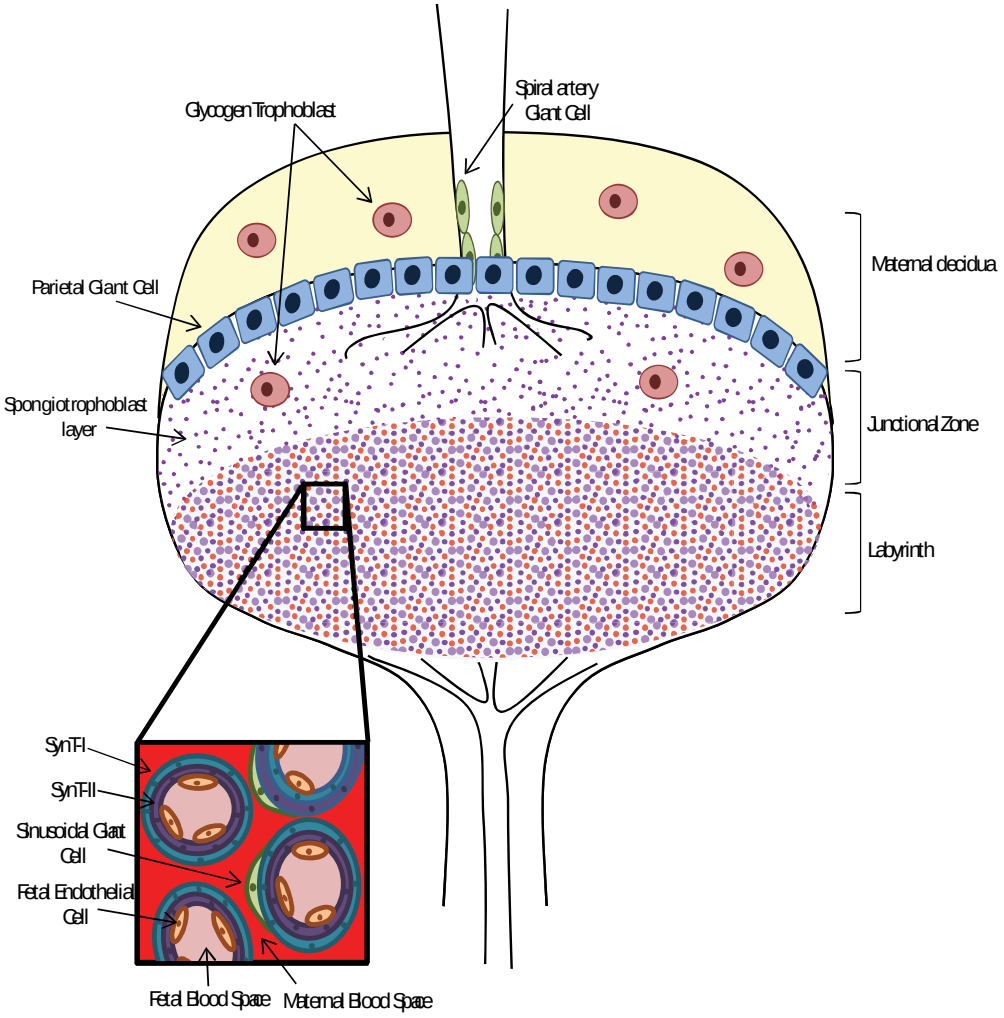

Figure 1.2. Structures and cells in the mouse placenta.
In mouse, the labyrinth is the functional structure where gas/nutrient exchange occurs. Maternal blood is separated from fetal blood by three layers of trophoblasts (SynT-I, SynT-II and sinusoidal giant cells). The junctional zone, which contains spongiotrophoblast, provides support and gives rise to trophoblast giant cells (TGCs) and glycogen trophoblasts. Both TGCs and glycogen trophoblasts are only modestly invasive compared to the human extravillous trophoblasts (EVTs). Figure from Soncin et al., 2015.

Mouse	Human
Trophoblast Stem / Labyrinthine Progenitor Cell	Cytotrophoblast (CTB)
SynT-I/SynT-II (Syncytiotrophoblast)	Syncytiotrophoblast (STB)
Spongiotrophoblast	Cell Column Trophoblast
Parietal Giant Cell	Extravillous Trophoblast (EVT)
Glycogen Trophoblast	Interstitial EVT
Spiral Artery Giant Cell	Endovascular EVT

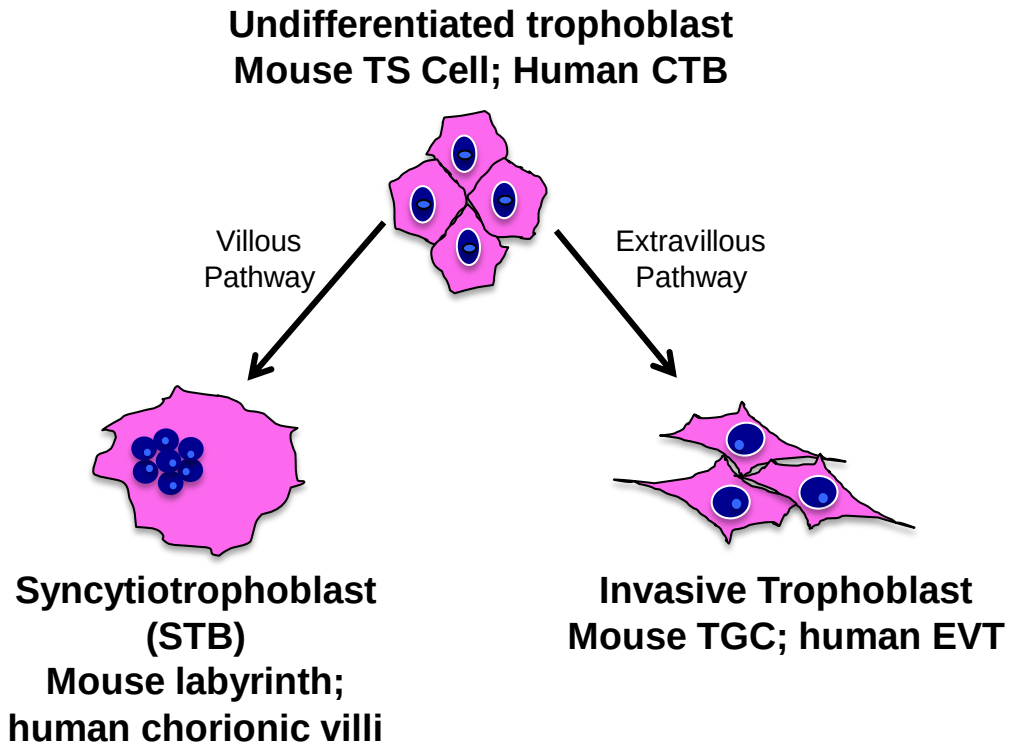

Figure 1.3. Trophoblast subtypes in mouse and human.
(A) Table listing functionally and/or structurally analogous mouse and human trophoblast subtypes. **(B)** Schematic of trophoblast differentiation into villous and extravillous lineages and the respective subtypes in mouse and human. Figures adapted from Soncin et al., 2015 and Li and Parast 2014.

In the first trimester placenta, the villous core is surrounded by two layers of trophoblast; a single layer of mononuclear CTB which then fuse together to form the overlying multinucleated syncytiotrophoblast (STB) layer (Figure 1.4). STBs are in direct contact with maternal blood, and they facilitate nutrient, gas and waste exchange. In humans, STBs also secrete human chorionic gonadotrophin (hCG), which is an important hormone for maintenance of pregnancy (Muyan and Boime, 1997).

In addition to the villous component, there is also an extravillous compartment in the human placenta. This compartment consists of CTB cell columns, which anchor a proportion of the chorionic villi to the uterus. Cell column CTBs are analogous to mouse spongiotrophoblast in expression of ASCL2 (Mash2). Cell column CTBs are precursors to invasive trophoblast, and are termed extravillous trophoblast (EVT) in human. Analogous to mouse TGC, EVT are polyploid, although they do not undergo endoreduplication. As the major invasive trophoblast, EVT remodel the maternal spiral arterioles in order to establish the maternal-fetal interface (Hunkapiller and Fisher, 2008).

1.2 Trophoblast differentiation: mouse and human

Mice offer a sound model for studying proper placental development, both *in vivo* and *in vitro*, due to the capacity for genetic manipulation and derivation of TS cells. Mouse trophoblast stem cells (mTSC) are derived from E3.5 blastocysts or from the ectoplacental cone region of an E8.5 embryo, in the presence of feeders (irradiated mouse embryonic fibroblasts, MEFs), FGF4, and heparin. *In vitro*, self-renewal can be sustained indefinitely under these conditions; upon removal of feeders/FCM, FGF4 and heparin, mTSC stop dividing and differentiate, over a period

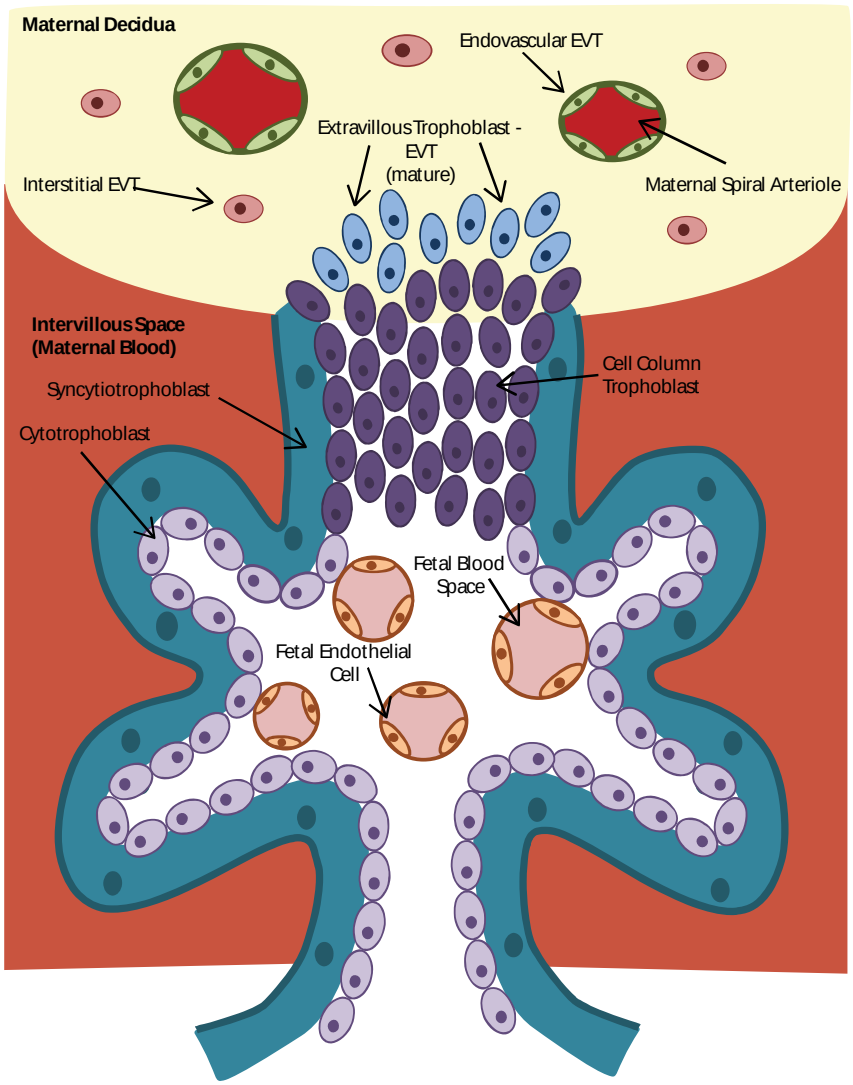

Figure 1.4. Structures and cells in the human placenta.
Cross-section of a chorionic villi, which is the functional structure for gas and nutrient exchange. In the first trimester, maternal blood is separated from the fetal blood by two layers of trophoblast, the syncytiotrophoblast (STB) and the cytotrophoblast (CTB) stem cells. Later in gestation, the continuous CTB layer disappears and only sparse CTBs are visible at term. The EVTs arise from the trophoblast cell column, and are highly invasive, penetrating up to one-third of the thickness of the uterus. Endovascular EVTs extensively remodel maternal spiral arterioles to ensure correct blood supply to the growing embryo. Figure from Soncin et al., 2015.

of 7 days, into both STB and TGC, with a preference towards the latter lineage *in vitro*. *In vivo*, TS cells contribute to all trophoblast subtypes when injected into blastocysts (Tanaka et al., 1998) and can rescue trophoblast-based placental defects (Takahashi et al., 2006).

While mice can be useful as a starting point for placental research, there remain many differences with human, including differences in placental morphology, trophoblast subtypes, and early developmental processes. For instance, the reciprocal expression of the transcription factors Oct4 and Cdx2 (in the ICM and trophectoderm, respectively) in the mouse is not maintained in higher vertebrates, including cattle, pig, and human (Berg et al., 2011; Chen et al., 2009; Ezashi et al., 2011; Strumpf et al., 2005). In the latter organisms, Cdx2 does not repress Oct4, and both genes are co-expressed in the trophectoderm of the late blastocyst (Berg et al., 2011). It is therefore important to compare findings in mice and mTSC to human trophoblast.

There are multiple ways to study human trophoblast differentiation. One way is to use an explant model of first-trimester human placenta, which maintains the normal spatial and functional relationships between the various cell populations, as well as proliferative capacity of the mononuclear CTB proliferation in vitro for a limited time period (Forbes et al., 2008). Another model is to isolate primary CTB from human placenta of any gestational age, although there are slight differences in culture conditions of CTBs isolated from different trimesters. This method is widely used to study terminal trophoblast differentiation into STB or EVT (Lee et al., 2007; Ezashi et al., 2011). However, there are some limitations to this latter model; once the cells are removed from the in vivo environment, the CTBs have a limited capacity to proliferate and cannot be maintained in culture for longer than 7-10 days, which means they have

to be repeatedly isolated. Additionally, only first trimester isolated CTB are able to differentiate into both STB and EVT; after the first trimester, EVT differentiation capacity declines precipitously (McMaster et al., 1995). There are also other limitations with primary CTB isolation, including limited cell number from first trimester placentas due to the size, as well as restricted access to first and second trimester tissue. Another way to study human trophoblast differentiation is to use human trophoblast cell lines (Hohn et al., 1998; King et al., 2000; Shiverick et al., 2001; Zhang et al., 2002). JEG3, a choriocarcinoma cell line, shows features of both STB and EVT. HTR-8, which are immortalized first trimester CTB, are mostly used as a model of EVT. The benefit of using trophoblast cell lines is that they are easy to grow and maintain, but the cells show major differences in comparison to primary cells, both in terms of marker expression and function (Graham et al., 1994; Hohn et al., 1998).

More recently, hESC have been used to study trophoblast differentiation (Amita et al., 2013; Bai et al., 2012; Das et al., 2007; Wu et al., 2008; Xu et al., 2002; Yu et al., 2011). Two methods have been used to obtain trophoblast from hESC: 1) Culturing embryoid bodies on Matrigel (Gerami-Naini et al., 2004), but more commonly, 2) addition of bone morphogenetic protein 4 (BMP4) in the presence of FCM, to hESC plated as a monolayer on Matrigel (Xu et al., 2002). Trophoblast induction has been verified by expression of various markers, including CDX2, KRT7, GCM1, hCG subunits, and by hCG secretion (characteristic of STB) and surface HLA-G expression (characteristic of EVT) (Das et al., 2007; Xu et al., 2002). BMP4, a member of the TGF-β superfamily, uses a set of receptors (BMPR1A, BMPR1B, and BMPR2) and activates a set of SMAD transducers (SMAD1/5/8) (ten Dijke and Hill, 2004) by phosphorylation. BMP signals through binding of a hetertetrameric complex consisting of two dimers of

type 1 and type 2 serine/threonine kinase receptors BMPR1A, BMPR1B and BMPR2 (Wang et al., 2014). The constitutively active type 2 receptor activates the type 1 receptor by transphosphorylation. The active type 1 receptor can then phosphorylate downstream SMADs 1, 5 and 8, which then associate with SMAD4. Type 1 receptors are required for signaling, but type 2 is required for ligand binding, so both are necessary for BMP signaling. In some cells, it has been found that BMPR1A and BMPR1B have overlapping functions (Yoon et al., 2005).

The BMP4 signaling pathway is naturally antagonized by the Activin/Nodal (also members of the TGF-β superfamily) pathway. These two pathways both compete for access to SMAD4, which is necessary to form SMAD complexes, followed by translocation into the nucleus and transcriptional regulation of target genes (ten Dijke and Hill, 2004). This is why addition of Activin/Nodal inhibitors to hESC also results in trophoblast differentiation (Wu et al., 2008).

Recently, trophoblast induction downstream of BMP4 has come into question, with one group indicating that hESC, being derived from ICM and with striking similarities to mouse post-implantation epiblast stem cells (mEpiSCs), should not have the potential to differentiate into trophoblast (Bernardo et al., 2011). However, unlike all other studies which use BMP4 in the presence of FCM, this study used chemically defined media, which, with the addition of BMP4, resulting in only a very small proportion (4-8%) of KRT7-positive trophoblast. More recently, Amita et al. (2013), contested these findings through a comparative study of culture and differentiation conditions, and confirmed the presence of functional trophoblast following FCM+BMP4 treatment (Amita et al., 2013). Mouse embryonic stem cells, derived from pre-implantation embryos, have also been shown to differentiate into trophoblast when

plated on laminin and treated with BMP4 (Hayashi et al., 2010). Interestingly, undifferentiated mTSCs secrete Bmp4 and express receptors for this factor (Murohashi et al., 2010); however, mice lacking bmpr1a or bmpr2 appear able to survive through implantation, though they die shortly thereafter (Mishina et al., 1995; Nagashima et al., 2013). More recently, Graham et al. have shown that Bmp signaling may play a role in specification of both extraembryonic endoderm and ectoderm (Graham et al., 2014). Nevertheless, the question of how BMP4 affects mTSC maintenance and differentiation remains.

1.3 Placentation: the role of oxygen

The early embryo develops under conditions of low oxygen tension (physiologic hypoxia), during which time placental growth predominates (Jauniaux et al., 2003). Numerous mechanisms are activated downstream of hypoxia, leading to the various cellular responses. These include signaling pathways like Notch and Wnt, which are downstream of hypoxia-inducible factor (HIF) (Simon and Keith, 2008). Other cellular responses affected by hypoxia include endoplasmic reticulum (ER) stress pathway (Koumenis and Wouters, 2006), mTOR signaling (Arsham et al., 2003), and epigenetic modifications, including changes in histone methylation and acetylation (Yang et al., 2009).

The HIF complex is a heterodimer consisting of an α subunit and a β, or Aryl Hydrocarbon Receptor Nuclear Translocator (ARNT), subunit (Figure 1.5A). There are multiple α subunits, including HIF-1α, HIF-2α, and HIF-3α, the best studied of which is HIF-1α (Simon and Keith, 2008). Both HIF-1α and ARNT are relatively ubiquitously expressed; however, while HIF-1β/ARNT is largely insensitive to changes in O_2, HIF-α subunits are acutely regulated by hypoxia, being stabilized under low oxygen

conditions (Figure 1.5B). Once stabilized, the HIF-α subunit complexes with HIF-1β/ARNT and acts as a transcription factor by binding to HIF response elements (HRE) located within O_2-regulated target genes (Bruick, 2003). Targets of HIF include genes that mediate hypoxic adaptations, such as glucose transporters, angiogenic factors, and hematopoietic growth factors (Simon and Keith, 2008).

Functional HIF complexes are necessary for proper embryonic and placental development. Abnormal trophoblast differentiation and placental function are seen in transgenic mice missing one or more of the HIF-1 subunits (Kozak et al., 1997; Iyer et al., 1998; Adelman et al., 2000; Cowden Dahl et al., 2005). Hypoxia and HIF also play a role in the differentiation of trophoblasts *in vitro*. Wild type mTSC differentiate almost exclusively into spongiotrophoblasts, but not STB or TGC, when exposed to hypoxia (Adelman et al., 2000). Additionally, when mTSC are derived from ARNT null embryos, they differentiate exclusively into STB instead of spongiotrophoblast or TGC (Maltepe et al., 2005). Finally, rat placentas exposed to hypoxia develop more invasive trophoblast (Rosario et al., 2008); rat TS cells cultured under hypoxia differentiate preferentially into invasive giant cells, a process which is HIF complex-dependent (Chakraborty et al., 2011). This highlights the role of hypoxia and the importance of an intact HIF complex during proper trophoblast differentiation and placental development in rodents.

In the human placenta, hypoxia is thought to inhibit differentiation, and promote proliferation, of trophoblast in early gestation (Genbacev et al., 1997); in fact, prior to maternal blood freely oxygenating the placenta in late first trimester, HIF-1α and HIF-2α proteins are highly expressed in villous trophoblast, with expression declining with increasing gestational age (Pringle et al., 2010).

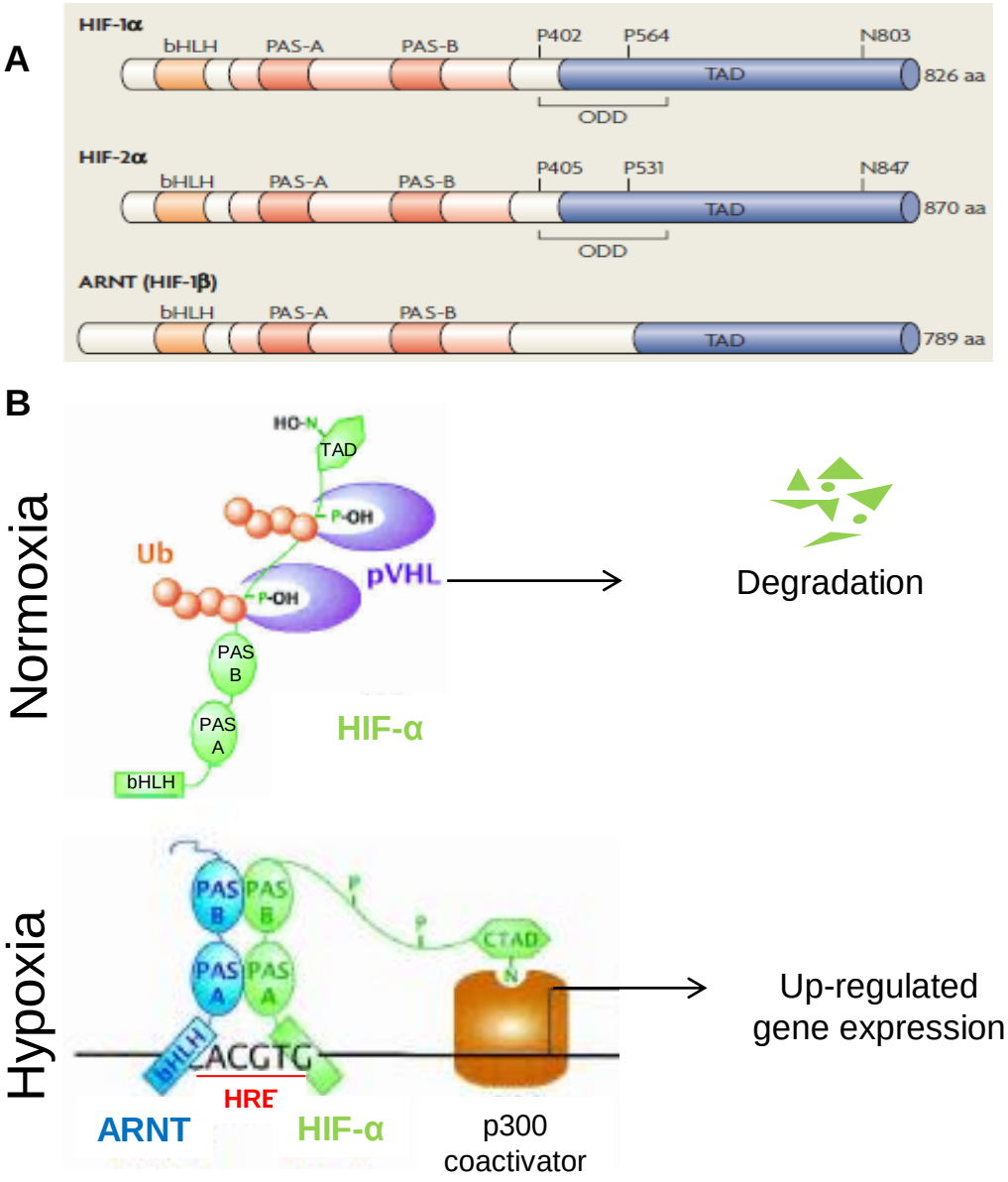

Figure 1.5. Hypoxia Inducible Factor Complex.
(A) Hypoxia-inducible factor (HIF) complex is a heterodimer consisting of an α subunit and a β, or ARNT, subunit. There are multiple α subunits, including HIF-1α and HIF-2α, which are regulated by hypoxia. ARNT is constitutively expressed and is largely insensitive to changes in O_2. **(B)** The HIF-α subunit is degraded in normoxia, but stabilized under low oxygen and can bind to ARNT serving as a transcription factor by binding to HIF response elements (HRE) located within O_2-regulated target genes. Figures from Simon and Keith 2008 and Bruick 2003).

Much less is known about the role of hypoxia and HIF in establishment of the trophoblast lineage in early human embryogenesis. One study has shown that in BMP4-treated hESC, hypoxia inhibits terminal differentiation of trophoblast, as seen by decreased hCG secretion, indicating inhibition of STB differentiation (Das et al., 2007).

Chapter 2

Materials and Methods

2.1 Mouse trophoblast stem cell culture

Mouse trophoblast stem cells (mTSC) were derived from E3.5 blastocysts from wild-type Sv129 mice on murine embryonic feeder cells (MEF) and cultured as previously described (Tanaka 1998). Cells were adapted to feeder-free conditions and were cultured in RMPI-based growth media containing 70% feeder-conditioned media (FCM), 25ng/ml FGF4 (Sigma-Aldrich) and 1ug/ml Heparin (Sigma-Aldrich). Differentiation was induced by removing FCM, FGF4 and Heparin for up to seven days. Minimal growth media containing 2.5% FBS and 10ng/ml Activin A (Stemgent) (to compensate for effects of FCM) was used for experiments using 1ug/ml Noggin (R&D Systems). Minimal differentiation media containing 2.5% FBS was used for experiments using 100ng/ml BMP4 (R&D Systems). Both BMP4 and Noggin treatments were started after serum starvation for 5 hours to minimize any effects of possible BMP4 present in FBS. Cells were cultured at 37°C at 95% room air and 5% CO_2.

2.2 Human placental samples: isolation and culture of primary cytotrophoblast and explants

All fetal and placental tissues were collected under a protocol approved by the Human Research Protections Program Committee of the UCSD Institutional Review Board; all patients gave informed consent for collection and use of these tissues.

First trimester cytotrophoblast were isolated from 8-10 week gestational age placentas. Areas rich in chorionic villi were minced, washed in PBS, and subjected to three sequential digestions: Digestion I: 300 U/ml of DNase I (Sigma-Aldrich) and 150 U/ml collagenase, and 50 U/ml hyaluronidase (Stemcell Technologies); Digestion II and III: 0.25% trypsin (Gibco) and 300 U/ml of DNase I. The pelleted cells from the second

and third digests were pooled and resuspended in HBSS (Thermo Fisher Scientific), and separated on a Percoll (Sigma-Aldrich) gradient. Cell plating was optimized by plating cells on Laminin (50 ug/ml, Santa Cruz Biotechnologies), Collagen IV (8 ug/cm^2, Sigma-Aldrich) or Fibronectin (20 ug/ml, Sigma-Aldrich). Plating was best on Fibronectin and was used for subsequent experiments. Cells were grown in media containing DMEM/F12 (Gibco), 20% fetal bovine serum (FBS, Sigma-Aldrich), 50X Penicillin-Streptomycin (10,000 units of penicillin, 10,000 ug Streptomycin in 100ml, Thermo Fisher Scientific), and 500X Gentamycin (10mg/ml, Gibco) and cultured for 4 days.

Term placentas were obtained and processed within one hour after cesarean section delivery. Following washing in PBS with antibiotics, the villous tissue was minced and transferred to a cell dissociation sieve and rinsed with PBS extensively. Three enzyme digestion steps were carried out, each using 0.25% trypsin and 300U/ml DNase I. Again, only the second and third digests were used in subsequent Percoll gradients. The pelleted cells from the second and third digests were pooled, resuspended in HBSS, and cytotrophoblast separated on Percoll gradient. Cell purity was determined by EGFR FACS; the majority of preps were >95% EGFR positive. Term CTB were seeded at a density of 10^6 cells per ml of Iscove's modified Dulbecco's medium (IMDM, Corning Cellgro) supplemented with 10% FBS and 50X Penicillin-Streptomycin (10,000 units of penicillin, 10,000 ug Streptomycin in 100ml, Thermo Fisher Scientific), and cultured for up to 7 days.

Explants were dissected from 6-8 week gestation age placentas by removing floating chorionic villi. Explants were placed into tissue culture-treated 24-well plates (BD Biosciences) in 500ul serum-free DMEM/F12 media (Gibco). Explants either had

no treatment, +10ng/ml EGF (R&D Systems), or +100ng/ml BMP4 (R&D Systems) and were cultured in 3% O_2 for 24 hours. Supernatant was collected for hCG ELISA assay. Explants were removed and put into a cassette with eosin (Leica), then into formalin to be processed for histologic evaluation. For experiments looking at effect of BMP4 treatment in isolated first trimester CTB, CTB were treated with 100 ng/ml BMP4 for 72 hours in serum-free media.

2.3 Human embryonic stem cell culture and differentiation

The human embryonic stem cell (hESC) aspect of the research was performed under a protocol approved by the UCSD Institutional Review Board and Embryonic Stem Cell Research Oversight Committee.

Prior to differentiation, hESC (WA09/H9 clone) were cultured under feeder-free conditions in StemPro (Invitrogen) medium with 12ng/mL recombinant basic fibroblast growth factor (bFGF) (Invitrogen) on Geltrex (BD biosciences) coated plates. Cells were passaged with StemDS (ScienCell Research Lab) every 3 to 5 days.

For traditional “one-step” trophoblast differentiation, hESC were removed from StemPro and cultured in feeder-conditioned medium supplemented with 10 ng/mL human BMP4 (R&D Systems) for the indicated number of days.

For the two-step trophoblast differentiation, hESC were first cultured in a StemPro-based minimal medium (EMIM, Erb et al., 2011) containing KO DMEM/F12 (Gibco), 1% Insulin-Transferrin-Selenium Mix (Sigma-Aldrich), 1% NEAA (Gibco), 2mM L-Glutamine (Corning), 0.1mM 2-mercaptoethanol (Gibo), and 2% BSA (Gemini Bio Products) for 2 days to remove any lingering effects of the StemPro supplement. The cells were then cultured in EMIM +10ng/mL human BMP4 (R&D Systems) to induce trophoblast lineage specification. After 3 or 4 days, the cells were split with 0.05%

trypsin+EDTA (Gibco) on Geltrex-coated plates in the presence of feeder-conditioned medium supplemented with 10 ng/mL human BMP4 (R&D Systems) for the indicated number of days.

2.4 Cell lines and culture conditions

The human choriocarcinoma cell line JEG3 was obtained from the American Type Culture Collection (Rockville, MD). The human immortalized extravillous trophoblast cell line HTR-8 was a kind gift from Dr. Charles Graham (Queen's University, Kingston, ON). JEG3 cells were grown in Dulbecco's modified Eagle's medium (DMEM) (Corning Cellgro) supplemented with 10% fetal bovine serum (FBS) (Sigma-Aldrich) and 100X Penicillin-Streptomycin (10,000 units of penicillin, 10,000 ug Streptomycin in 100ml, Thermo Fisher Scientific). HTR-8 cells were grown in RPMI-1640 medium (Corning Cellgro) also supplemented with 10% FBS and 100X Penicillin-Streptomycin (10,000 units of penicillin, 10,000 ug Streptomycin in 100ml, Thermo Fisher Scientific).

2.5 Hypoxic culture

For hypoxia, cells were cultured in an XVIVO system (Biospherix). For all experiments in hypoxia, media was changed and cells were lysed (for either RNA or protein analysis) or fixed (for flow cytometry) in the XVIVO work chamber, under the indicated oxygen tension.

2.6 Constructs for downregulation of ARNT

pLKO.1 based scrambled shRNA was obtained from Addgene (Cambridge, MA). A set of five Mission shRNA Lentiviral constructs targeting human *ARNT* gene were purchased (Sigma-Aldrich). HEK293FT cells were transfected with shRNA

constructs, Delta 8.2 and VSV-G using Lipofectamine 2000 (Sigma-Aldrich) according to the manufacturer's instructions. Lentiviral supernatants were concentrated with PEG-it virus precipitation solution (System Biosciences). The concentrated viral particles were then incubated with target cells in the presence of 10 mg/mL polybrene (Sigma-Aldrich). Packaging and infection efficiency were tested using a GFP-expressing lentivirus (in the same pCMV-lentiviral construct as used for ARNT). Of the five *ARNT*-specific shRNA constructs, three worked best, based on protein knockdown in HEK293T cell; therefore, subsequent experiments were performed with this subset of three shRNAs pooled together. For primary isolated CTBs, cells were transiently infected for 4 days. For hESC, cells were stably infected; after 3 days of infection, cells were treated with 5ug/mL puromycin (Sigma-Aldrich) to select stably transduced cells over at least 3 passages. Infection efficiency was determined by GFP expression. Knockdown efficiency was determined by western blot.

2.7 Immunostaining of cells and tissues

For immunohistochemistry on formalin-fixed, paraffin-embedded human placental explants, serial sections were stained with rabbit anti-KRT7 (Abcam), mouse anti-Ki67 (Dako), rabbit anti-HIF-1alpha (Epitomics) or rabbit anti-HIF-2alpha (Lifespan Biosciences) primary antibodies and counterstained using Hematoxylin by using a Ventana Discovery Ultra automated immunostainer with standard antigen retrieval and reagents per the manufacturer's protocol.

For immunofluorescence staining of hESC, cells grown on geltrex-coated coverslips were fixed with 4% paraformaldehyde, then permeabilized with 0.5% Triton X-100 and incubated with primary antibodies, including rabbit anti-OCT4 (Abcam), rabbit anti-KRT7 (Abcam), mouse anti-p63 (4A4, Sigma-Aldrich), mouse anti-HLA-G

(4H84, Abcam), rabbit anti-KLF4 (Sigma-Aldrich), and mouse anti-hCGb (Abcam), and visualized by Alexa fluor 488 or 594 conjugated secondary antibodies (Invitrogen). For nuclear staining, cells were incubated with DAPI (Invitrogen) for 5 minutes.

All stained tissues and cells were imaged by using either a Leica DM IRE2 inverted fluorescence microscope or a Leica DM2500 transmitted light microscope.

2.8 Western blot analysis

After washing with ice-cold phosphate-buffered saline, cells were scraped in lysis buffer containing 1% Triton X-100 and 0.5% SDS, 150mM NaCL in 50mM Tris pH7.5, with 100x HALT protease inhibitor (Thermo Fisher Scientific), and 100x EDTA (Thermo Fisher Scientific). Samples were sonicated for 15 seconds at 20% amplitude, spun at 14,000 rpm for 10 minutes to pellet any insoluble material, and the supernatant was collected. Protein concentration of each sample was determined using a BCA protein assay reagent (Thermo Fisher Scientific). Samples were mixed with 10X sodium dodecyl sulfate (SDS)-polyacrylamide gel electrophoresis sample buffer (20 mmol/L Tris, pH 8.0, 2% SDS, 2 mmol/L dithiothreitol, 1 mmol/L Na_3VO_4, 2 mmol/L ethylenediamine tetraacetic acid, and 20% glycerol) plus 5% 2-mercaptoethanol (BioRad) and boiled for 10 minutes. 30 µg of total cellular protein was separated by 10% SDS-polyacrylamide gel electrophoresis and then transferred to polyvinylidene difluoride (PVDF) membranes. The membranes were blocked for 1 hour at room temperature in 20 mmol/L Tris, pH 8.0, 150 mmol/L NaCl, and 0.05% Tween 20 (Thermo Fisher Scientific) (TBS-T) containing 5% nonfat dried milk (BioRad). For phopho-SMAD1/5/8, membranes were blocked and antibody was incubated in 5% bovine serum albumin (Sigma-Aldrich). The membranes were then incubated with the primary antibody overnight at 4°C. Primary antibodies included rabbit anti-HIF1α

(Cayman Chemical), mouse anti-ARNT (BD Biosciences), mouse anti-beta-actin (Sigma-Aldrich), rabbit anti-SMAD1 (Cell Signaling Technologies), and rabbit anti-phospho-SMAD1/5/8 (Ser463/465, Cell Signaling Technologies). Following three washes in TBS-T, the membranes were incubated with the appropriate horseradish peroxidase (HRP)-conjugated secondary antibodies (Jackson Immunoresearch) for 1 hour at room temperature, then washed with TBS-T three times. The labeled proteins were visualized using the enhanced chemiluminescence (ECL) kit (Thermo Fisher Scientific).

2.9 Flow Cytometry

For flow cytometric analysis, cells were fixed with 4% paraformaldehyde (PFA); Cells were incubated with antibodies at room temperature for an hour, washed and resuspended in an appropriate volume of FACS buffer (1x PBS, 10% FBS). Flow cytometric analysis was done using a BD FACS-Canto Flow Cytometer (BD Biosciences). Antibodies used for FACS included PE-conjugated mouse anti-HLA-G (MEM-G/9, ExBio), APC-conjugated mouse anti-EGFR (BioLegend).

2.10 Measurement of secreted total hCG, Hyperglycosylated hCG and MMP2

Cell culture supernatants were collected and stored in -80°C. Levels of total hCG were quantified using hCG ELISA Kit (Calbiotech Inc.) according to the manufacturer's protocol. Hyperglycosylated hCG (H-hCG) was quantified by electrochemiluminescent procedure using specific antibodies at Quest Diagnostics. Levels of secreted MMP2 were quantified using MMP2 ELISA kit (Abcam). The results were normalized to DNA content, using DNA isolated from the DNEasy Blood and Tissue Kit (Qiagen).

2.11 RNA isolation, quantitative reverse-transcriptase PCR, and gene expression microarray

For both cells and tissues, total RNA was extracted with the mirVana RNA Isolation Kit (Ambion) according to the manufacturer's protocol. For quantitative reverse-transcriptase PCR (qRT-PCR), purity and concentration of the samples were assessed with NanoDrop ND-1000 Spectrophotometer (Thermo Fisher Scientific). cDNA was prepared from 500ng RNA using iScript (Bio-Rad) in a 20 uL reaction, and diluted 1:5 with nuclease-free water. Quantitative reverse transcriptase PCR (qRT-PCR) was performed using 4 uL of the diluted cDNA, along with 625 nM of each primer and POWER SYBR Green PCR master mix (Applied Biosystems) in a total reaction volume of 20 µL. qRT-PCR was performed using a System 7300 instrument (Applied Biosystems) and a one-step program: 95°C, 10 min; 95°C, 30 sec, 60°C, 1 min, for 40 cycles. Relative mRNA expression levels were determined by the $\Delta\Delta C_T$ method using 18S rRNA as a housekeeping gene and normalized to day 0 unless otherwise stated. Data are shown as relative mRNA expression with standard deviation. All primer pairs (Table 2.1) were checked for specificity using BLAST analysis and melting curve to ensure amplification of a single product with the appropriate size and melting temperature. Samples amplified for specific BMP Receptor subtypes were loaded into a gel to check for band size.

Table 2.1. List of primers used for quantitative real-time PCR.

Primer Name	Primer sequence
MOUSE	
18S	F 5'-CGC GGT TCT ATT TTG TTG GT-3' R 5'-AAC CTC CGA CTT TCG TTC TTG-3'
Bmpr1a	F 5'-ATG CAA GGA TTC ACC GAA AG-3' R 5'-AAC AAC AGG GGG CAG TGT AG-3'
Bmpr1b	F 5'-AGC AGC TGA GAA CCT CGC CG-3' R 5'-GCT CTC TCC GTG TCC GCG TG-3'
Bmpr2	F 5'-ATA GGC GTG TGC CAA AAA TC-3' R 5'-ATT GTC AAT GGT GTG CTG GA-3'
Bmp4	F 5'-TGA TAC CTG AGA CCG GGA AG-3' R 5'-CTG GAG CCG GTA AAG ATC CC-3'
SynA	F 5'-CCC TTG TTC CTC TGC CTA CTC-3' R 5'-TCA TGG GTG TCT CTG TCC AA-3'
Tpbpa	F 5'- GGA AGT CCC TGC TGT TTT TG -3' R 5'-AGA GAG TGG CGA TGG GTT TT-3'
HUMAN	
18S	F 5'-CGC CGC TAG AGG TGA AAT TCT-3' R 5'-CGA ACC TCC GAC TTT CGT TCT-3'
TP63	F 5'-CTG GAA AAC AAT GCC CAG A-3' R 5'-AGA GAG CAT CGA AGG TGG AG-3'
KLF4	F 5'-ACC TAC ACA AAG AGT TCC CAT C-3' R 5'-TGT GTT TAC GGT AGT GCC TG-3'
ID2	F 5'-GAC GAA GGG AAG CTC CAG CGT GT-3' F 5'-CTG ACC GCG AGG GAA GGC GA-3'
TEAD4	F 5'-CAG TAT GAG AGC CCC GAG AA-3' F 5'-TGC TTG AGC TTG TGG ATG AA-3'
CGB	F 5'-TGA GAT CAC TTC ACC GTG GTC TCC-3' R 5'-TTT ATA CCT CGG GGT TGT GGG G-3'
POU5F1	F 5'-TGG GCT CGA GAA GGA TGT G-3' R 5'-GCA TAG TCG CTG CTT GAT CG-3'
CDX2	F 5'-TGG ACA CGG ACC ACC AG-3' R 5'-GCT CTG GGA CAC TTC TCA GAG G-3'
HLAG	F 5'-CAG ATA CCT GGA GAA CGG GA-3' R 5'-CAG TAT GAT CTC CGC AGG GT-3'
STRA13	F 5'-CGT TGA GGC TGC GGT CAT GGA G-3' R 5'-CGC GGA CTG CTG CTT CTT TGG-3'
BMP4	F 5'-TTG TCT CCC CGA TGG GAT TC-3' F 5'-CAA ACT TGC TGG AAA GGC TCA-3'
BMPR1A	F 5'-ATC ACA GGA GGG ATC GTG GA-3' F 5'-AGA CAC AAT TGG CCG CAA AC-3'
BMPR1B	F 5'-GGG TGG AGT TCA GCC TAC TC-3' F 5'-TTC CTG CAC TTC GCA AAA GC-3'
BMPR2	F 5'-GGG TAA GCT CTT GCC GTC TT-3' F 5'-AAC CTC GCT TAT GGC TGC AT-3'
ITGA6	F 5'-GGC GGT GTT ATG TCC TGA GTC-3' F 5'-AAT CGC CCA TCA CAA AAG CTC-3'
ITGA5	F 5'-GGC TTC AAC TTA GAC GCG GAG-3' F 5'-TGG CTG GTA TTA GCC TTG GGT-3'

Table 2.1. List of primers used for quantitative real-time PCR. Continued

Primer Name	Primer Sequence
HUMAN	
ITGA1	F 5'-CTG GAC ATA GTC ATA GTG CTG GA-3' F 5'-ACC TGT GTC TGT TTA GGA CCA-3'
SYNA	F 5'-GTC ACT GTC TGT TGG ACT TAC T-3' F 5'-CGG GTG AGT TGG GAG ATT AC-3'
PPARG	F 5'-CCC AAG TTT GAG TTT GCT GTG-3' F 5'-CAG GGC TTG TAG CAG GTT GT-3'
TEAD2	F 5'-CAG GCC TCT GAG CTT TTC CA-3' F 5'-GGA GGT CAG TAG ATG GGG GA-3'
ARNT	F 5'-CCC TAG TCT CAC CAA TCG TGG ATC-3' F 5'-GTA GCT GTT GCT CTG ATC TCC CAG-3'
VEGFA	F 5'-AGG CCA GCA CAT AGG AGA GA-3' F 5'-TTT CTT GCG CTT TCG TTT TT-3'
ANKRD37	F 5'-GTC GCC TGT CCA CTT AGC C-3' F 5'-GCT GTT TGC CCG TTC TTA TTA CA-3'
SLC2A1	F 5'-ATA CTC ATG ACC ATC GCG CTA G-3' F 5'-AAA GAA GGC CAC AAA GCC AAA TG-3'
EGFR	F 5'-CTA AGA TCC CGT CCA TCG CC-3' F 5'-GGA GCC CAG CAC TTT GAT CT-3'

For RNA to be used for gene expression microarray, total RNA was purified using the MirVana RNA Isolation Kit (Ambion). Total RNA was quantified using the Ribogreen reagent (Lifetech, Inc.) using a Qubit fluorometer (Thermo Fisher Scientific), and quality-controlled on an Agilent 2100 Bioanalyzer (Agilent). Only those RNA samples with an RNA integrity number (RIN) > 8.0 were subjected to further gene expression analysis. Two hundred nanograms of input total RNA was amplified and labeled using the TotalPrep kit (Ambion). The labeled product was then hybridized to Illumina HT12 arrays and scanned on a BeadArray Reader (Illumina, Inc.) according to the manufacturer's instructions.

2.12 Analysis of gene expression profiling data

Probes were filtered with a detection-*P* value cut-off of 0.01, and normalized by using the LUMI package in R with the RSN (Robust Spline Normalization) method. I used Qlucore software to explore and analyze microarray gene expression data sets. I viewed my data in a Principal Component Analysis. For both primary CTB and hESC, I used shScramble control cells as my wild-type conditions for analysis in chapter 4. For primary CTB, I assessed freshly isolated (Day 0), Hypoxia (Day 4) and Normoxia (Day 4). For hESC cultured using the one-step method, I assessed day 0, and hypoxia or normoxia (days 2, 4, 6 and 8). For hESC culture using the two-step method, I assessed CTB (Day 3) and Hypoxia (CTB+2) and Normoxia (CTB+2). To look at the effect of ARNT knockdown, Scramble shRNA-treated cells were compared to ARNT shRNA-treated cells. Heatmaps of gene expression were generated first by filtering for variance (v=0.01) and then applying a multi-group statistical analysis (ANOVA) ($q \leq 0.05$) unless otherwise stated. Probes that were significantly upregulated in hypoxia were selected and the probe list was exported from Qlucore. The list of probes was

then subjected to gene ontology analysis using METASCAPE (Metascape.org) to assess genes upregulated in hypoxia, or for shARNT samples, genes that are significantly unchanged between normoxia and hypoxia. Probe lists, with fold change data, are provided in Appendix A, and gene ontology information is provided in Appendix B.

For primary CTB, I compared gene expression of Day 0, Hypoxia Day 4, and Normoxia Day 4 to gene expression data of sorted CTB (EGFR single positive cells) and sorted EVT (HLA-G single positive cells) that were obtained by flow cytometry-assisted cell sorting. To obtain the populations of sorted CTB or sorted EVT, freshly isolated first trimester trophoblast were stained with PE-conjugated mouse anti-HLA-G (87G, Biolegend) and APC-conjugated mouse anti-EGFR (BioLegend) and sorted using a BD Influx (BD Biosciences). For my comparison, I used probes that had a fold change of 1.3 or higher for my primary CTB samples or a fold change of 2.0 or higher for the sorted CTB and sorted EVT samples.

2.13 Statistical analysis

For first trimester isolated CTB, data presented are mean ± standard deviation of five separate placentas. For hESC-derived trophoblast, data presented are mean ± standard deviation of three replicate wells of a single prep of cells. Paired t-test was performed and P values below 0.05 were taken to indicate a statistically significant difference between the populations sampled.

Chapter 3

The role of BMP4 signaling during trophoblast lineage specification, self-renewal and differentiation

3.1 Role of BMP4 in mouse trophoblast stem cell maintenance

It is known that during mouse development, mouse trophoblast stem cells (mTSC) secrete BMP4, which in turn induces mesoderm induction in the post-implantation epiblast (Winnier et al., 1995; Murohashi et al., 2010); however, BMP4 receptors are also expressed in extraembryonic ectoderm, where mTSC reside *in vivo* (Mishina et al., 1995). Additionally, mice lacking Bmp Receptor Type 1a (Bmpr1a) or Bmp Receptor Type 1b (Bmpr2) survive through implantation, although they die soon thereafter (Mishina et al., 1995; Nagashima et al., 2013). BMP4 is also involved in maintenance of pluripotency in mouse embryonic stem cells (mESC), although in the presence of laminin, it has also been shown to induce trophoblast differentiation (Hayashi et al., 2010). More recently, it has been shown that inhibition of BMP signaling may interfere with establishment of trophectoderm in the early mouse embryo (Graham et al., 2014). Nevertheless, the question of how BMP4 affects trophoblast lineage specification, self-renewal and differentiation remains.

I first addressed the role of BMP4 in trophoblast self-renewal and differentiation in the mTSC model. First, I determined if BMP4 or its receptors are expressed in mTSC at various timepoints of differentiation by RT-PCR. I found expression of Bmpr1a, which helps to phosphorylate Phospho-Smad 1/5/8, as well as expression of Bmp Receptor type 2 (Bmpr2) (Figure 3.1A). Bmp4 and Bmpr1b were also expressed, albeit at lower levels. Expression of all transcripts was greatest at day 1 of differentiation. I next wanted to confirm that Bmp4 signaling is active; therefore, I assessed Phospho-SMAD1/5/8 and total SMAD1 levels in both undifferentiated and differentiated mTSC and confirmed there is indeed phosphorylated SMAD1/5/8 in the undifferentiated state (Figure 3.1B).

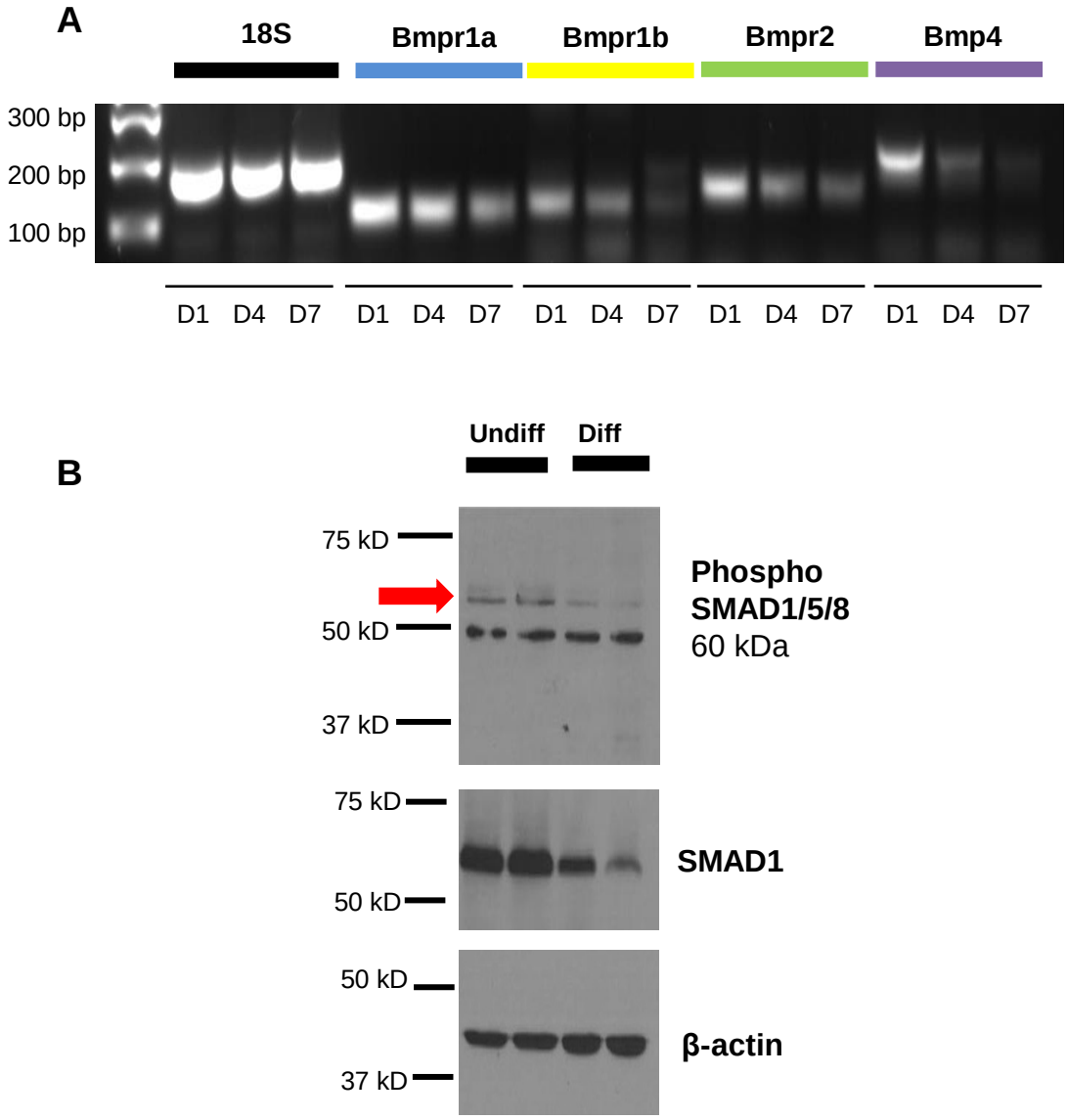

Figure 3.1. BMP4 receptors and signaling in mouse trophoblast stem cells (mTSC).
(A) BMP4 and BMP Receptor types in mTSC were analyzed by PCR on amplified DNA at days 1, 4 and 7. **(B)** Western blot for Phospho SMAD 1/5/8 (correct band indicated by arrow), total SMAD1 and beta Actin in undifferentiated (Undiff) or differentiated (Diff) mTSC.

Based on the evidence that the receptors for BMP4 are expressed and signaling is active in undifferentiated mTSC, I hypothesized that BMP4 helps maintain mTSC in an undifferentiated state. In order to determine the effect of BMP4 on maintenance vs. differentiation of mTSC, I designed two experiments: 1) treating with BMP4 during mTSC differentiation, and 2) treating undifferentiated mTSC with Noggin, an inhibitor of BMP4 signaling. For both experiments I used media containing minimal (2.5%) fetal bovine serum (FBS) to minimize any effect of possible BMP4 present in serum.

To confirm normal BMP4 signaling in minimal media, I found that Phopho-SMAD1/5/8, which is present in undifferentiated mTSC, is reduced as the cells differentiate (Figure 3.2A). However, in the presence of BMP4, differentiating mTSC maintained phopho-SMAD1/5/8 (Figure 3.2A). To evaluate the effect of BMP4 signaling on differentiation status of mTSC, I examined relative mRNA expression of markers of syncytiotrophoblast (STB) differentiation and spongiotrophoblast, a precursor to trophoblast giant cell (TGC) differentiation. I found that BMP4 significantly reduced the expression of Spongiotrophoblast marker Tpbpa (Figure 3.2B).

To assess the effect of BMP4 on mTSC maintenance, I inhibited BMP4 directly by treating cells with Noggin while the cells are in growth media. To confirm the effects of Noggin, I saw reduced expression of Phopho-SMAD1/5/8 during Noggin treatment of undifferentiated mTSC (Figure 3.3A). Additionally, I found that Noggin significantly increased relative mRNA expression of Tpbpa, a TGC precursor (Figure 3.3B).

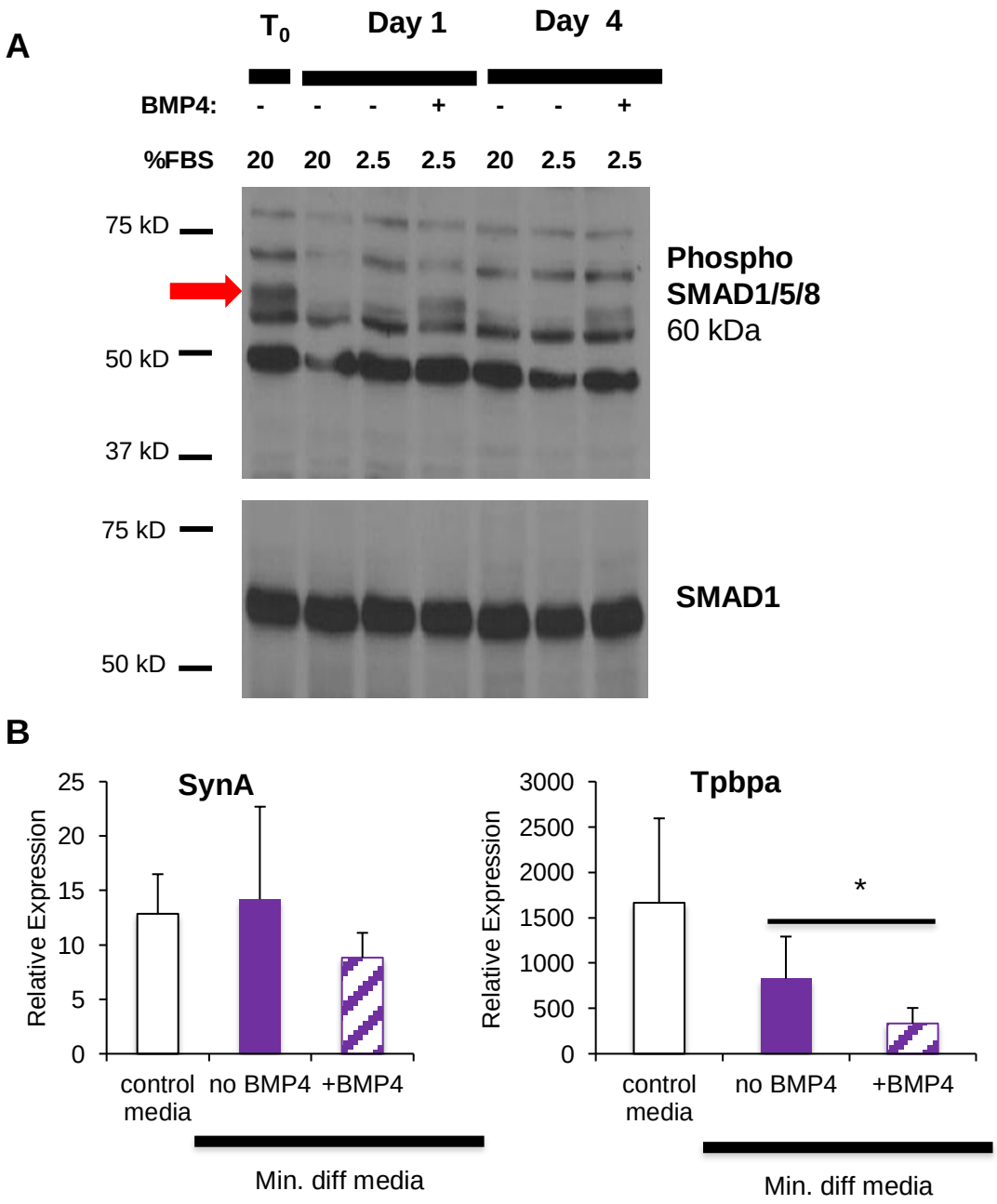

Figure 3.2. Effect of BMP4 treatment during mTSC differentiation.
(A) Western blot for Phospho SMAD1/5/8 in undifferentiated mTSC, mTSC differentiating in normal or minimal serum media, and upon treatment with BMP4 (100ng/ml) treatment **(B)** qRT-PCR analysis of syncytiotrophoblast marker SynA and spongiotrophoblast marker Tpbpa. Values adjusted to undifferentiated state and normalized to 18S ribosomal RNA. *p<0.05.

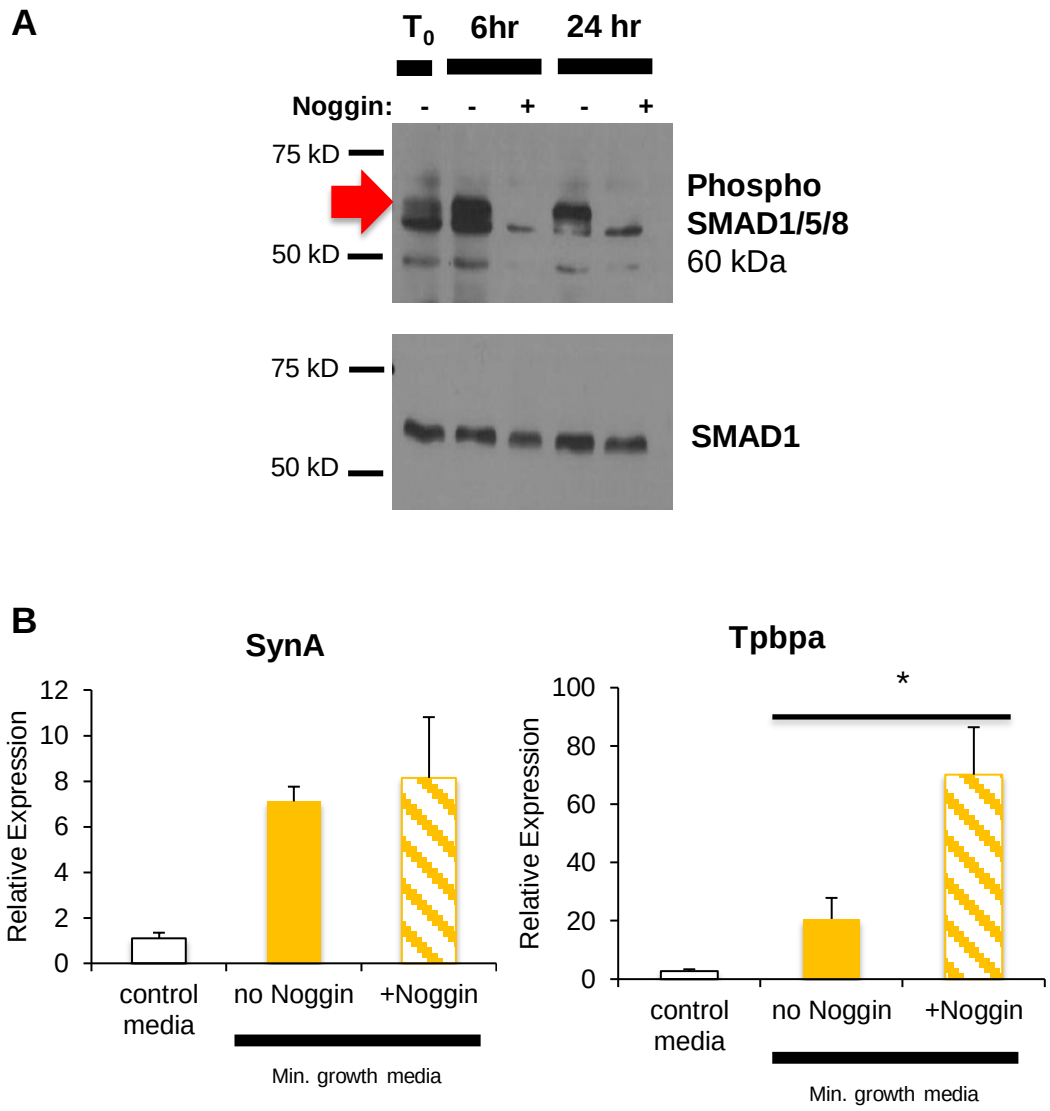

Figure 3.3. Effect of BMP4 inhibition in undifferentiated mTSC.
(A) Western blot for Phospho SMAD1/5/8 in undifferentiated mTSC in minimal growth media, and with treatment with Noggin (1ug/mL), an inhibitor of BMP4. **(B)** qRT-PCR analysis of syncytiotrophoblast marker SynA and spongiotrophoblast marker Tpbpa. Values adjusted to undifferentiated state and normalized to 18S ribosomal RNA
*p<0.05.

3.2 Effect of BMP4 in primary human cytotrophoblasts

In humans, BMP4 is known to induce trophoblast from human embryonic stem cells (hESC) (Xu et al). However, the role of BMP4 has not been assessed in isolated primary human cytotrophoblasts (CTB). I used RT-PCR to assess expression of BMP4 and its receptors in human primary CTB isolated from first trimester placenta. BMP4 and BMP Receptors 1A and 2 were expressed, while BMP Receptor 1B was not expressed, (Figure 3.4A). These results were confirmed by assessing relative mRNA expression by qRT-PCR (Figure 3.4B).

In order to determine if BMP4 affects maintenance of primary human CTB, I treated explants from first trimester chorionic villi with BMP4. Each villus is comprised of a dual layer of STB and CTB surrounding a stromal core. The two layers of trophoblast can be seen by H&E staining, as well as by expression of KRT7, a pan-trophoblast marker (Figure 3.5A). I looked for expression of Ki67, a marker of proliferation, which is expressed in the nuclei of proliferative CTB located in the inner layer, but not in STB, the outer trophoblast layer. When explants were treated with EGF, a pro-differentiation factor (Forbes et al., 2008), the percentage of Ki67-expressing CTB decreased compared to untreated explants (Figure 3.5B). When explants were treated with BMP4, Ki67 similarly decreased compared to untreated explants (Figure 3.5A and B).

To further assess the effect of BMP4 in human CTB differentiation, I measured hCG secretion from primary CTBs isolated from first trimester, second trimester and term placentas treated with or without BMP4 for the specified number of days (Figure 3.6A). I did not find any difference in hCG secretion at any gestational age

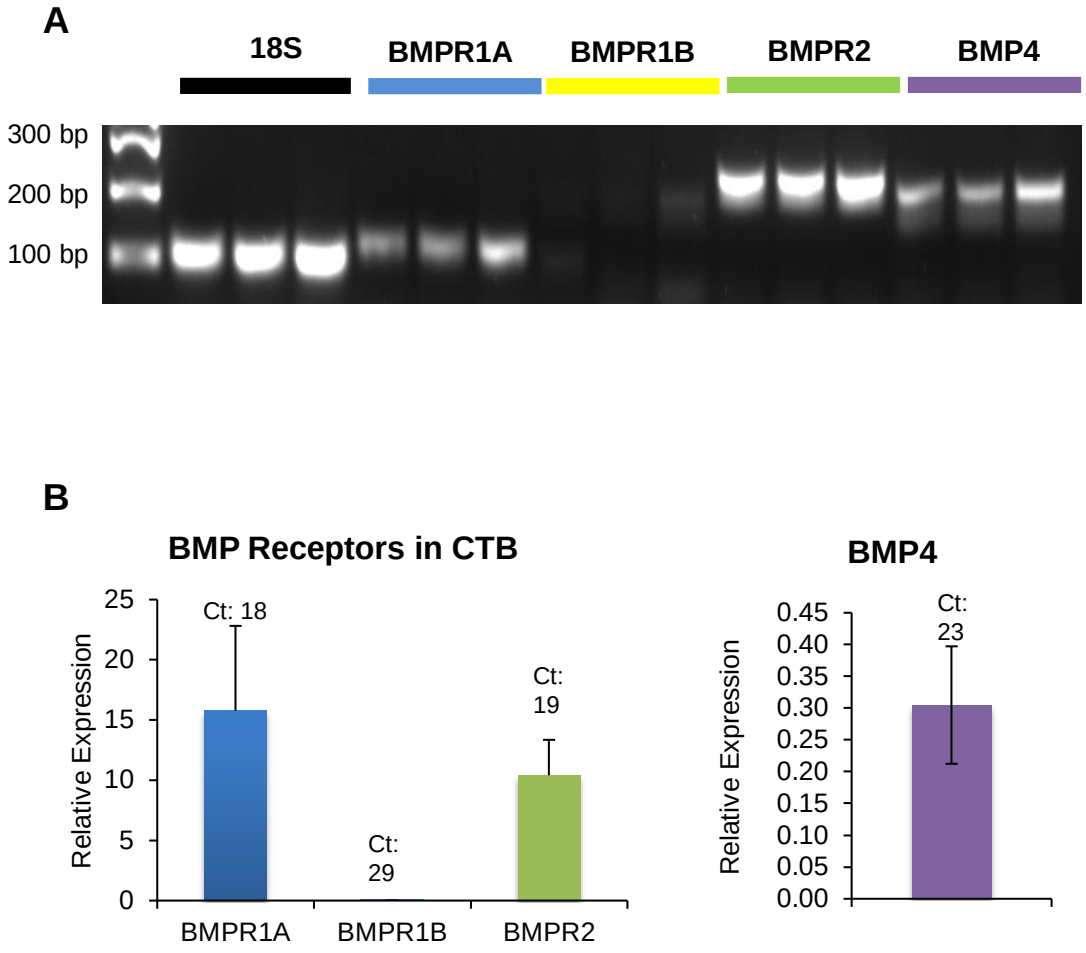

Figure 3.4. BMP4 receptors and signaling in isolated first trimester trophoblast.
(A) BMP4 and BMP Receptor types in primary CTB isolated from first trimester placenta were analyzed by PCR and **(B)** confirmed by qRT-PCR. Values adjusted to freshly isolated CTB and normalized to 18S ribosomal RNA.

A

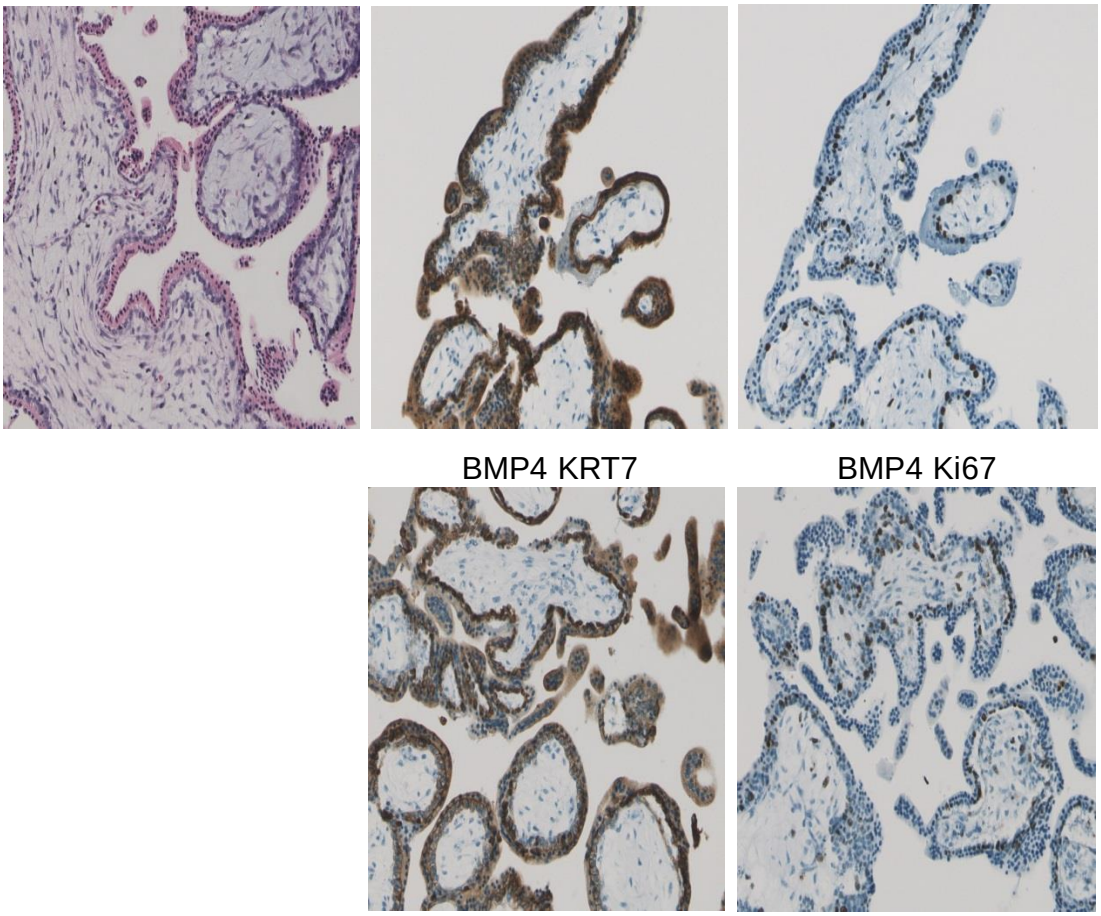

B

Treatment	% of Ki67^{+} CTB	Std. Dev.
Untreated	38.2	12.2
+EGF	18.7*	5.1
+ BMP4	23.7*	5.5

Figure 3.5. BMP4 treatment of first trimester villous explants.
(A) H&E staining shows the double layer of cytotrophoblast (CTB) and syncytiotrophoblast surrounding each villi. KRT7 (pan-trophoblast marker) and Ki67 staining of untreated explants or explants treated with BMP4 (100 ng/ml) and cultured at 3% O_2 for 24 hours in serum-free media. **(B)** Percentage of Ki67+ proliferative CTB in untreated, EGF-treated (10 ng/ml) and BMP4-treated explants. * $p < 0.05$ compared to control.

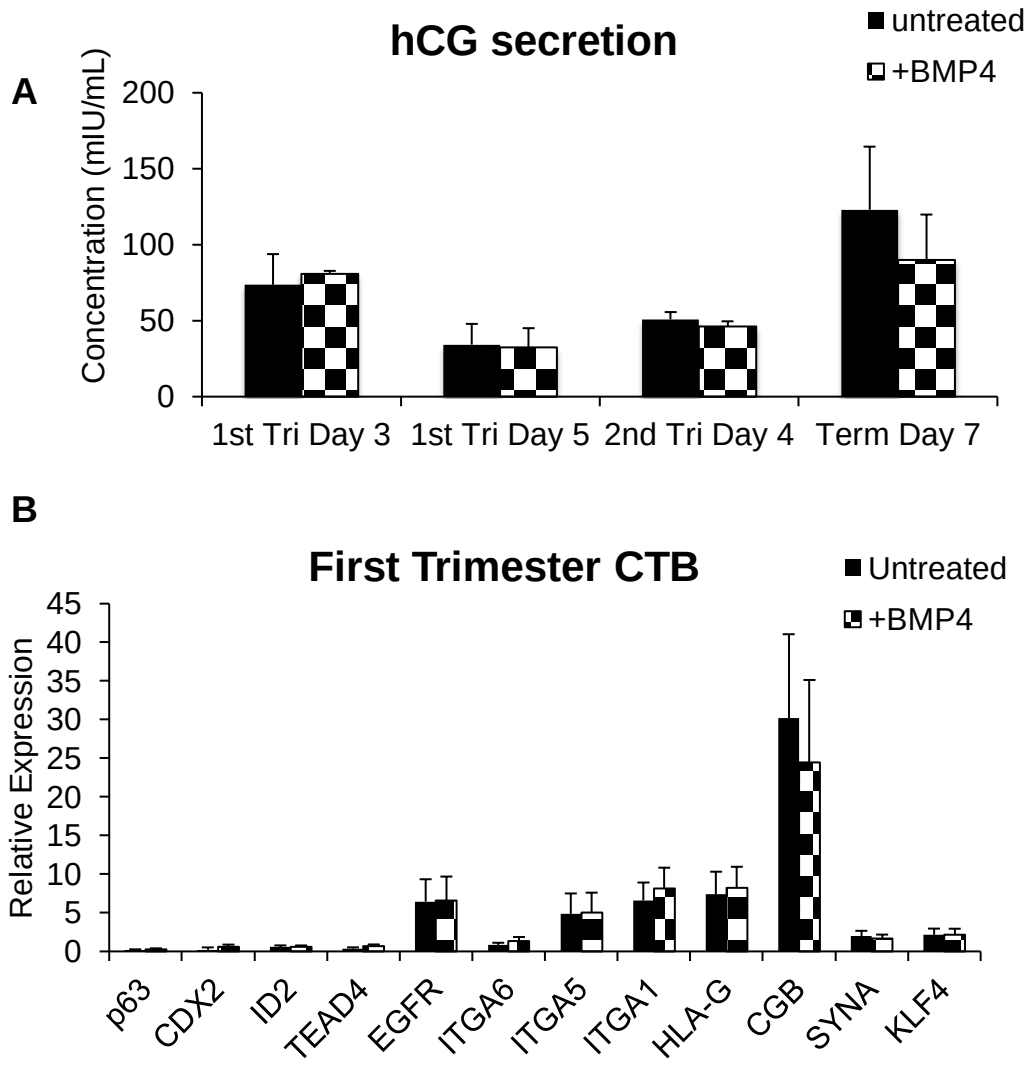

Figure 3.6. Effect of BMP4 on differentiation of isolated primary cytotrophoblasts (CTB).
(A) hCG secretion of primary CTB isolated from first trimester, second trimester and term placentas treated with or without BMP4 (100 ng/ml) was measured by ELISA. **(B)** qRT-PCR analysis of first trimester isolated CTB found no significant differences in expression of trophoblast differentiation markers between untreated and BMP4 treatment.

compared to untreated. Next I checked expression of multiple markers of differentiation by qRT-PCR in isolated first trimester CTB, but found no significant difference in expression of lineage-specific markers (Figure 3.6B) with BMP4 treatment. There was also no significant difference in expression of differentiation markers in BMP4-treated second trimester and term CTB (data not shown).

3.3 The effects of BMP4 signaling during human trophoblast lineage specification, maintenance, and differentiation

Since the discovery of trophoblast induction upon BMP4 treatment of hESC (Xu et al., 2002), numerous other studies have used the model to study trophoblast differentiation (Das et al., 2007; Wu et al., 2008; Erb et al., 2011; Yu et al., 2011). In the presence of feeder conditioned media (FCM) and BMP4, POU5F1-expressing pluripotent hESC differentiate into CTB and continue to differentiate into STB and EVT (Figure 3.7A). The cells undergo obvious morphologic changes from tight colonies of pluripotent hESC to flattened epithelial-like trophoblast (Figure 3.7B). Recently, a single study called into question trophoblast induction downstream of BMP4, indicating that the cells had features of mesoderm and were possibly more similar to extraembryonic mesoderm, rather than extraembryonic ectoderm (Bernardo et al., 2011). In order to confirm the identity of BMP4-treated hESC, we subjected these cells to microarray-based genome-wide gene expression profiling alongside a series of fetal and placental tissues and isolated cells. Gene probes that were specifically differentially expressed in each tissue type were filtered out, and analysis by hierarchical clustering showed that BMP4-treated hESC were most similar to placental tissue and isolated primary

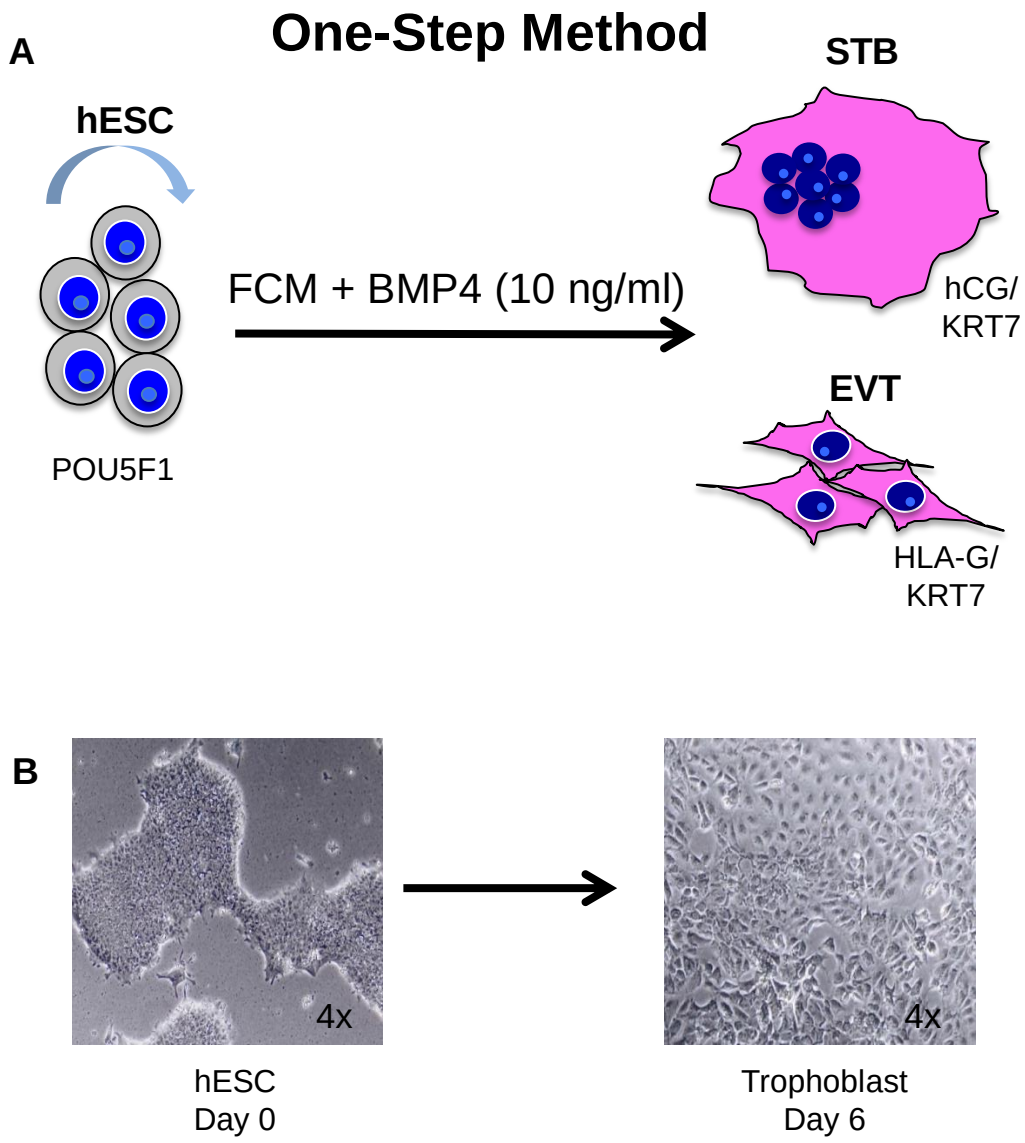

Figure 3.7. One-step method of BMP4-induced trophoblast differentiation of human embryonic stem cells (hESC).
(A) Self-renewing hESC maintained under feeder-free conditions with bFGF differentiate into KRT7 positive trophoblast subtypes after culture in feeder-conditioned medium supplemented with 10 ng/ml BMP4 for up to 8 days. BMP4-treated hESC undergo a p63/KRT7/CDX2 triple-positive CTB "stem cell" state prior to terminal differentiation into HLA-G positive EVT and hCG-secreting STB. **(B)** Cells undergo morphologic changes from tight colonies of pluripotent stem cells to flattened epithelial-like trophoblast.

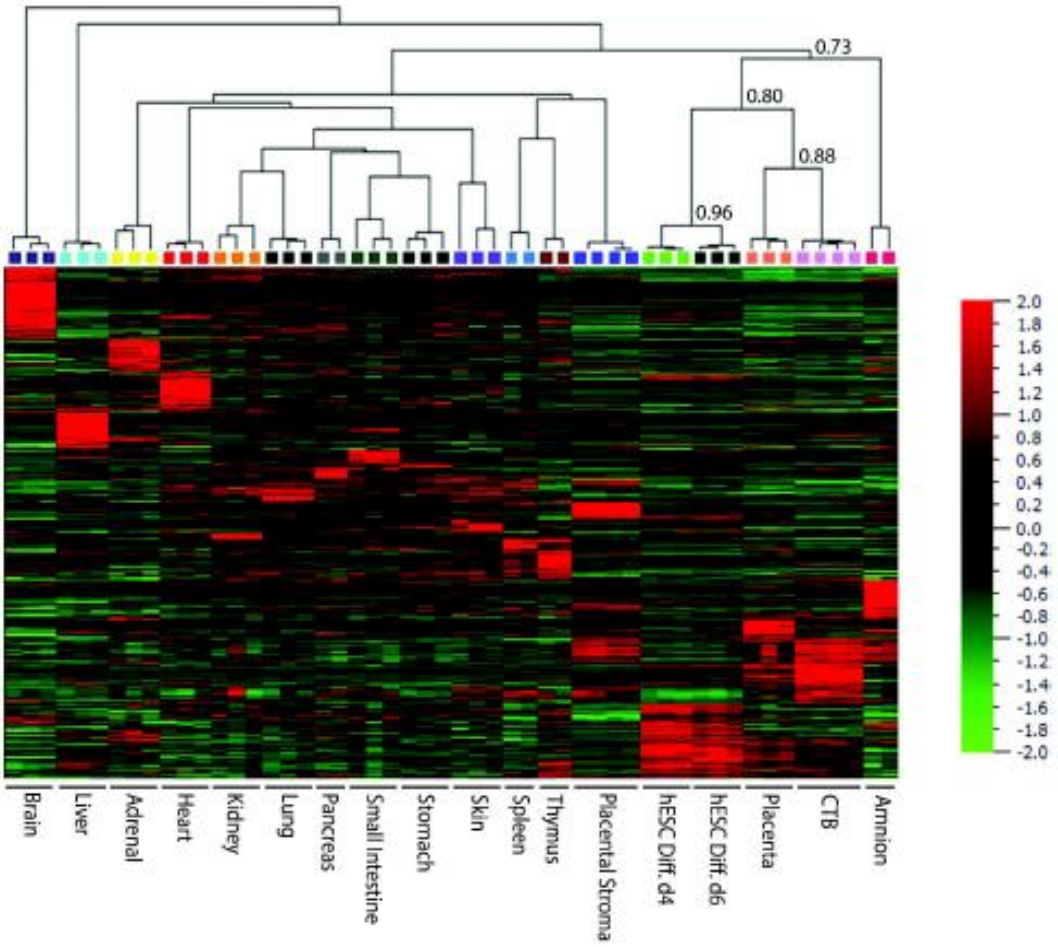

Figure 3.8. BMP4-treated hESC most closely resemble placenta and primary CTB and express trophoblast-associated genes.
Hierarchical clustering shows that hESC treated with FCM-BMP4 at days 4 and 6, most closely resemble placental tissues and primary CTB. Pearson correlation coefficients are shown for the FCM-BMP4-day4/day6/placental tissue/CTB cluster.

CTB, clustering away from placental stroma and amnion (Figure 3.8).

Previously, the delta-N isoform of the nuclear protein TP63 was identified as a marker of proliferative CTB in the human placenta (Lee et al., 2007). Our lab has recently determined that BMP4-treated hESC undergo a CTB stem cell-like state, which is characterized by expression of the delta N isoform of p63. dNp63 is induced downstream of BMP4 treatment during trophoblast differentiation of hESC along with other trophoblast associated genes. Samples analyzed at days 0, 2, 4, and 6 of differentiation showed evidence of progressive differentiation, with some early trophoblast progenitor-associated genes, such as *STRA13, CDX2* and *dNp63* being induced on days 2-4, and genes associated with terminally-differentiated trophoblast, including *HLAG*, *CGA*, and *CGB1* being induced later, on day 6 (Figure 3.9 and Figure 3.10).

Differentiation was further confirmed by immunofluorescence, with POU5F1 present and KRT7 absent in undifferentiated hESC (Figure 3.11). As the cells differentiate into trophoblast, POU5F1 is downregulated and by day 5 of BMP4 treatment, the cells were uniformly $p63^{+}/KRT7^{+}$ CTB. By day 7, the CTB further differentiated into HLA-$G^{+}/KRT7^{+}$ EVT and $hCG^{+}/KLF4^{+}$ STB at day 7. Functional differentiation was confirmed by secretion of hCG and hyperglycosylated hCG, indicating STB and EVT differentiation, respectively (Figure 3.12) (Guibourdenche et al., 2010).

More recently, our lab has developed a “two-step” method of trophoblast differentiation from hESC (Figure 3.13A). Instead of the traditional “one-step” method of treating with BMP4 every day in the continued presence of FCM, we first switch the

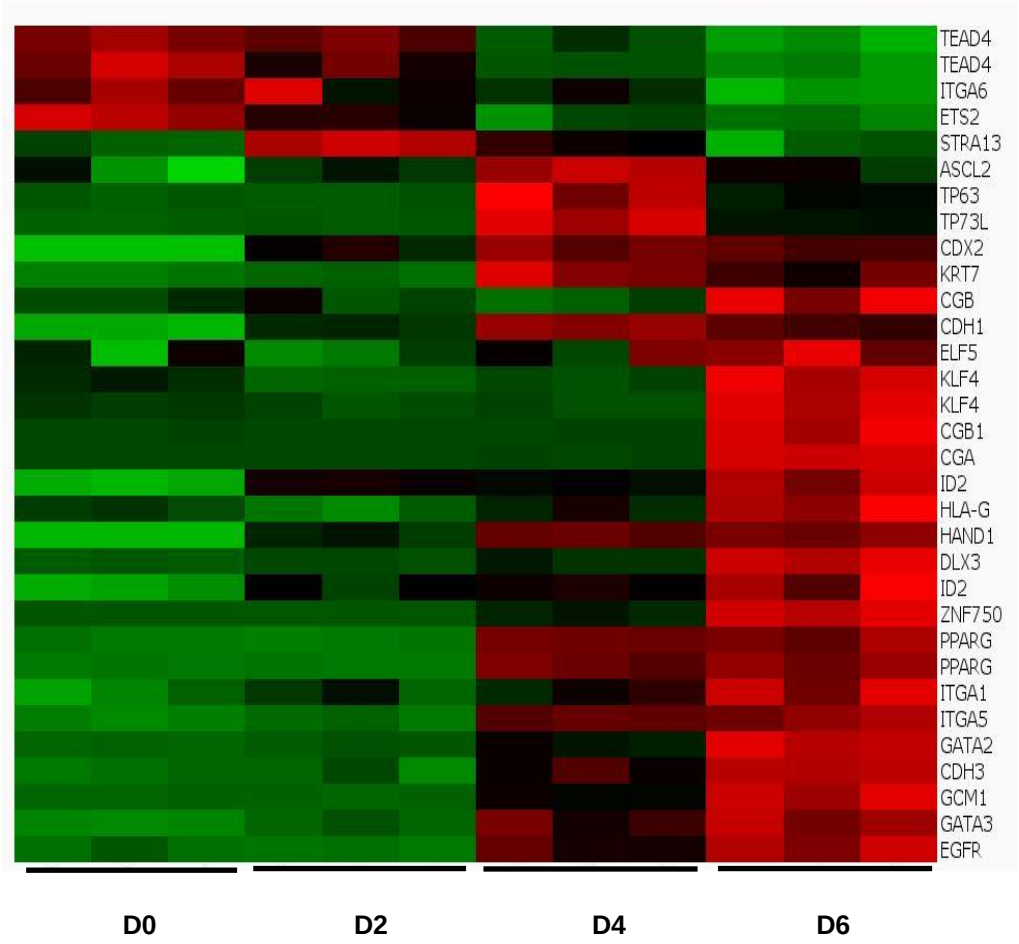

Figure 3.9. Expression patterns of known trophoblast-associated genes. Heatmap of human trophectoderm-specific transcription factor expression during hESC-derived trophoblast differentiation. Some genes are represented by multiple probes on the heatmap.

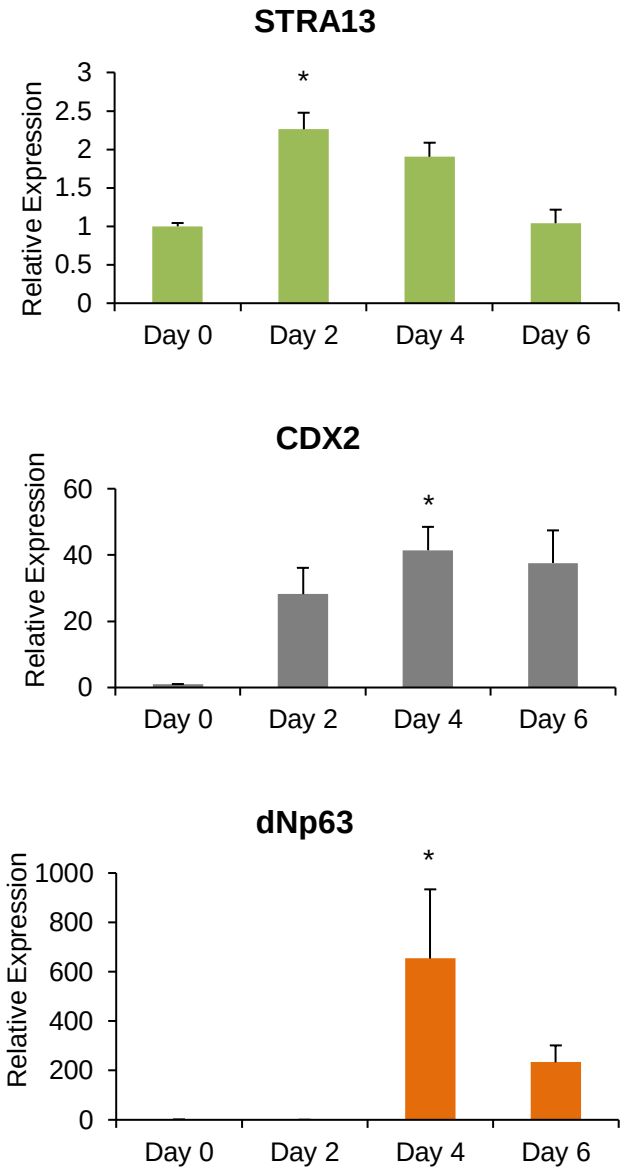

Figure 3.10. Expression of trophoblast progenitor-associated genes. qRT-PCR analysis of trophoblast progenitor-associated markers during one-step differentiation of BMP4-treated hESC. Values adjusted to undifferentiated state and normalized to 18S ribosomal RNA *p<0.05.

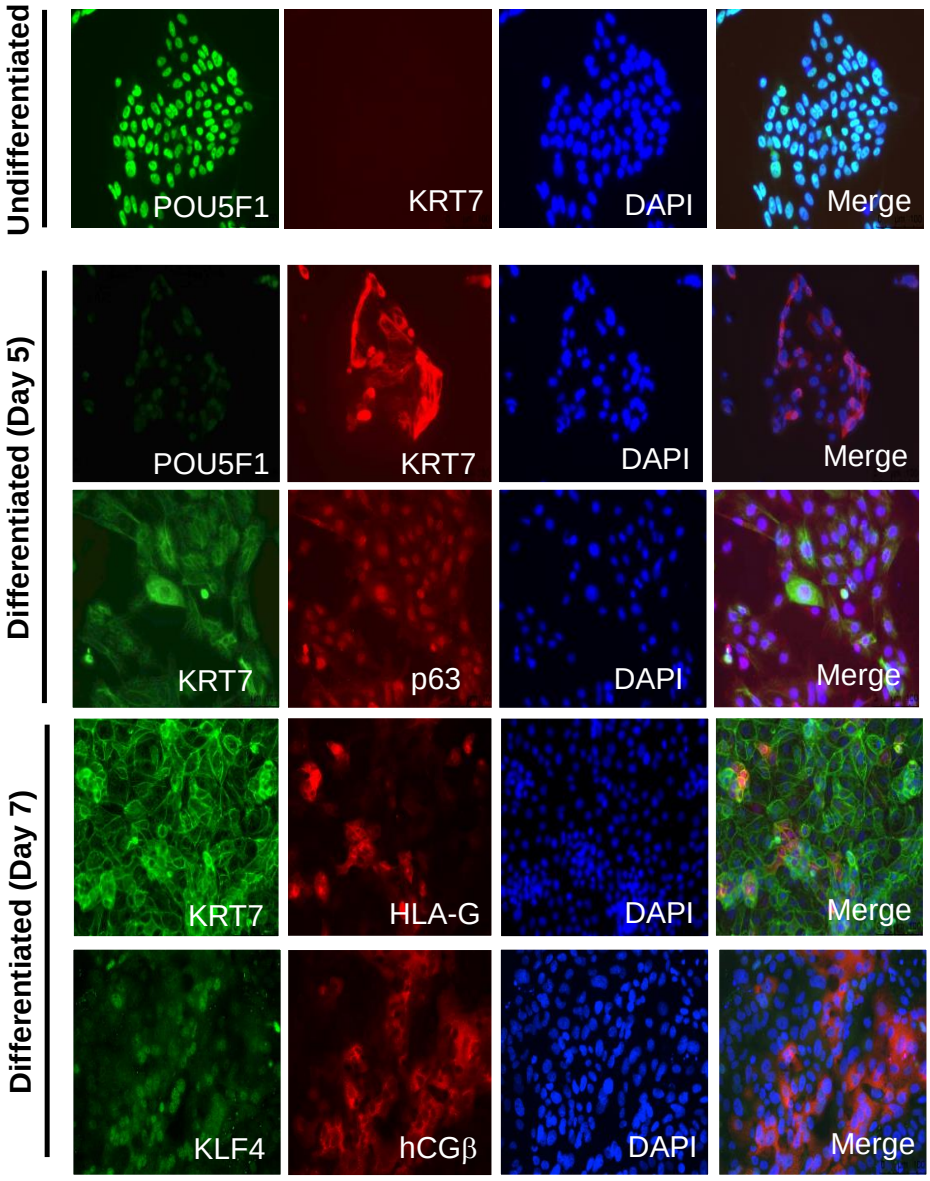

Figure 3.11. BMP4 treatment of hESC induces a trophoblast phenotype. Immunofluorescence staining of undifferentiated hESC and differentiated hESC-derived CTB at day 5 and 7. Staining shows a transition through a p63+/KRT7+ cytotrophoblast phenotype at day 5, prior to differentiating into HLA-G+/KRT7+ and KLF4+/hCGβ+ trophoblast, characteristic of EVT and STB, respectively.

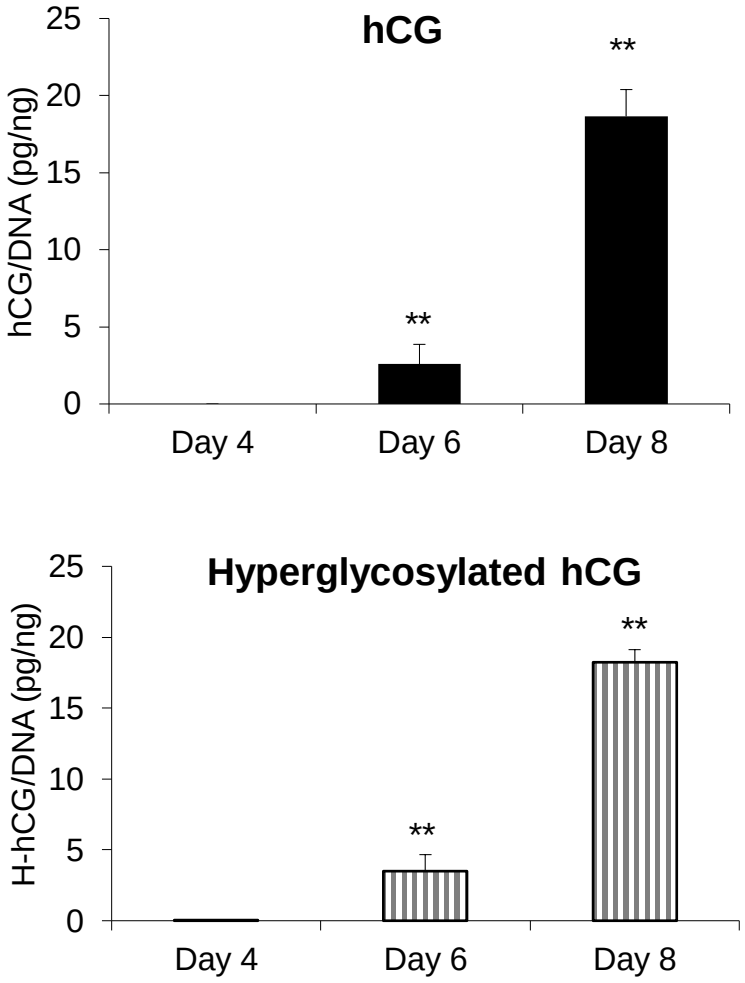

Figure 3.12. BMP4 treatment in hESC-derived CTB induces hCG and hyperglycosylated hCG secretion.
FCM-BMP4-treated hESC secrete hCGβ, including a hyperglycosylated form, which is unique to EVT. Data are normalized to DNA content and are expressed as mean ± s.d. of triplicate samples. **p<0.01.

pluripotent hESC to minimal media for two days, in order to remove any lingering effects of culture in growth factor-rich StemPro media. We then start BMP4 treatment still in the presence of the minimal media for 3-4 days and obtain a pure population of CTB cells, which is confirmed by EGFR expression by flow cytometry (Figure 3.13C). These hESC-derived CTB can be replated, and when switched to media containing FCM plus BMP4, they further differentiate into STB and EVT. The transition from pluripotent hESC colonies to epithelial-like CTB and differentiated trophoblast can be seen morphologically (Figure 3.13B). This two-step method enables efficient and uniform CTB induction of hESC upon BMP4 treatment, allowing the ability to keep the cells in the CTB progenitor stage longer than in the one-step method, where the FCM causes the cells to rapidly and stochastically terminally differentiate. Markers of CTB, including *CDX2*, *TP63* and *PPARG*, increase between days 1 through 4 (Figure 3.14). Surface expression of CTB marker EGFR is co-expressed with KRT7 at day 4 (Figure 3.14B). Only when cells are switched from minimal media to FCM plus BMP4 do the cells further differentiate into both EVT and STB, as seen by HLA-G expression on the surface of EVT (Figure 3.15A) and by secretion of hCG by STB (Figure 3.15B).

Chapter 3, in part, contains material that appears in Development 2013. Li Yingchun, Moretto-Zita Matteo, Soncin Francesca, Wakeland Anna, Wolfe Lynlee, Leon-Garcia Sandra, Pandian Raj, Pizzo Donald, Cui Li, Nazor Kristopher, Loring Jeanne F, Crum Christopher P., Laurent Louise C., Parast Mana M. The Company of Biologists Ltd. 2014. The dissertation author was co-investigator and co-second author of this paper.

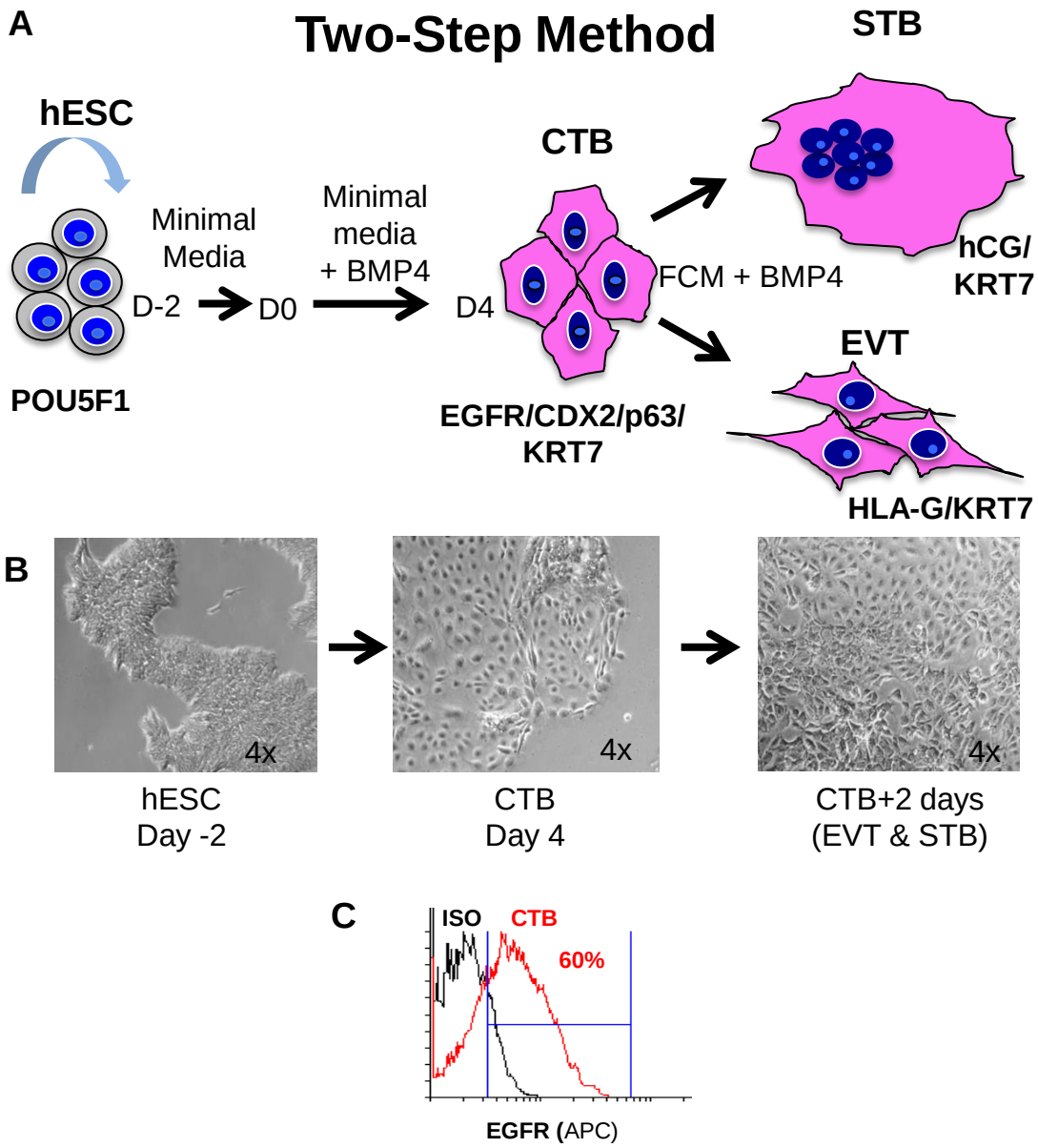

Figure 3.13. New two-step method of BMP4-induced trophoblast differentiation of hESC.
(A) Undifferentiated hESCs are switched to minimal media for two days to remove lingering growth factor supplement effects. BMP4 (10 ng/ml) is added for 3-4 days as the cells undergo a p63/KRT7/CDX2 triple-positive CTB "stem cell" state prior to switching to FCM+BMP4 to obtain terminal differentiation into HLA-G positive EVT and hCG positive STB. **(B)** hESC undergo morphologic changes during trophoblast lineage specification and differentiation. **(C)** CTB population at day 4 is analyzed by flow cytometry for surface EGFR expression.

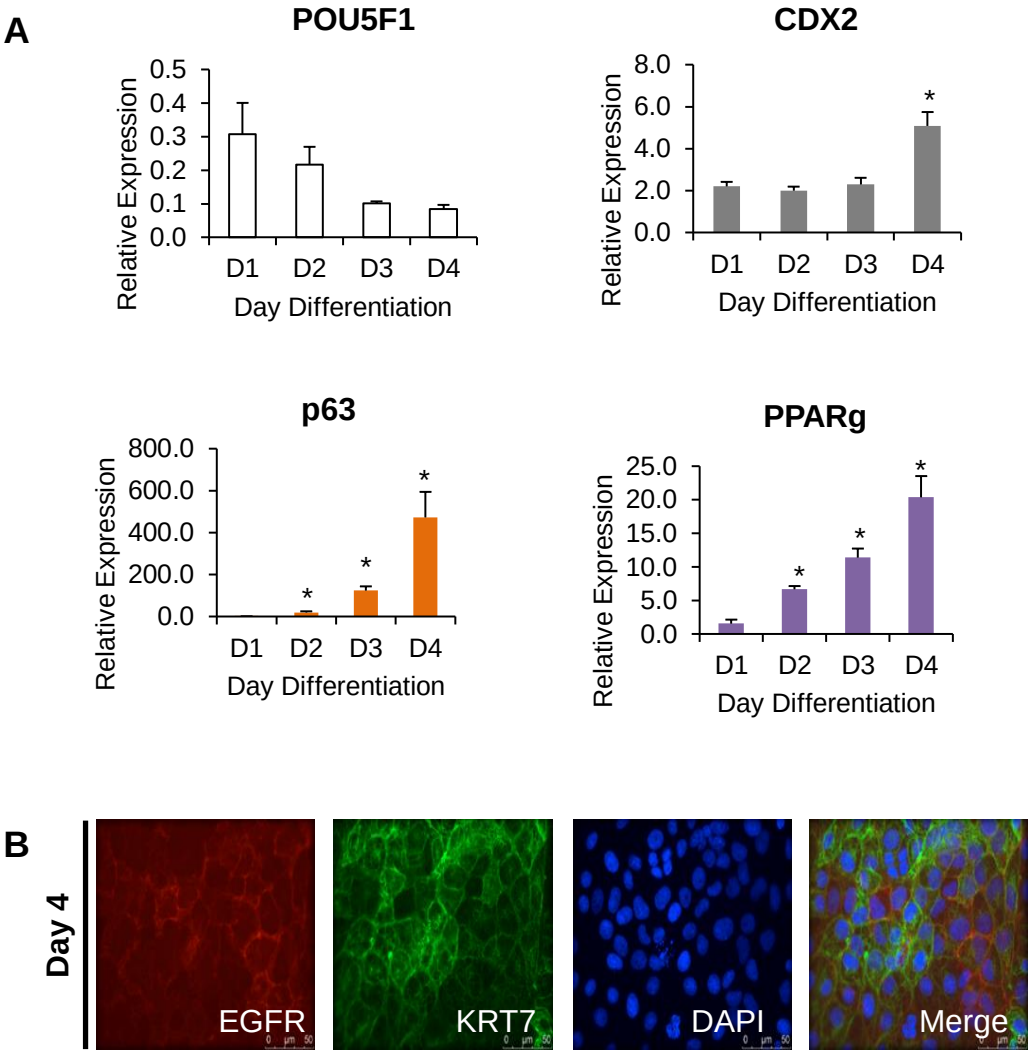

Figure 3.14. CTB differentiation in the first step of the Two-Step Method. **(A)** qRT-PCR analysis of CTB markers during the first four days of CTB differentiation of BMP4-treated hESC. **(B)** Surface expression of CTB marker EGFR is co-expressed with KRT7 at day 4. Values adjusted to undifferentiated hESC at day 0 and normalized to 18S ribosomal RNA *p<0.05.

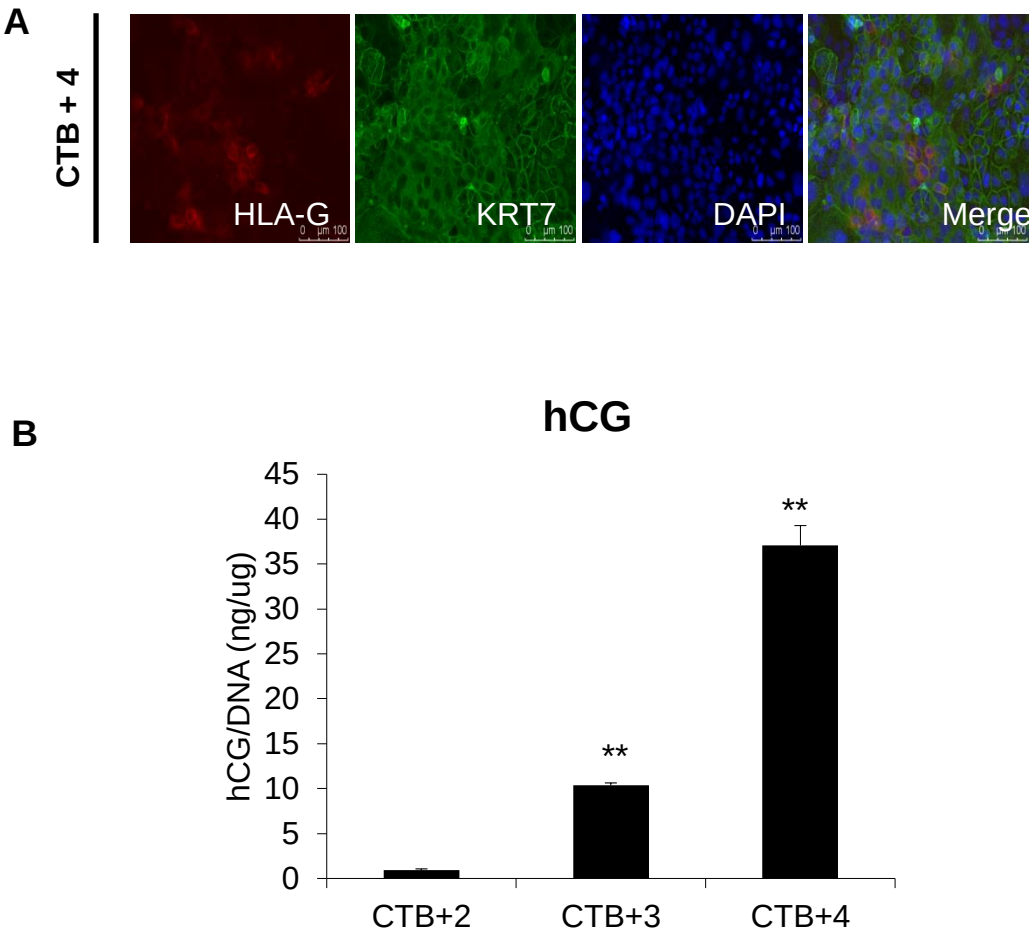

Figure 3.15. Terminal trophoblast differentiation in the second step of the Two-Step Method.

(A) Surface expression of EVT marker HLA-G is co-expressed with KRT7 at day 4 post-replating of CTB. **(B)** hCG secretion during differentiation at 2, 3 and 4 days after replating CTB in FCM+BMP4 was measured by ELISA. Data are normalized to DNA content and are expressed as mean ± s.d. of triplicate samples. **p<0.01.

Chapter 4

The role of hypoxia in trophoblast lineage specification and differentiation

4.1 Introduction

The role of hypoxia has been studied in various trophoblast models. In human embryonic stem cell (hESC)-derived trophoblast, hypoxia has been shown to inhibit hCG hormone production, indicating that it may inhibit terminal differentiation of these cells into syncytiotrophoblast (STB) (Das et al., 2007). In a classic study using human placental explants, hypoxia was found to inhibit trophoblast differentiation and instead promote proliferation of cytotrophoblast. In more recent years, rodent models have been used to find that hypoxia promotes differentiation into invasive trophoblast. These conflicting results prompted me to further investigate the role of hypoxia signaling, both in the context of BMP4-induced trophoblast lineage specification and during trophoblast differentiation, particularly into extravillous trophoblast (EVT).

4.2 Establishing culture conditions for hypoxic culture

In order to culture trophoblast in hypoxia, I used a hypoxia chamber to maintain cells in continuous culture, change media and collect timepoints at steady oxygen levels, without the need for re-oxygenation. In order to determine optimal conditions of hypoxia, I measured hCG secretion in normoxia (20% O_2) and at a range of oxygen tensions, including 8%, 5% and 2% O_2 (Figure 4.1). Levels of hCG at 8% O_2 were similar to levels secreted in normoxia. At 5% and 2% O_2, hCG levels were further reduced, with the lowest levels of hCG correlating to the lowest oxygen levels. Based on this experiment, as well as published oxygen concentrations in the uterus during implantation and early placentation, I proceeded with my experiments using 20% O_2 for normoxia, 5% O_2 as physiologic hypoxia during trophoblast lineage specification and 2% O_2 as physiologic hypoxia during early placentation for the following

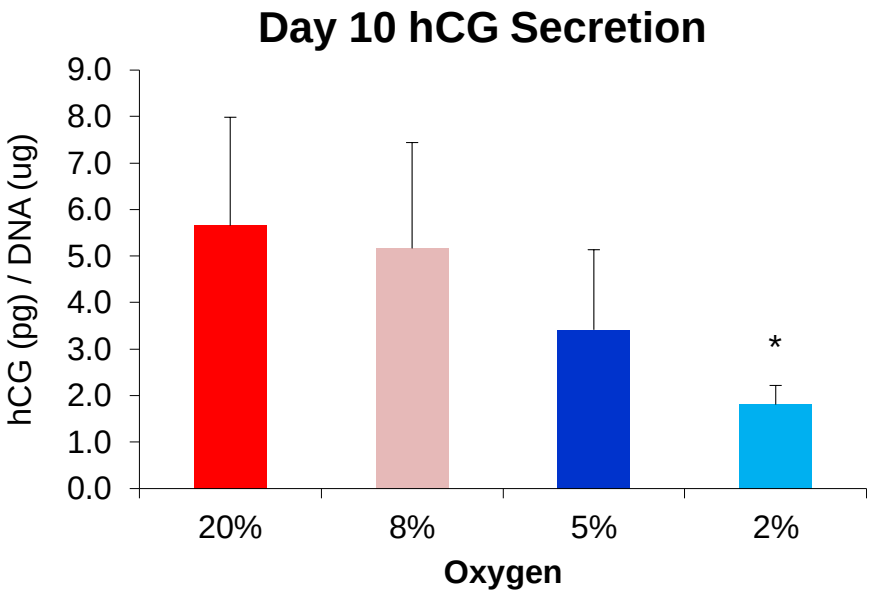

Figure 4.1. Effect of decreasing oxygen levels on hCG secretion.
hCG secretion of hESC-derived CTB at 20% (normoxia), 8%, 5% and 2% O_2 was measured by ELISA. Data are normalized to DNA content and are expressed as mean ± s.d. of triplicate samples. *p<0.05.

experiments using trophoblast cell lines, isolated primary CTB and hESC-derived trophoblast.

4.3 Using trophoblast cell lines to determine hypoxic effect on trophoblast differentiation

I wanted to determine if two human trophoblast cell lines, HTR-8 and JEG3, could be used to study the effect of hypoxia on trophoblast differentiation. HTR-8 cells are immortalized from first trimester trophoblast using simian virus 40 large T antigen and differentiate only into extravillous lineage (Graham et al., 1993). JEG3 cells are a choriocarcinoma cell line and can differentiate into both EVT and STB. In order to utilize these cells to address the effect of hypoxia on human trophoblast differentiation, I first needed to assess if these trophoblast cell lines respond to hypoxia by changing their differentiation status. I used qRT-PCR to look at EVT marker expression during differentiation of HTR-8. I saw significantly increased expression of *HLA-G* but not *ITGA1* (Figure 4.2). I next checked the hypoxia response of the JEG3 cells our lab obtained from Dr. Dongbao Chen (Reproductive Medicine, UCLA) and found that there was no significant expression of *HLA-G* and *ITGA1* in hypoxia compared to normoxia (Figure 4.3A).

In addition, when I assessed surface HLA-G expression by flow cytometry in hypoxia, the cells were completely negative, which is the opposite of previously-published reports (Figure 4.3B). I obtained new JEG3 cells from ATCC and checked for hypoxia response. The new JEG3 cells expressed surface HLA-G, and had higher expression in hypoxia compared to normoxia (Figure 4.3C). JEG3 cells secreted hCG as expected, and hCG levels were significantly reduced in hypoxia, another previously-documented response (Figure 4.3D). However, neither the HTR-8 or JEG3

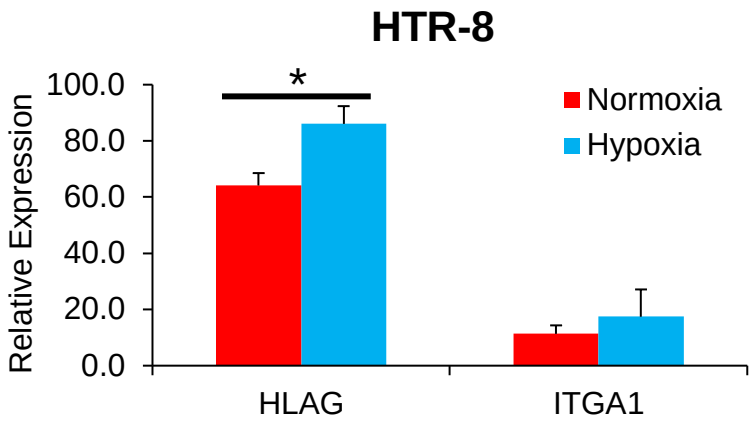

Figure 4.2. Expression of EVT markers in the trophoblast cell line HTR-8. qRT-PCR analysis of expression of EVT markers HLA-G and ITGA1 at day 2 differentiation in normoxia or hypoxia (2% O_2). Values normalized to 18S ribosomal RNA *p<0.05.

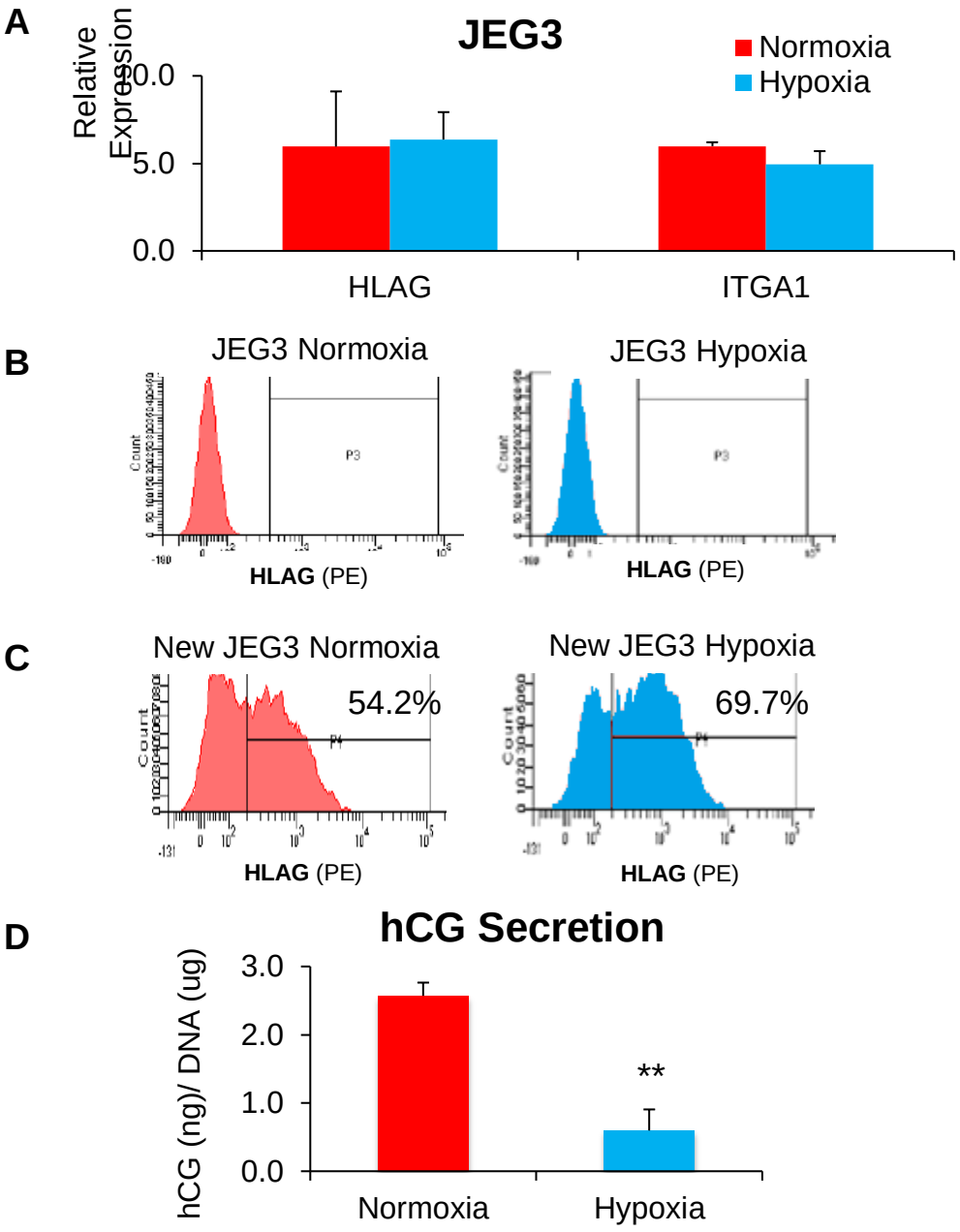

Figure 4.3. Expression of EVT markers in the choriocarcinoma cell line JEG3.

(A) qRT-PCR analysis of EVT markers HLA-G and ITGA1 at day 3 differentiation in normoxia or hypoxia (2% O_2). Values normalized to 18S ribosomal RNA. **(B)** Flow cytometry for surface HLA-G expression on JEG3 cultured in normoxia or hypoxia. **(C)** Flow cytometry of new JEG3 from ATCC cultured in normoxia or hypoxia. **(D)** hCG secretion of JEG3 cultured in normoxia or hypoxia was measured by ELISA. Data are normalized to DNA content and are expressed as mean ± s.d. of triplicate samples. **p<0.01.

cells secreted matrix metalloproteinase 2 (MMP2), which is secreted by EVT to help the digest the uterine ECM and aid invasion. Based on these findings, I concluded that other than hCG secretion in JEG3, the two trophoblast cell lines did not show a major or consistent response to hypoxia, so I decided to next try primary isolated CTB for future experiments to better evaluate hypoxia and trophoblast differentiation.

4.4 Hypoxia increases differentiation of isolated cytotrophoblast into extravillous trophoblast

In addition to determining which oxygen levels to use for experiments, the plating conditions needed to be optimized for using primary CTB isolated from first trimester placentas. I conducted multiple experiments to determine the best seeding density (1.5x10^6 cells/mL), media (DMEM/F12, 10% fetal bovine serum, penicillin/streptomycin and gentamycin), timepoints to change media (day 1 after plating and day 3), and end timepoint for cell collection (day 4). I also assessed which extracellular matrix (ECM) to use in order to get optimal plating of the CTB. The cells plated best on Fibronectin and also plated well on Collagen IV (Figure 4.4). The cells did not plate well on Laminin, all floating by day 1. Next, I assessed trophoblast differentiation of first trimester CTB when plated in 20%, 5% or 2% O_2 on either Fibronectin or Collagen IV. I found similar results for both ECM; as oxygen levels decreased, the percentage of EGFR+/HLA-G+ cells increased (Figure 4.4). I also assessed MMP2 and found that as oxygen decreased from 20% to 5% to 2% O_2, the level of MMP2 secretion increased (Figure 4.5A). To determine how hypoxia affects differentiation into STB, I assessed hCG levels by ELISA, since hCG is secreted by STB specifically. I found that hCG secretion was highest in normoxia, and greatly

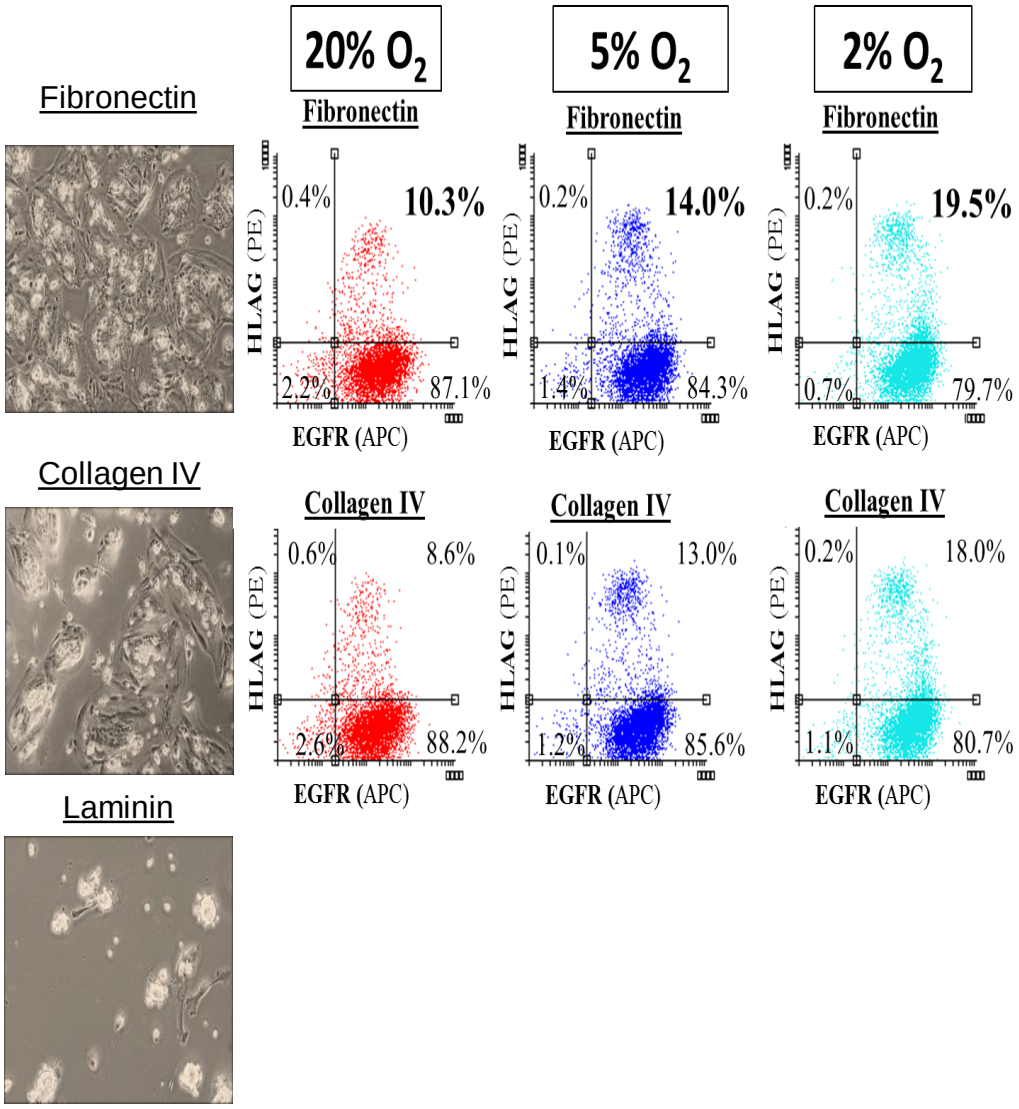

Figure 4.4. Extracellular matrix and low oxygen promote extravillous trophoblast differentiation of isolated primary CTB.
First trimester CTB were isolated (modified Kliman method) and plated on fibronectin, collagen IV or laminin (cells did not survive) and cultured under 20%, 5% or 2% oxygen for 4 days. CTB cultured on Fibronectin and Collagen IV were analyzed by flow cytometry for expression of EGFR (CTB marker) and HLA-G (EVT marker).

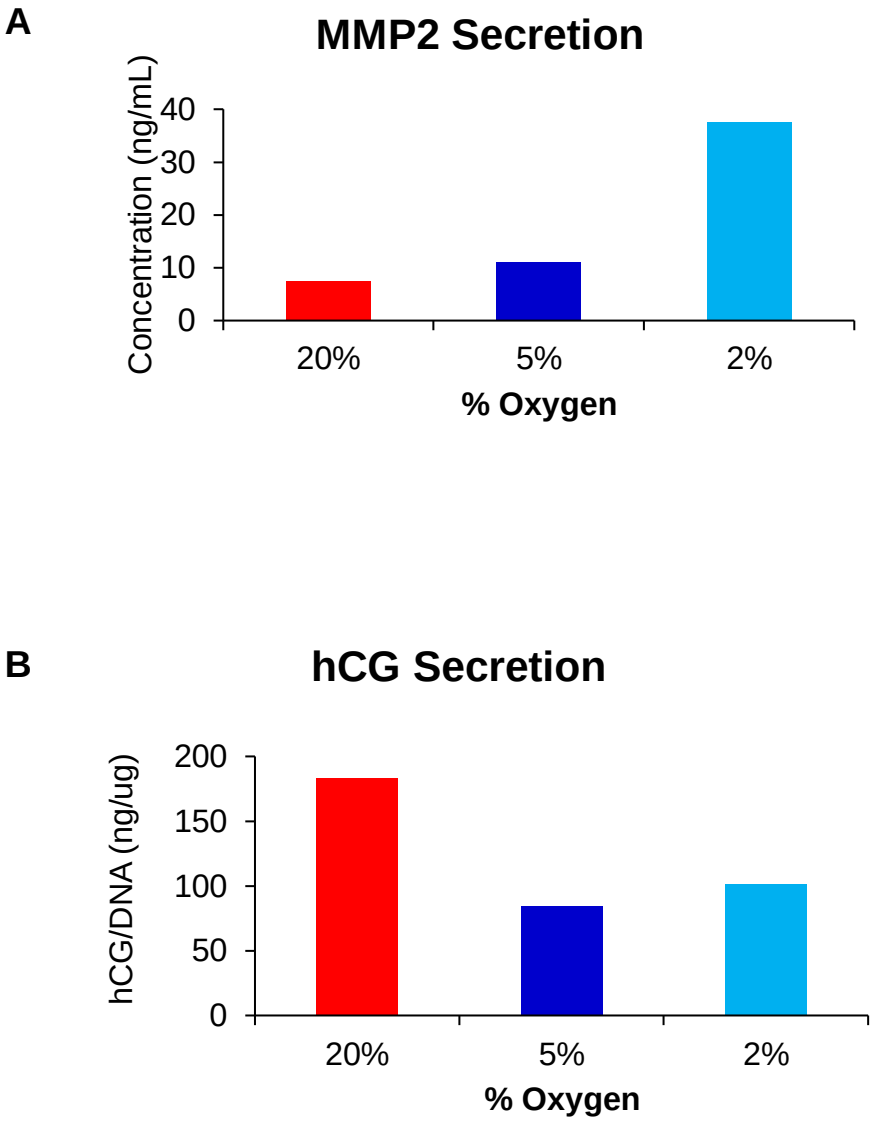

Figure 4.5. Effect of oxygen secretion of matrix metalloproteinase 2 (MMP2) and hCG by isolated primary CTB.
(A) MMP2 secretion at oxygen levels of 20%, 5% and 2% was measured by ELISA. MMP2 is secreted by EVT. **(B)** hCG secretion at oxygen levels of 20%, 5% and 2% was measured by ELISA . hCG is secreted by STB. n=1

decreased in both 5% and 2% O_2 (Figure 4.5B). After this initial experiment, I decided to proceed by using Fibronectin and 2% O_2 for the level of hypoxia.

Next I decided to further assess the effect of hypoxia on first trimester CTB differentiation. Using four different placentas, I assessed expression of EVT-specific markers. I found that, in conditions of hypoxia, *HLA-G*, *ITGA1* and *TEAD2* all were significantly increased compared to normoxia (Figure 4.6A). Surface expression of HLA-G by flow cytometry showed a significant increase in EVT differentiation compared to normoxia (Figure 4.6B). Additionally, MMP2 secretion was higher in hypoxia compared to normoxia (Figure 4.6C). Conversely, hCG secretion was significantly and drastically reduced in hypoxia compared to normoxia (Figure 4.6D).

4.5 Gene expression profiling of isolated CTB

Subsequently, I decided to look at global gene expression patterns of isolated CTB in conditions of hypoxia compared to normoxia. I subjected freshly isolated CTB (Day 0), along with cells that were plated for four days in normoxia or hypoxia (2% O_2), to microarray-based genome-wide gene expression profiling. Principal Component Analysis (PCA) showed that the cells clustered first based on whether they were freshly isolated or cultured *in vitro* (Figure 4.7). The second component showed the effect of oxygen on cultured cells. I next wanted to confirm whether trophoblast differentiation-associated gene expression was occurring in the correct patterns. Gene expression analysis of a list of known human trophoblast-associated genes showed CTB genes upregulated in day 0, including *CDX2*, *ELF5*, *TP63*, *ITGA6* and *ID2* (Figure 4.8). The analysis also showed that the trophoblast-associated genes that are upregulated in hypoxia are markers of EVT, including *HLA-G*, *ITGA1*, *TEAD2*

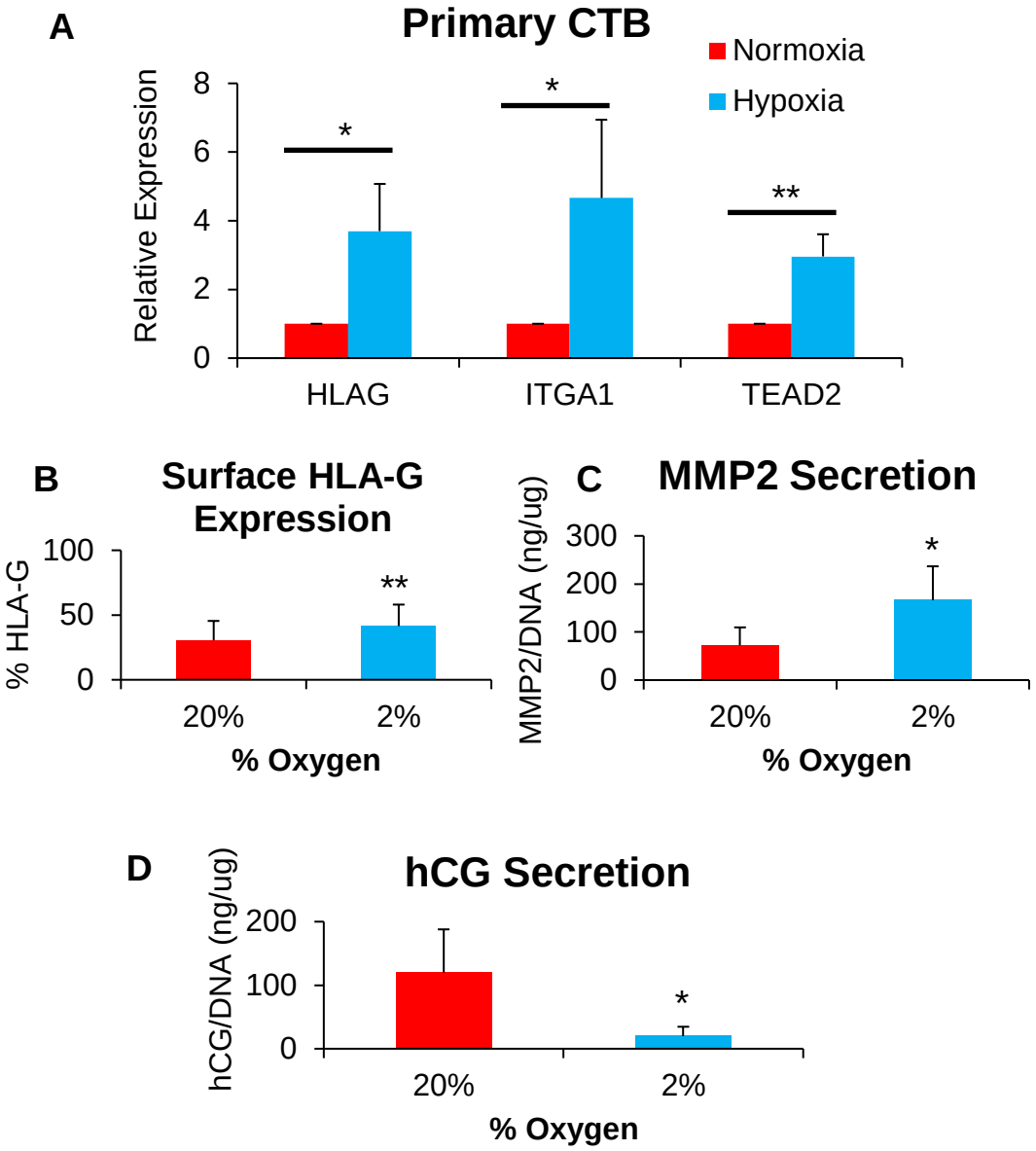

Figure 4.6. Hypoxia increases differentiation of primary CTB into EVT and decreases STB differentiation.
(A) qRT-PCR analysis of EVT markers HLA-G, ITGA1 and TEAD2 in primary CTB isolated from first trimester. Values adjusted to freshly isolated (day 0) and normalized to 18S ribosomal RNA **(B)** Surface HLA-G expression in normoxia and hypoxia measured by flow cytometry. **(C)** MMP2 secretion in normoxia and hypoxia measured by ELISA and normalized to DNA content. **(D)** Decreased hCG secretion in hypoxia compared to normoxia, measured by ELISA and normalized to DNA content . n=4 *p<0.05 **p<0.01.

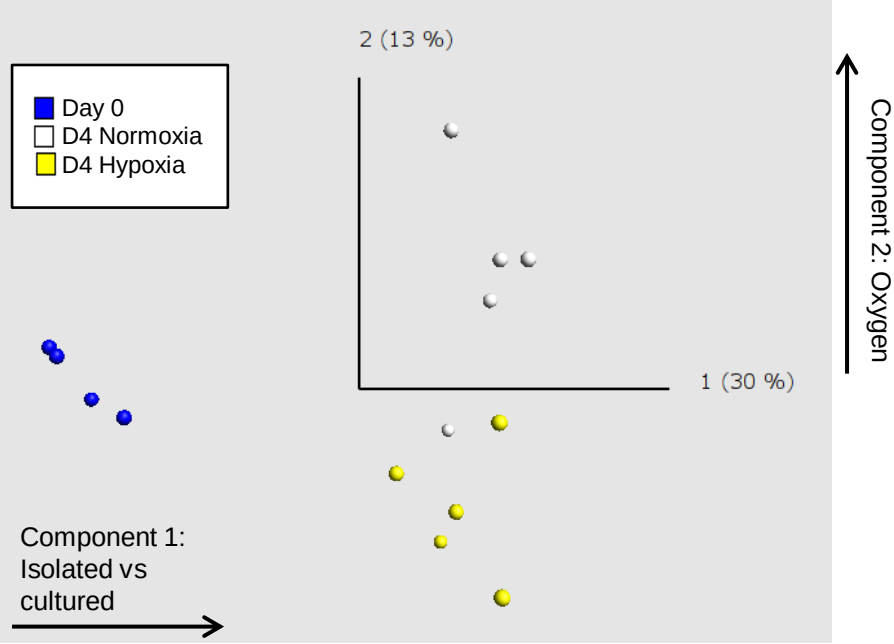

Figure 4.7. Principal Component Analysis (PCA) of primary CTB.
PCA shows that the first principal component (horizontal axis) distinctly separates primary CTB isolated from first trimester based on whether the samples were freshly isolated or cultured. The second principal component (vertical axis) accounts for the differences due to effect of oxygen (20% vs 2% O_2)

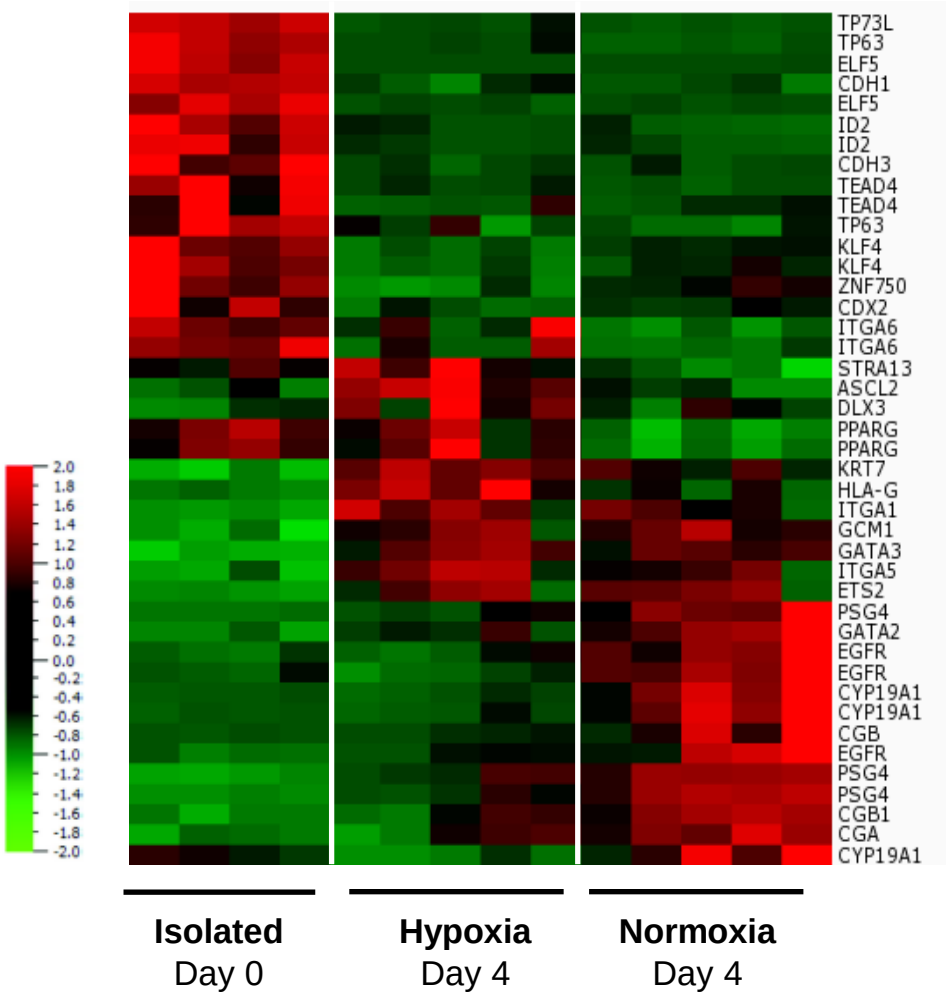

Figure 4.8. Heatmap of trophoblast-specific gene expression in primary CTB. Gene expression of primary CTB isolated from first trimester and cultured for 4 days in hypoxia (2% O_2) or normoxia. Only statistically significant gene probes were shown (ANOVA $q<0.05$) and subjected to hierarchical clustering. Some genes are represented by multiple probes on the heatmap.

and *ASCL2*. Markers of STB differentiation, such as *CGB* and *PSG4*, are upregulated only in normoxia and are reduced in conditions of hypoxia.

In order to identify important genes that are upregulated downstream of hypoxia, I looked at global expression of genes at day 0, and day 4 in hypoxia, and day 4 in normoxia. After filtering for variance of the probes and applying multi-group statistical analysis based on oxygen, hierarchical clustering showed a group of 825 probes that were specifically upregulated in hypoxia compared to normoxia (Figure 4.9). I took the list of probes, and after removing duplicates, subjected the list to gene ontology analysis using Metascape software in order to assess the types of genes upregulated in hypoxia (Figure 4.10A). I found enrichment of 10 groups of genes, including hypoxia, focal adhesion, and epithelial to mesenchymal transition. Next, I compared gene expression profiles of the isolated CTB (Day 0), Hypoxia (Day 4), and Normoxia (Day 4) samples to gene expression profiles of sorted CTB (EGFR single positive cells) and sorted EVT (HLA-G single positive cells) that were obtained by flow cytometry-assisted cell sorting (Figure 4.10B). I found that the samples in hypoxia shared the most genes with the sorted EVT, while the isolated CTB (day 0) shared the most genes with sorted CTB.

4.6 Hypoxia does not affect human trophoblast lineage specification

I next used hESC-derived trophoblast to assess what effect, if any, hypoxia has on trophoblast lineage specification. One unique use of this model (compared to primary isolated CTB) is the ability to study the early stages of induction of CTB from hESC. When I did a timecourse evaluating the first four days of trophoblast induction from hESC to CTB, I found EGFR started to be expressed on the surface of CTB at day 2 in normoxia, and reached peak levels (of greater than 60%) by day 4 (Figure

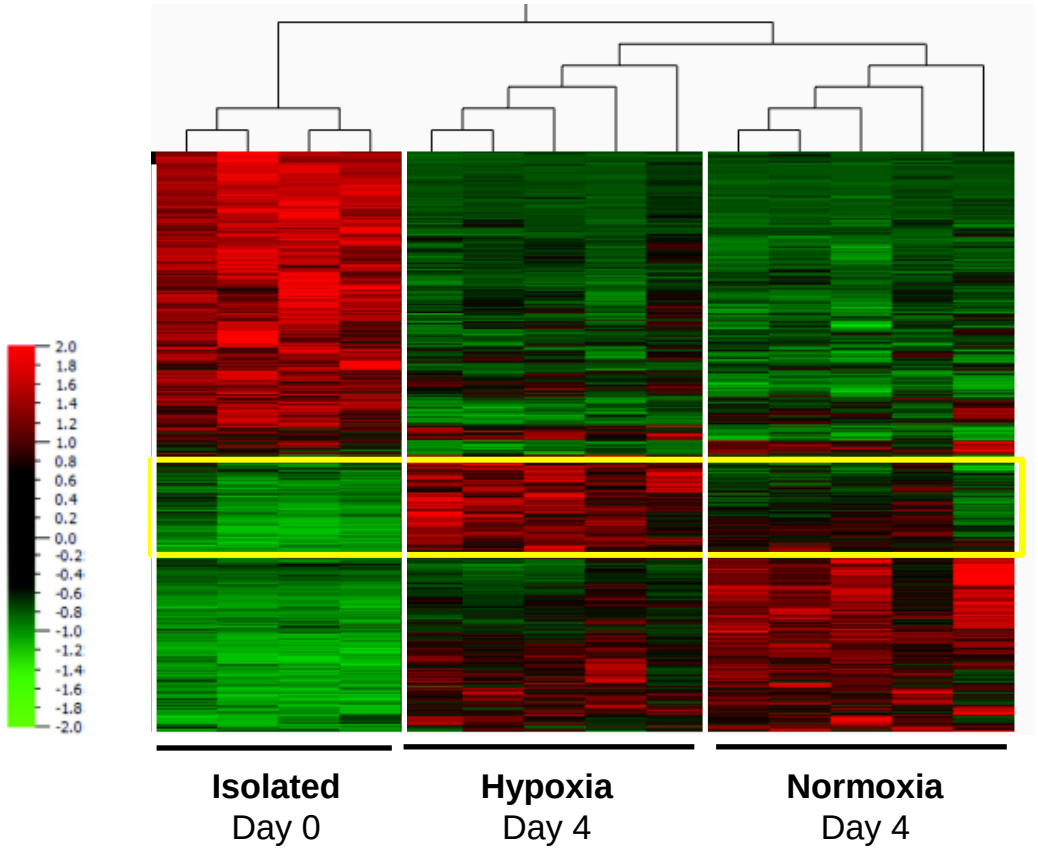

Figure 4.9. Heatmap of global gene expression in primary CTB. Genome-wide expression profile of primary CTB isolated from first trimester and cultured for 4 days in hypoxia (2% O_2) or normoxia. Samples and gene probes were subjected to hierarchical clustering and probes were filtered for variance (v=0.01). Only statistically significant gene probes were shown (ANOVA q<0.05). Highlighted cluster (yellow) indicates 825 gene probes that are upregulated in hypoxia compared to normoxia or day 0.

A

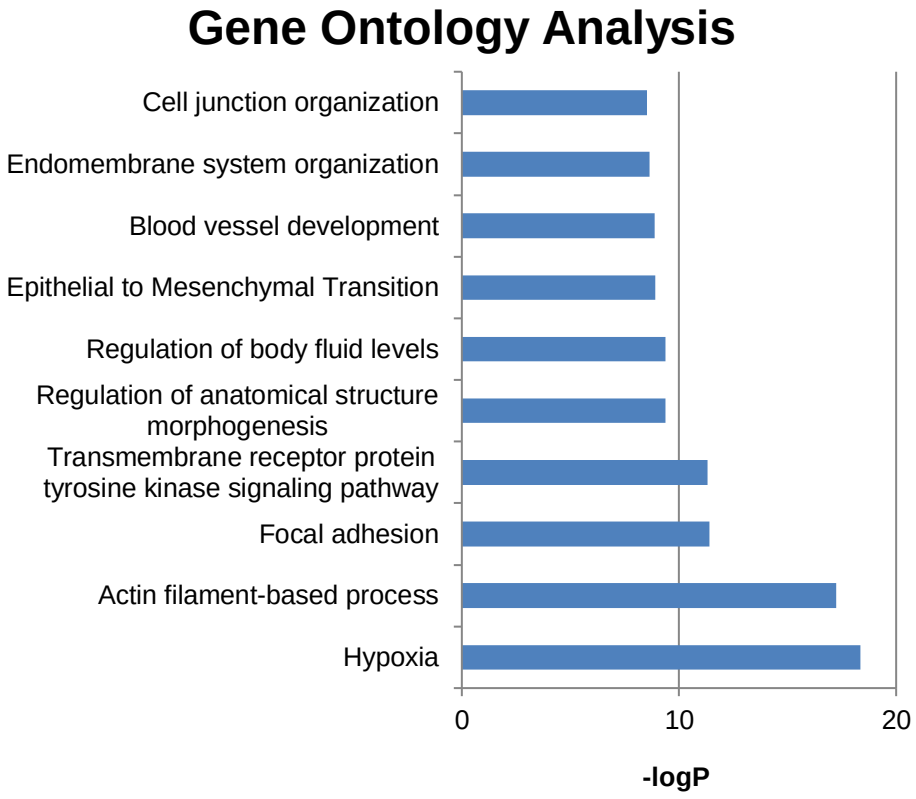

B

	Sorted CTB	Sorted EVT
Day 0	24%	0.7%
Normoxia	10%	16%
Hypoxia	1.3%	46%

Figure 4.10. Primary CTB cultured in hypoxia show EVT-like properties. **(A)** Gene ontology analysis of the 825 gene probes upregulated in hypoxia in primary CTB. Some of the enriched groups can be associated with EVT functions. **(B)** Comparison of statistically significant signature genes of isolated CTB (Day 0), Hypoxia CTB (Day 4), and Normoxia CTB (Day 4) to sorted CTB (EGFR single positive cells) and sorted EVT (HLA-G single positive cells) that were obtained by flow cytometry-assisted cell sorting.

4.11A). In hypoxia, there was no effect on trophoblast lineage specification, as the cells expressed the same levels of EGFR as cells in normoxia at each respective day. I assessed other CTB markers, including *CDX2* and *TP63* by qRT-PCR. The only significant difference was at day 2, when *TP63* had significantly higher expression in normoxia compared to hypoxia. Overall, however, hypoxia did not affect trophoblast lineage specification, either by promoting or delaying induction of CTB (Figure 4.11B).

4.7 Hypoxia increases differentiation of hESC-derived cytotrophoblast into extravillous trophoblast

I next asked what effect hypoxia has on terminal differentiation of hESC-derived CTB. Using the two-step method, I grew the cells to the CTB stage at day 4, and then split the cells using FCM+BMP4 into differing oxygen levels. I used flow cytometry to assess surface expression of EGFR, a marker of CTB, and HLA-G, a marker of EVT, looking specifically for the effect of oxygen on differentiation into EGFR+/HLA-G+ population of cells which represent EVT differentiation in vitro. I found that in normoxia (20% and 8% O_2), only 5% of cells differentiated into EVT. Hypoxia greatly increased the amount of EVT differentiation, as seen by an increase to ~14% EVT cells in hypoxia (2% O_2) (Figure 4.12A). This result was seen at each day of differentiation post-CTB stage, with hypoxia consistently resulting in the highest differentiation into EVT (Figure 4.12B). I also found that hypoxia significantly increased secretion of MMP2, a hallmark of EVT invasive function, and significantly decreased secretion of hCG, a hallmark of STB function (Figure 4.13A and B).

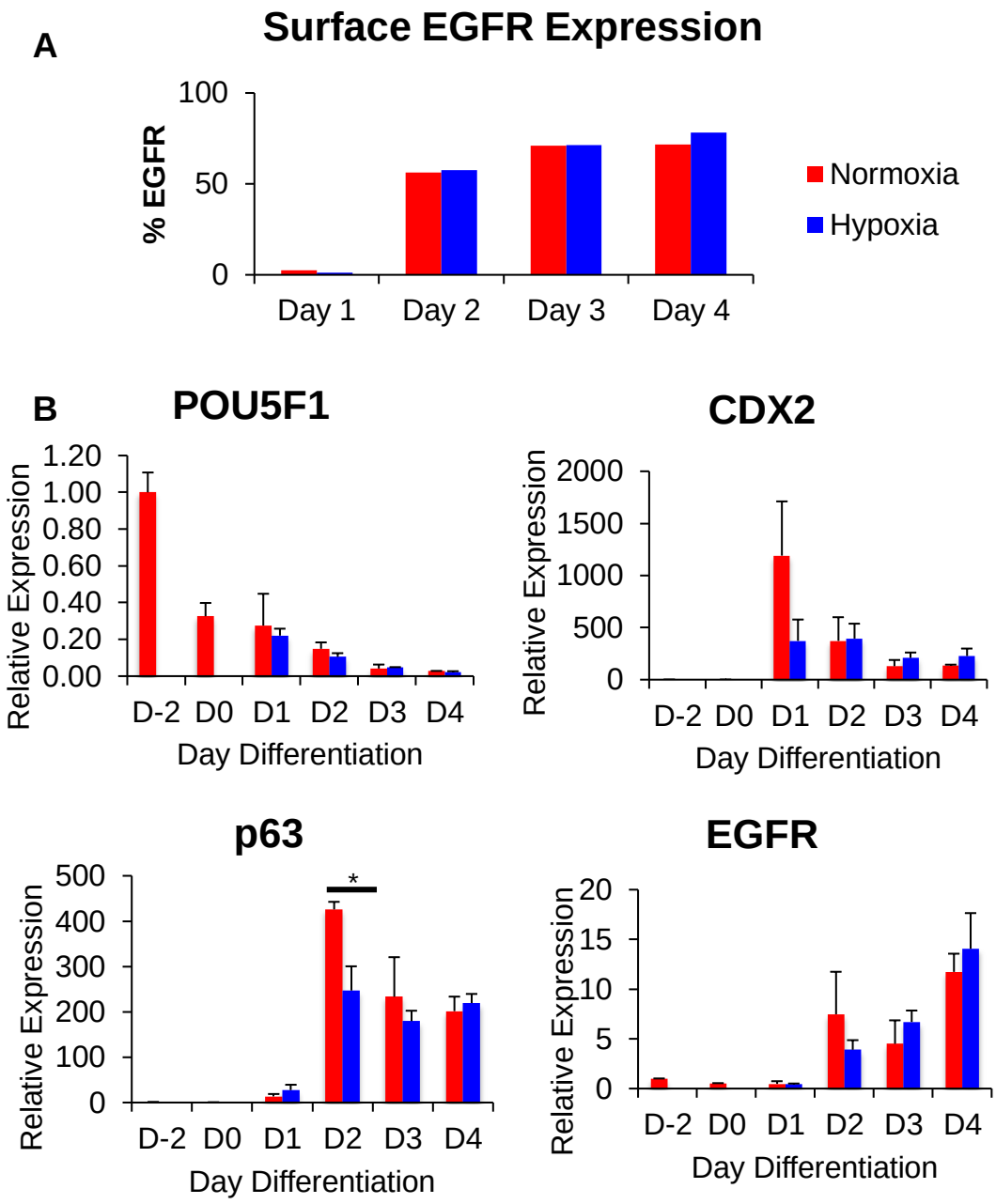

Figure 4.11. Hypoxia does not affect human trophoblast lineage specification of hESC-derived CTB.
(A) Surface EGFR at days 1, 2, 3 and 4 measured by flow cytometry. **(B)** qRT-PCR analysis of pluripotency marker POU5F1 and CTB markers CDX2, p63 and EGFR. The only significant difference between hypoxia (5% O_2) and normoxia was p63 at D2. $p<0.05$

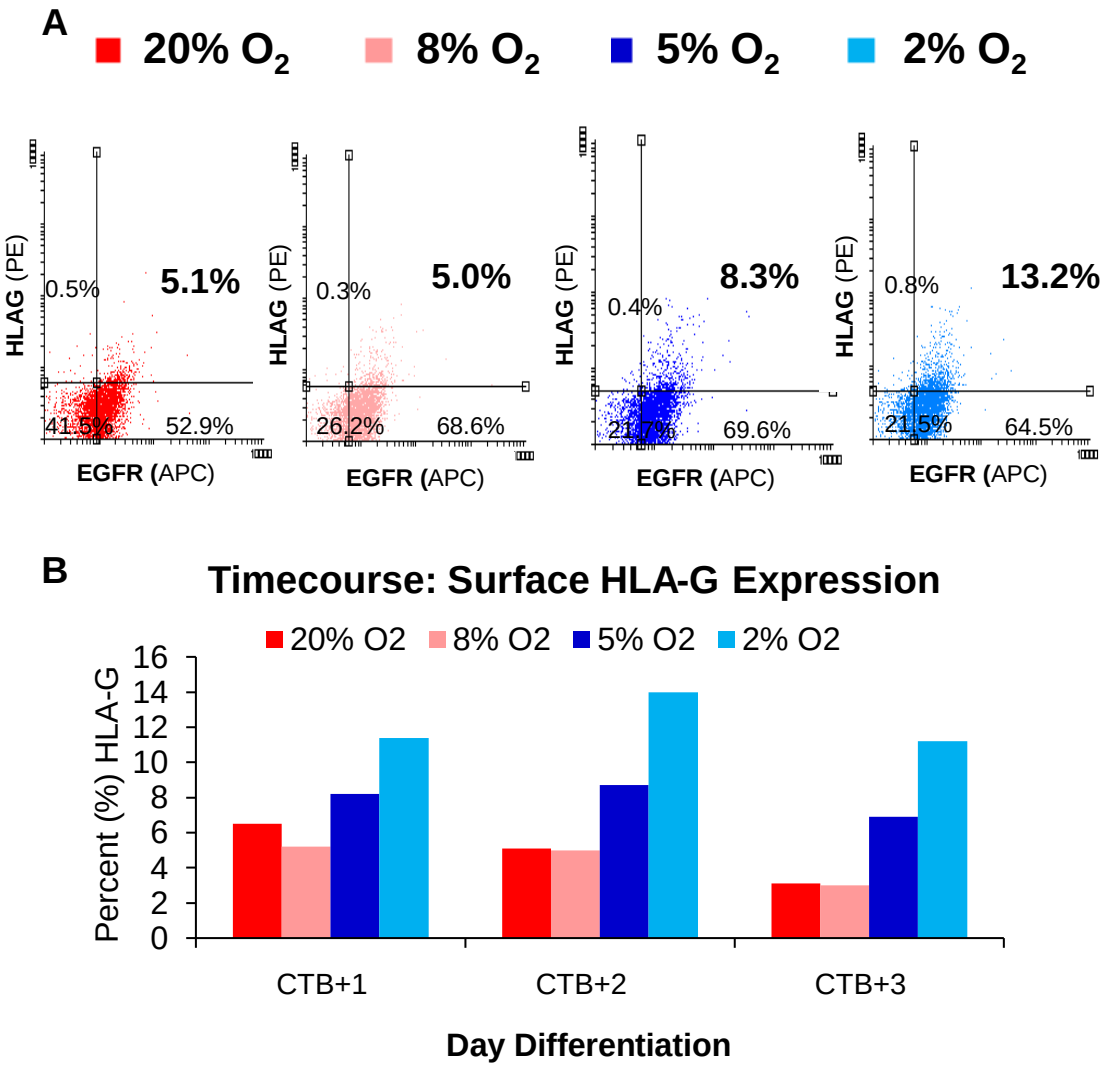

Figure 4.12. Increased EVT differentiation of hESC-derived trophoblast cultured in differing oxygen levels.
(A) Trophoblast derived from BMP4-treated hESC differentiated under different oxygen levels at 2 days post-CTB stage were assessed for surface HLA-G and EGFR by flow cytometry **(B)** Summary of flow cytometry (% HLA-G) for additional timepoints of differentiation at 1, 2, and 3 days post-CTB stage.

A

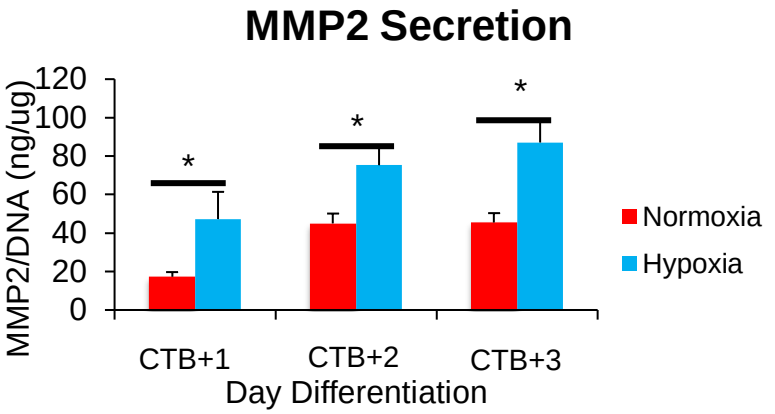

B

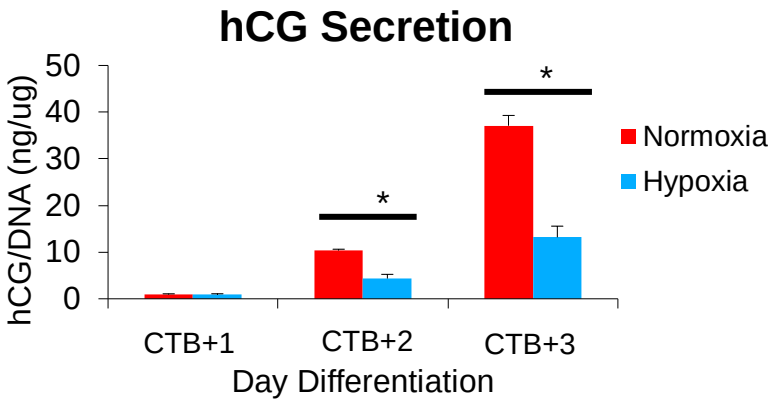

Figure 4.13. Hypoxia increases differentiation of hESC-derived CTB into EVT and decreases STB differentiation.
(A) MMP2 secretion in normoxia and hypoxia (2% O_2) measured by ELISA and normalized to DNA content. **(B)** Decreased hCG secretion in hypoxia compared to normoxia, measured by ELISA and normalized to DNA content . *p<0.05

4.8 Gene expression profiling of hESC-derived trophoblast in normoxia and hypoxia

I first subjected a timecourse of trophoblast differentiated using the traditional one-step method to microarray-based genome-wide gene expression profiling. I first viewed my data without statistics in a Principal Component Analysis (PCA) to look for unbiased patterns in my samples. PCA demonstrated that the samples very clearly separate primarily by differentiation, and secondarily by either hypoxia or normoxia (Figure 4.14). I next wanted to determine what effect hypoxia had on known trophoblast-associated markers. Multi-group comparison showed significantly (q=0.01) differentially expressed markers at each timepoint, with clear patterns of genes that are highly upregulated in either hypoxia or normoxia (Figure 4.15). Genes that were higher in normoxia compared to hypoxia at day 6 included genes associated with syncytiotrophoblast differentiation, such as *CGA*, *CGB*, *ERVFWD-1*, *ERVW-1* (genes important for syncytialization), *GCM1*, *GATA2* and *PSG4*. However, genes associated with extravillous differentiation, such as *HLA-G* and *ITGA1*, were higher in hypoxia. Interestingly, some genes that are associated with CTB were higher in hypoxia, such as *CDX2* and *CDH1*. However, some CTB-associated genes like *TFEB*, *TP63* and *ELF5* were higher in normoxia, not hypoxia. *TP63* was confirmed to be significantly higher in normoxia by the previous qRT-PCR (Figure 4.11B). Also of note, *PPARG*, *ASCL2* and *ITGA5*, which are associated with EVT differentiation, and *HAND1*, which in mice plays a role in mouse TGC differentiation (Hemberger et al., 2004), were all higher in hypoxia.

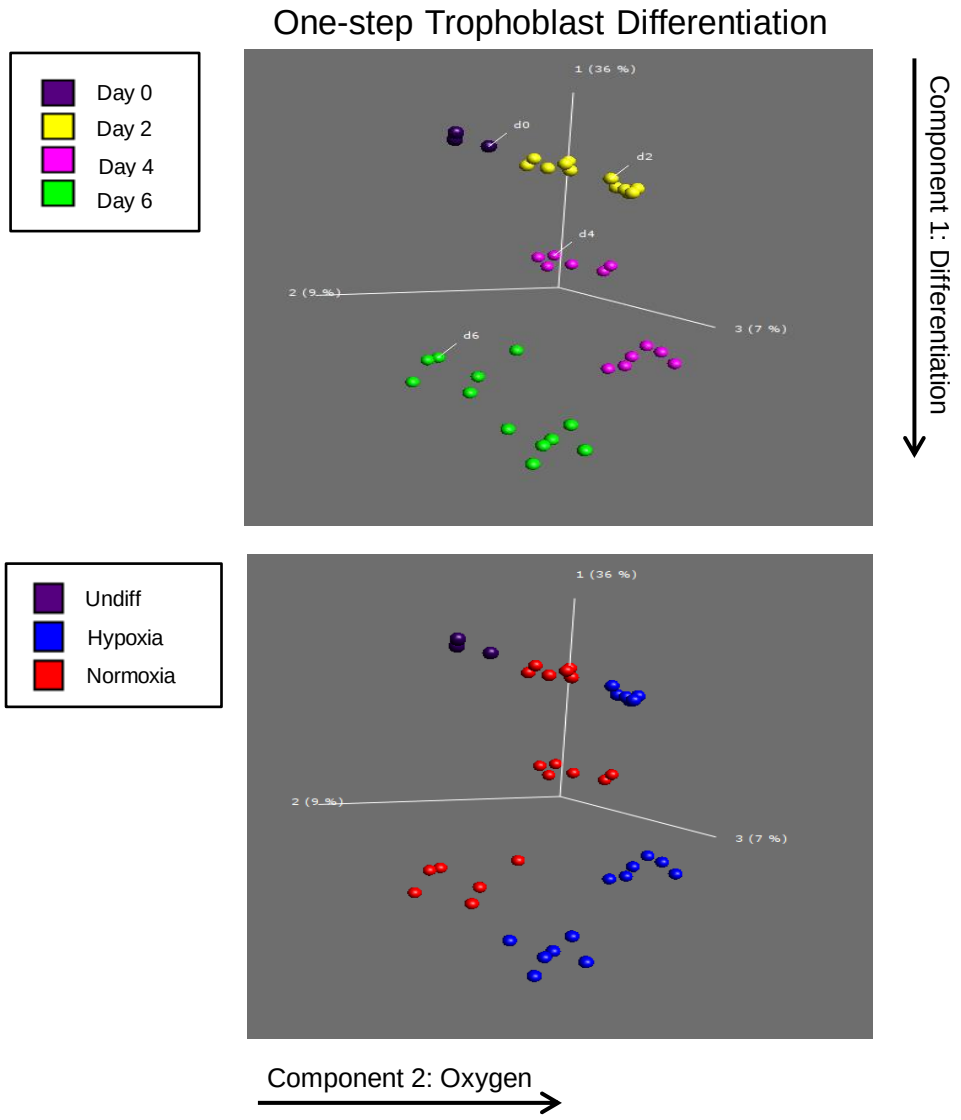

Figure 4.14. Principal Component Analysis (PCA) of hESC-derived trophoblast using the one-step method.
PCA shows that the first principal component (horizontal axis) distinctly separates hESC-derived CTB based on differentiation. The second principal component (vertical axis) accounts for the differences due to effect of oxygen (20% vs 2% O_2).

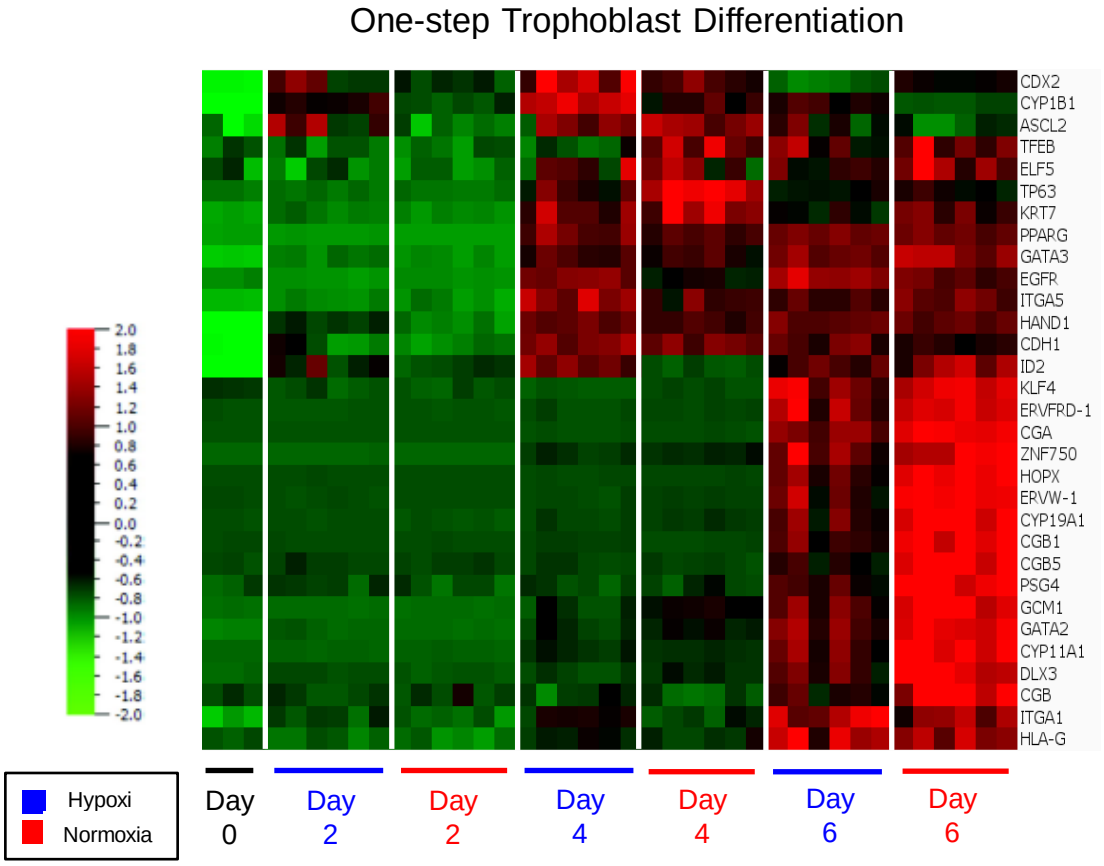

Figure 4.15. Heatmap of trophoblast-specific gene expression in hESC-derived CTB using the one-step method of differentiation.
Gene expression of hESC-derived CTB differentiated using the one-step method and cultured for 2, 4 or 6 days in hypoxia (2% O_2) or normoxia. Only statistically significant gene probes were shown (ANOVA $q<0.01$) and subjected to hierarchical clustering. Some genes are represented by multiple probes on the heatmap.

In order to learn more about what genes are upregulated in hypoxia during increased EVT differentiation, I performed trophoblast differentiation using the two-step method, with trophoblast in the second step cultured under conditions of either normoxia or hypoxia. I subjected selected samples (CTB, CTB+2 days in normoxia or CTB+2 days in hypoxia) to microarray-based genome-wide gene expression profiling. PCA again showed that the cells clustered first based on differentiation, and second based on culture in different levels of oxygen (Figure 4.16). I then confirmed expression of known trophoblast-associated genes. CTB-associated genes, including *CDX2*, *TP63*, *ELF5* and *TEAD4*, were significantly upregulated in CTB and were downregulated during terminal differentiation (Figure 4.17). The analysis also showed that hypoxia upregulated expression of EVT-associated genes, including *HLA-G*, *ITGA1*, and *ASCL2*. Differentiation in normoxia led to higher expression of *PSG4*, but *CGB* expression was only slightly higher than in hypoxia.

Next, I assessed which genes are upregulated downstream of hypoxia. I looked at global expression of genes in CTB, or CTB+2 in hypoxia or normoxia. After filtering for variance and applying multi-group statistical analysis based on oxygen tension, hierarchical clustering showed a group of 429 probes that were specifically upregulated in hypoxia compared to normoxia (Figure 4.18). In order to assess what types of genes are upregulated in hypoxia, I subjected the list of probes to gene ontology analysis using Metascape software (Figure 4.19). I found enrichment of 10 groups of genes, which included hypoxia, epithelial to mesenchymal transition, positive regulation of insulin secretion, and insulin signaling.

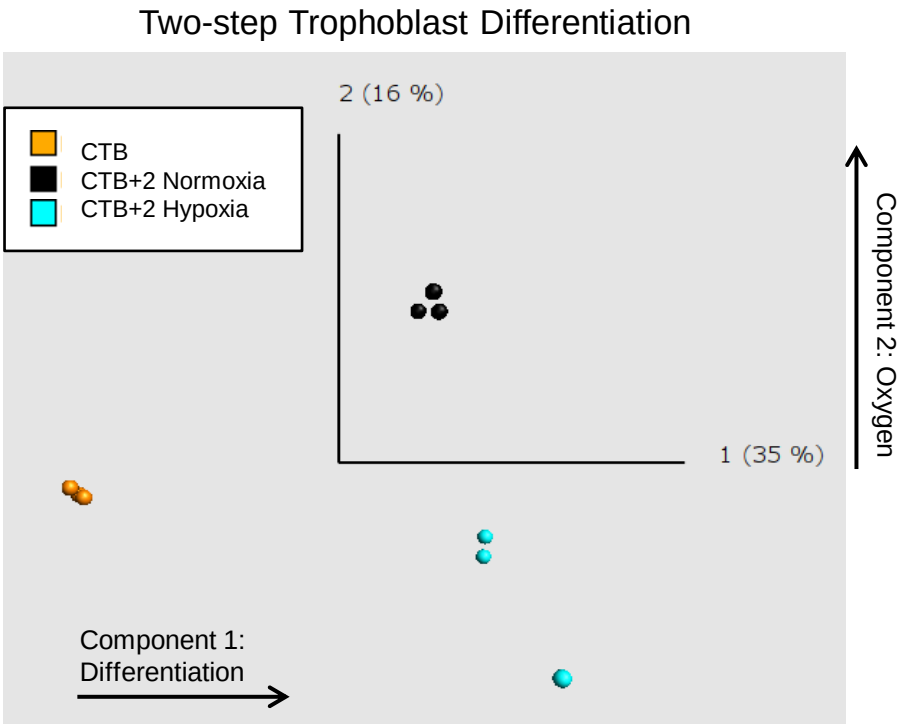

Figure 4.16. Principal Component Analysis (PCA) of hESC-derived trophoblast using the two-step method.
PCA shows that the first principal component (horizontal axis) distinctly separates hESC-derived CTB based on differentiation. The second principal component (vertical axis) accounts for the differences due to effect of oxygen (20% vs 2% O_2).

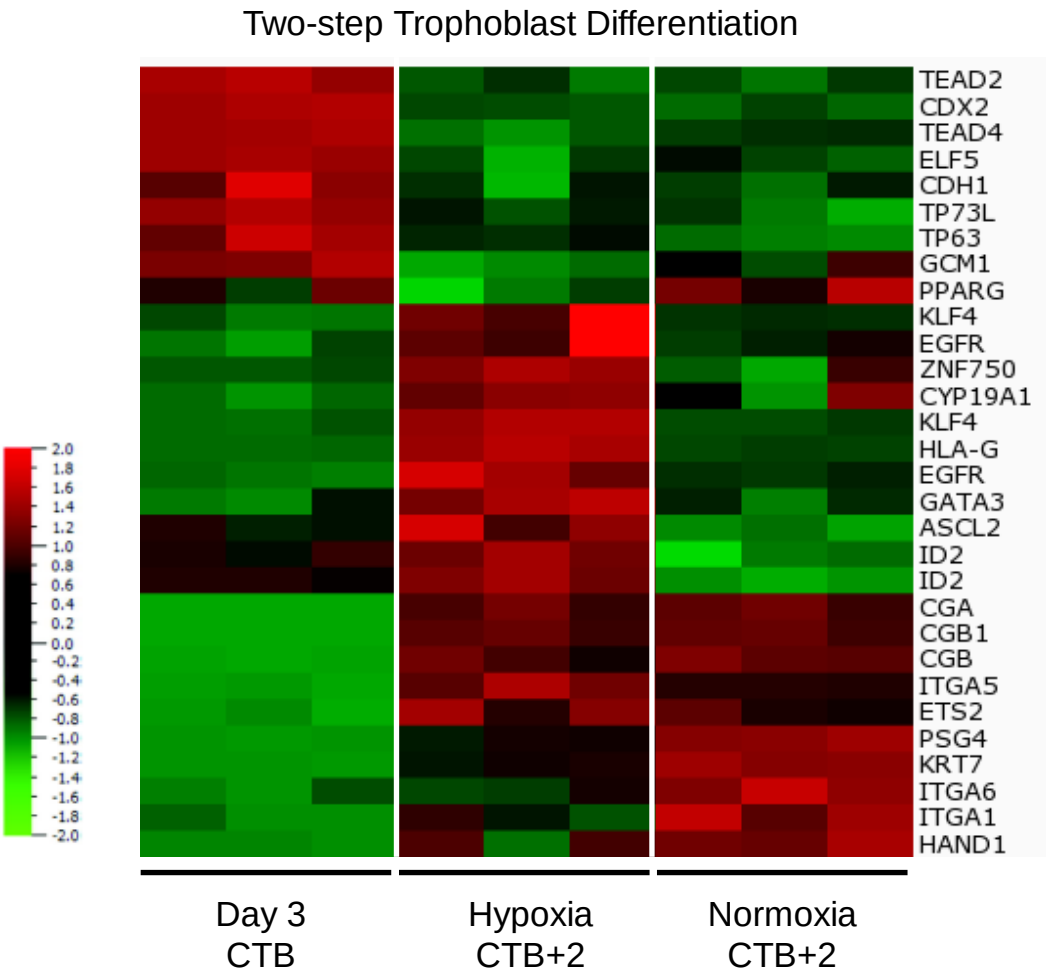

Figure 4.17. Heatmap of trophoblast-specific gene expression in hESC-derived CTB using the two-step method of differentiation.
Gene expression of hESC-derived CTB differentiated using the two-step method and comparing CTB (Day 3) or 2 days post-CTB cultured in hypoxia (2% O_2) or normoxia. Only statistically significant gene probes were shown (ANOVA $q<0.05$) and subjected to hierarchical clustering. Some genes are represented by multiple probes on the heatmap.

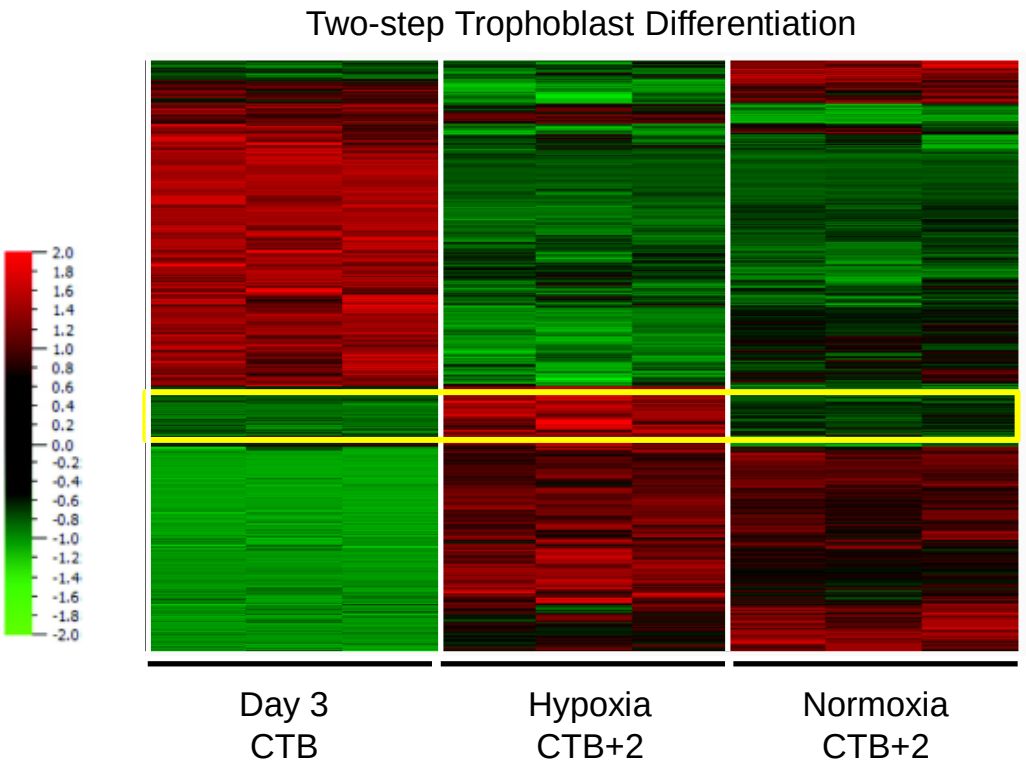

Figure 4.18. Heatmap of global gene expression in hESC-derived CTB. Genome-wide expression profile of hESC-derived CTB differentiated using the two-step method and comparing CTB (Day 3) or 2 days post-CTB cultured in hypoxia (2% O_2) or normoxia. Gene probes were subjected to hierarchical clustering and probes were filtered for variance (v=0.01). Only statistically significant gene probes were shown (ANOVA $q<0.05$). Highlighted cluster (yellow) indicates 429 gene probes that are upregulated in hypoxia compared to normoxia or CTB (day 3).

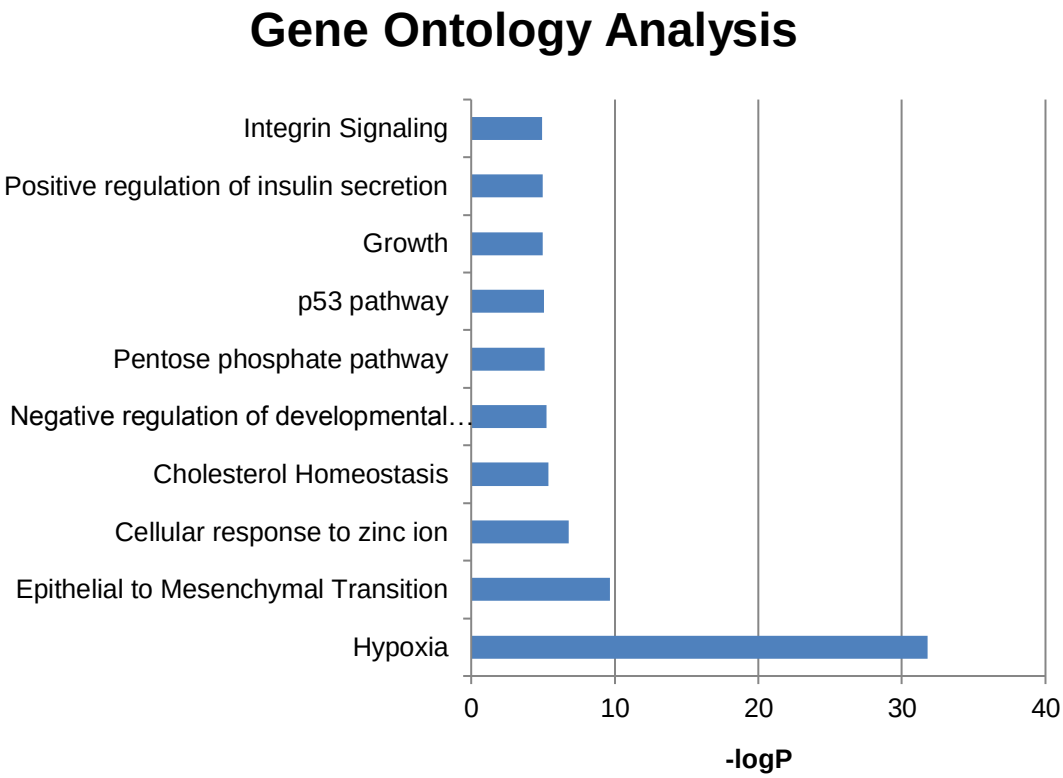

Figure 4.19. hESC-derived CTB cultured in hypoxia show EVT-like properties.
Gene ontology analysis of the 429 gene probes upregulated in hypoxia in hESC-derived CTB. Some of the enriched groups can be associated with EVT functions.

Chapter 5

The role of an intact HIF complex in hypoxia-mediated human trophoblast differentiation

5.1 Introduction

Hypoxia-Inducible Factor, or HIF, is a dimeric protein complex that plays an essential role in the cellular response to hypoxia. The HIF complex is composed of an oxygen-regulated α-subunit (usually either *HIF1α* or *HIF2α*) and a constitutively expressed β-subunit, or *ARNT*. An intact HIF complex is important for proper trophoblast differentiation and placentation in rodents. It is known that disruption of the intact HIF complex impairs invasive trophoblast differentiation. One study found mouse trophoblast stem cells (mTSC) derived from *Arnt*-null mice are unable to form invasive trophoblast, differentiating exclusively into syncytiotrophoblast (Maltepe et al., 2005). Another study found that hypoxia promotes differentiation of rat TSC into invasive trophoblast in a HIF-complex dependent process (Chakraborty et al., 2011). HIF subunits are highly expressed in first trimester human placenta (Pringle et al., 2010). However, the role of HIF complex during human trophoblast differentiation has not yet been determined.

5.2 Expression of HIF-1α and HIF-2α in early gestation human placenta

Previously, other groups have examined expression of HIF-1α and HIF-2α in human placenta by staining of tissue sections. Some reports have found both HIF-1α and HIF-2α localized in STB, villous CTB and fetoplacental vascular endothelium in first trimester, and that the abundance decreases significantly with increasing gestational age (Caniggia and Winter, 2002; Caniggia et al., 2000). Another study found both HIF-1α and HIF-2α present throughout gestation but that HIF-1α peaks at 7-10 weeks of gestation, and that HIF-2α peaks at 10-12 weeks of gestation (Ietta et al., 2006). To confirm these findings, we repeated the staining in first trimester (12 weeks of gestation) tissue (Figure 5.1). I found HIF-1α expressed in the nuclei of very

A

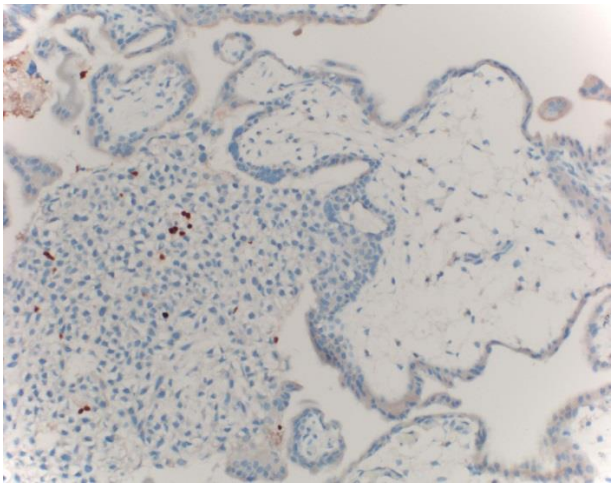

B

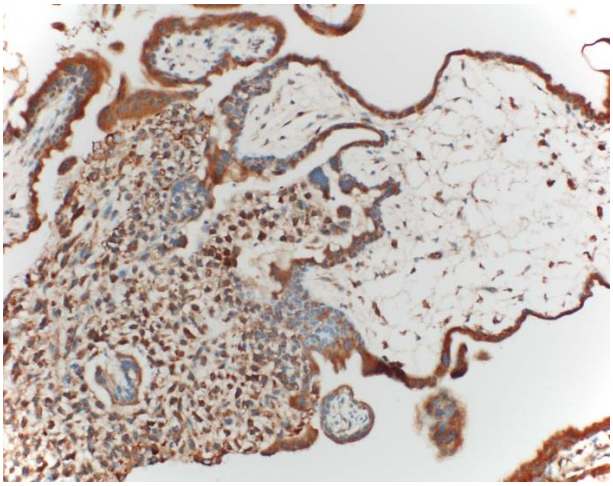

Figure 5.1. Expression of HIF-1α and HIF-2α in first trimester placenta. **(A)** First trimester (12 weeks gestational age) placental tissue stained for HIF-1α shows expression only in the nuclei of a few EVT located in the CTB cell columns. **(B)** First trimester (12 weeks gestational age) placental tissue stained for HIF-2α shows expression in the cytoplasm of CTB, STB and EVT. Brown, immunostaining of indicated marker; blue, hematoxylin-stained nuclei. 20x

few EVT located within the CTB cell columns. I found HIF-2α expressed in the cytoplasm of CTB, STB and EVT.

5.3 Knockdown of *ARNT* in primary isolated CTB

To determine if an intact and functioning HIF complex is required for differentiation of human primary isolated CTB, I infected isolated first trimester CTB with lentivirus expressing either *ARNT*-specific or scrambled shRNA. To downregulate ARNT, lentiviral shRNA was obtained by pooling the three clones which had previously shown the best knockdown in HEK293 cells: western blot of ARNT in these cells transfected with the each of five single shARNT clones, all five together, scrambled, or untransfected shows that clones A1, E4 and F4 were the most efficient at ARNT knockdown (Figure 5.2A). I infected freshly isolated CTB and collected the cells after 4 days of culture, without selection. Infection with a GFP-expressing lentivirus packaged at the same time as the shRNA clones showed >80% of CTBs to be GFP-positive at day 4 (Figure 5.2B). When I assessed knockdown efficiency by western blot, ARNT was expressed at day 0 and, in scrambled control, both in normoxia and hypoxia (Figure 5.3A). In the shARNT infected cells, ARNT was drastically downregulated both in conditions of normoxia and hypoxia. Morphologically, differentiated *ARNT*-shRNA-infected cells showed a similar epithelial phenotype to the scrambled control, and both had slightly fewer cells than the uninfected control (Figure 5.3B).

5.4 Comparative gene expression profiling of isolated CTB and ARNT knockdown

Next, I subjected the scrambled control or shARNT-infected primary CTBs to microarray-based gene expression analysis. I first wanted to assess the effect of shARNT globally. Previously, I had determined that 825 gene probes were significantly

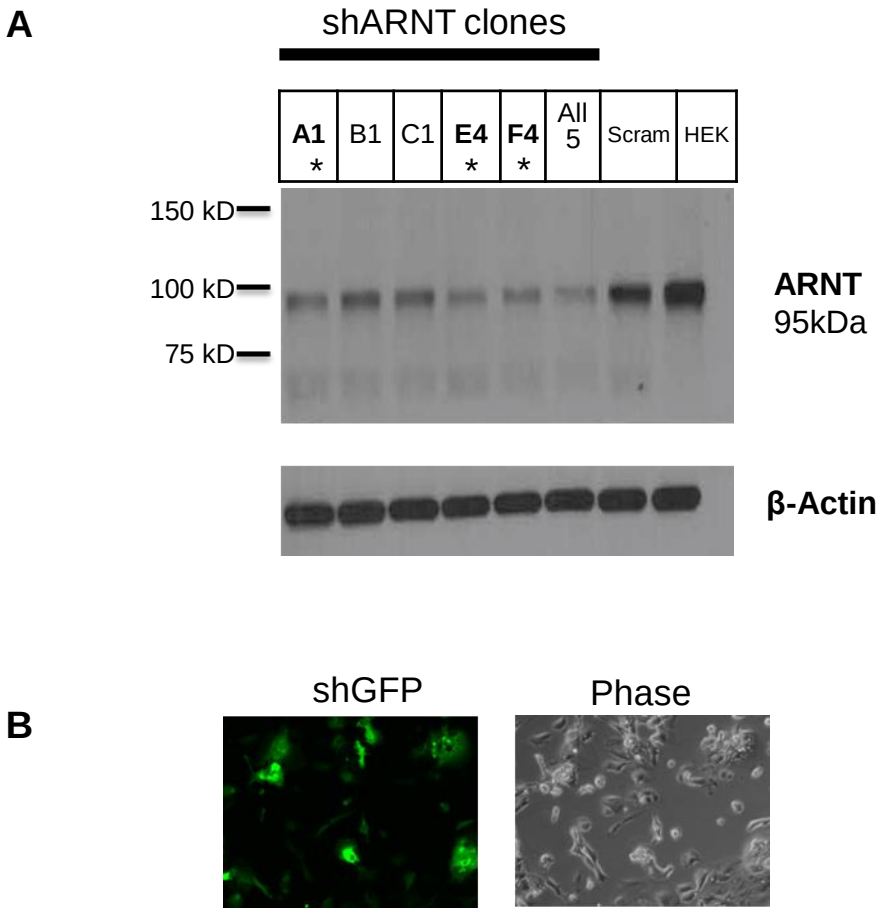

Figure 5.2. Making lentiviral shRNA for ARNT knockdown.
(A) Western blot for ARNT shows lentiviral transfection of HEK293 cells with each of the single lentiviral shARNT clones, all five clones together, shScramble (scram), or untransfected (HEK). * indicates clones with the most ARNT knockdown. **(B)** Infection with a GFP-expressing lentivirus packaged at the same time as the shRNA clones showed >80% of CTBs to be GFP-positive at day 4.

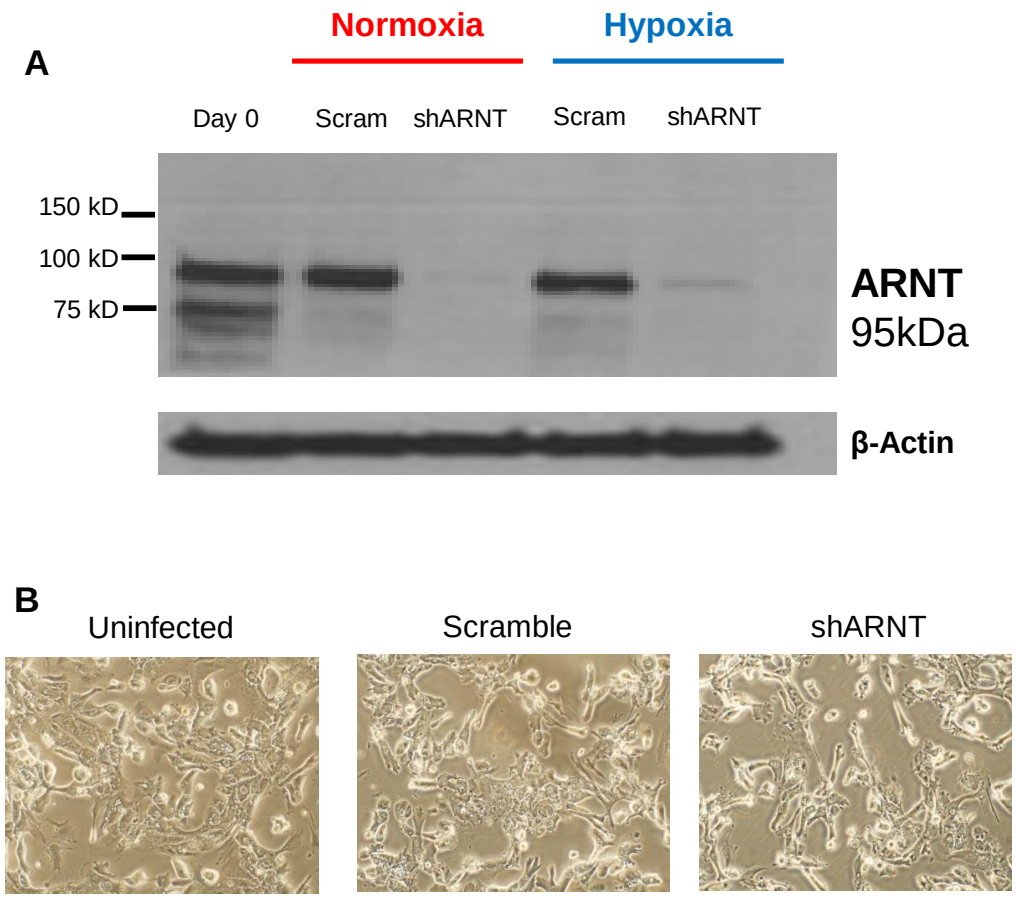

Figure 5.3. Knockdown of ARNT in primary CTB.
(A) isolated first trimester CTB were infected with lentivirus expressing either *ARNT*-specific or scrambled shRNA. Lentiviral shARNT was obtained by pooling the three clones which had previously shown the best knockdown in HEK293 cells. **(B)** Morphology of differentiated *ARNT*-shRNA-infected cells showed a similar epithelial phenotype to the scrambled control, and both had slightly fewer cells compared to uninfected control

upregulated in hypoxia in scrambled control (Figure 4.9). When I looked at the expression patterns of those probes in shARNT-infected CTBs, it was evident that knockdown of ARNT caused less upregulation of the hypoxia-induced probes (Figure 5.4). I determined how many of those probes were significantly changed in shARNT by applying multigroup analysis between just shARNT normoxia and shARNT hypoxia samples. I found that ~30% of the 825 probes were still significantly upregulated in hypoxia despite ARNT knockdown and resulting disruption of HIF complex signaling (Figure 5.5). However, hypoxic upregulation of the majority of probes (~70%) was abrogated in absence of ARNT, which represents the HIF-dependent hypoxia-induced genes in isolated CTB. I next characterized the potential role(s) this subset of genes plays by subjecting them to gene ontology analysis using Metascape software. I found enrichment of 10 groups of genes, including hypoxia, actin-based processes, focal adhesion, integrin-mediated signaling pathways and epithelial to mesenchymal transition (Figure 5.6).

5.5 Effect of ARNT knockdown on EVT differentiation of isolated CTB

In order to further assess the effect of ARNT knockdown on EVT differentiation of isolated CTB, I performed quantitative RT-PCR. First, I confirmed that *ARNT* is repressed in my shARNT-infected CTBs, and that shARNT-infected CTBs show a reduction of expression of known HIF complex targets *VEGFA* and *ANKRD37* compared to scrambled control (Figure 5.7 A-C). When I evaluated EVT-associated markers *HLA-G*, *ITGA1* and *TEAD2*, I saw significantly reduced expression in shARNT-infected CTB cultured in hypoxia (Figure 5.7 D-F). I next evaluated functional aspects of EVT differentiation by assessing expression of surface HLA-G, a hallmark of EVT differentiation. I found that in scramble control lentivirus-infected CTB, hypoxia

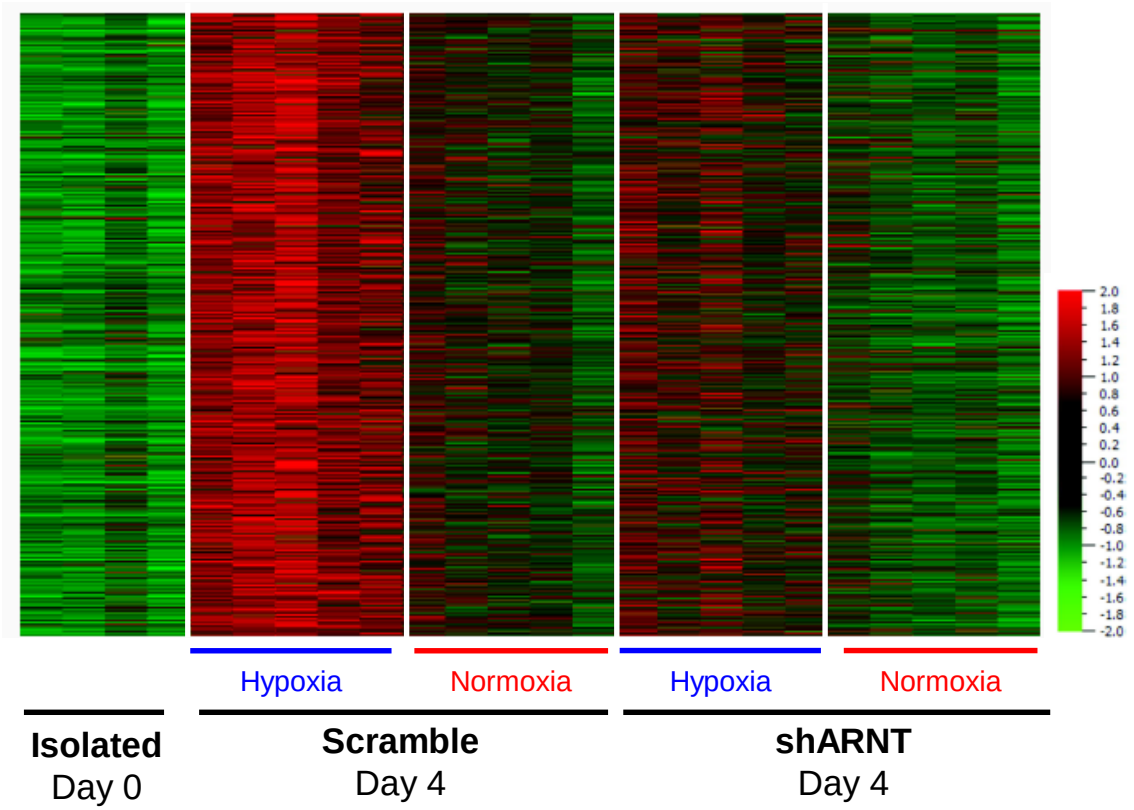

Figure 5.4. Effect of ARNT knockdown on gene expression of hypoxia-upregulated genes in primary CTB.
Expression patterns of genes significantly upregulated in scramble-infected primary CTB cultured in hypoxia compared to shARNT-infected cells.

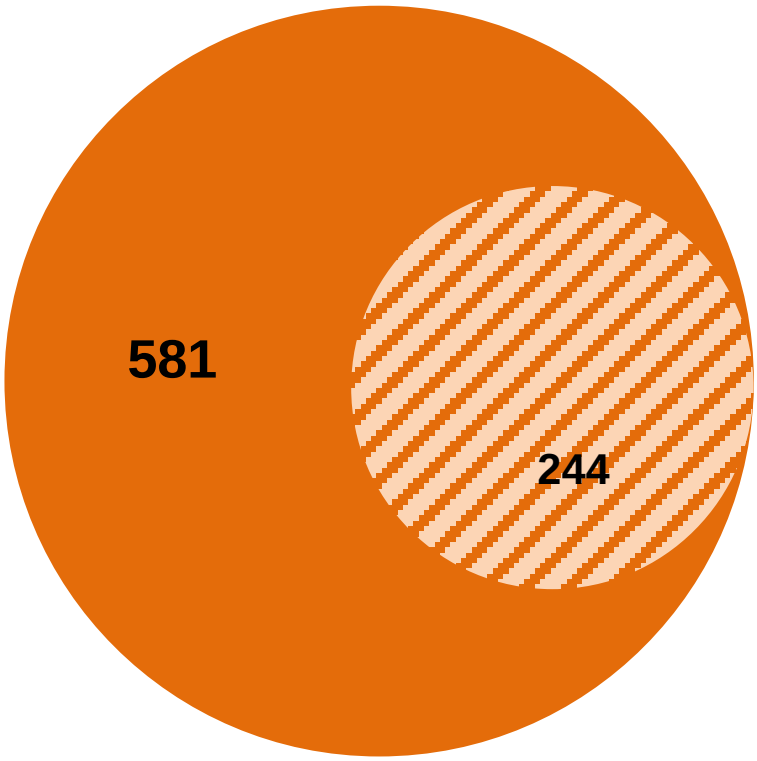

Figure 5.5. Graphic representation of potentially HIF-dependent and HIF-independent genes in shARNT primary CTB.
To identify HIF dependent genes in hypoxic conditions, I focused on the genes previously identified as significantly upregulated in hypoxia in scramble-infected primary CTB. I then identified which genes were still significantly upregulated in shARNT-infected primary CTB (244). Therefore, the genes that were unchanged (581) in shARNT-infected cells potentially are regulated by the HIF complex.

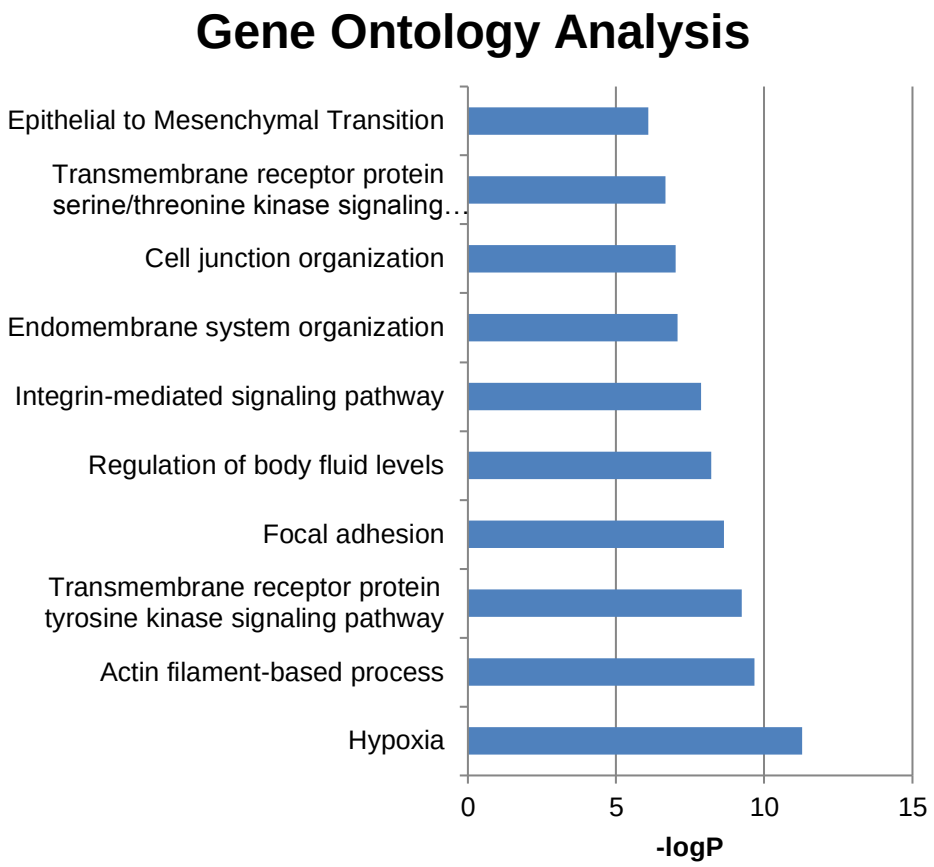

Figure 5.6. Gene ontology analysis of potentially HIF-dependent genes in primary CTB.
Gene ontology analysis of the HIF dependent genes (not upregulated in hypoxia after ARNT knockdown) in primary CTB. Some of the enriched groups can be associated with EVT functions.

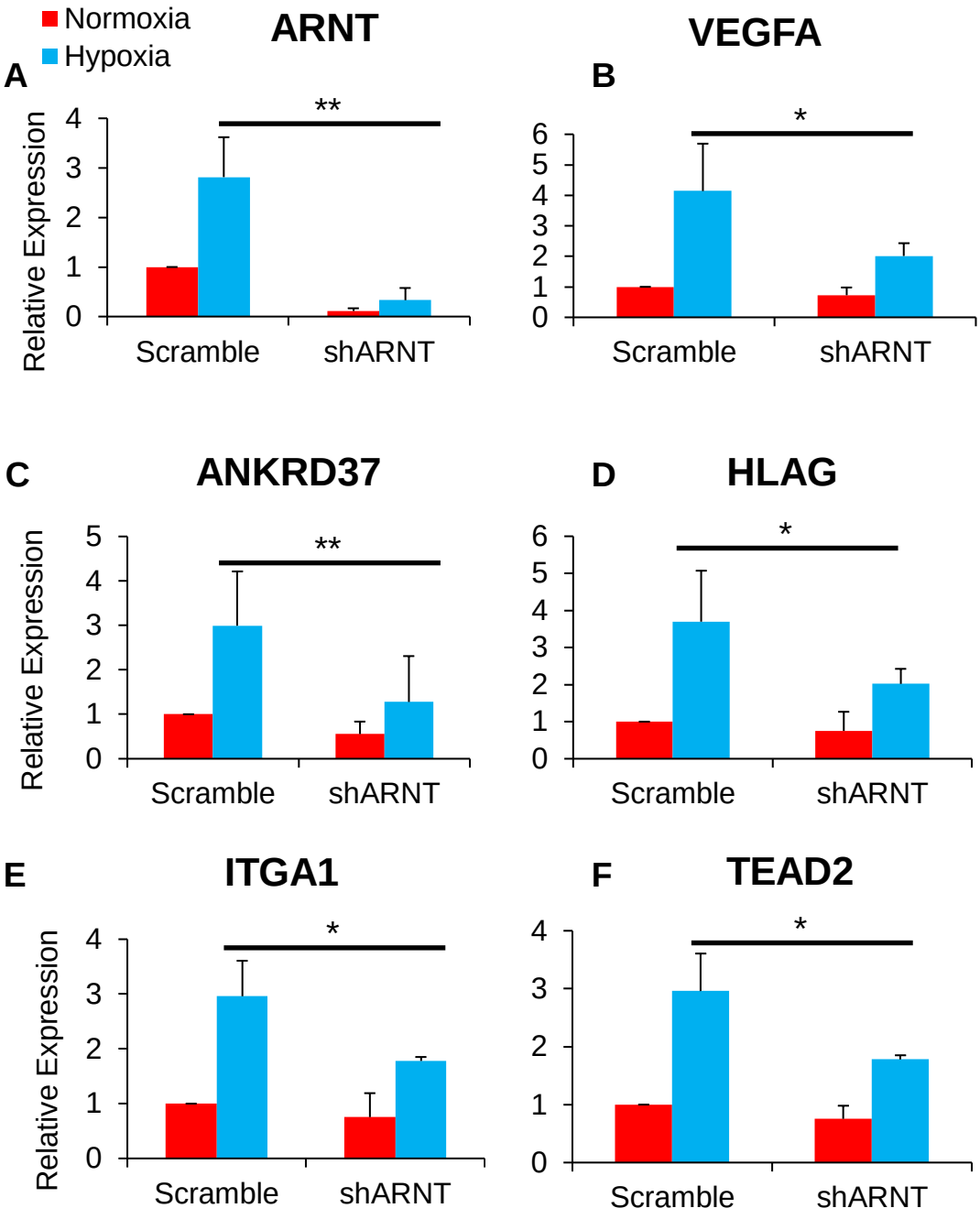

Figure 5.7. ARNT knockdown reduces expression of markers of EVT differentiation.

qRT-PCR analysis of ARNT **(A)** and targets downstream of HIF complex **(B)-(C)** and markers of EVT differentiation **(D)-(F)** in scramble or shARNT-infected primary CTB. Values adjusted to freshly isolated (day 0) and normalized to 18S ribosomal RNA. n=5 *p<0.05 **p<0.01

increased surface HLA-G expression, but in shARNT-infected CTBs there was significantly less surface HLA-G expression in response to hypoxia (Figure 5.8A). Likewise, levels of MMP2, secreted by EVT, were also significantly reduced in shARNT-infected compared to scrambled control CTB in hypoxia (Figure 5.8B). Secretion of hCG was reduced in hypoxia (as previously seen; see Figure 4.6D) in scramble control-lentivirus infected CTB (Figure 5.8C). This effect appeared to also be dependent on ARNT, with hCG levels remaining high in hypoxia in the absence of ARNT.

5.6 Knockdown of *ARNT* in hESC-derived trophoblast

To determine if an intact and functioning HIF complex is required for hESC-derived trophoblast differentiation, I infected pluripotent H9 hESC with lentivirus expressing the same 3-clone pool of shRNA against *ARNT* (Figure 5.2A) or with scrambled shRNA, and used puromycin to select for cells expressing the respective shRNA. The cells were confirmed to be stably infected by assessing ARNT expression by western blot in the undifferentiated state (Figure 5.9A). Infection did not affect pluripotency of the hESC as assessed by *POU5F1* expression, but did affect expression of HIF signaling target *SLC2A1* after 1 hour of hypoxia (Figure 5.9B). Once the cells were stably infected, I differentiated the cells using our lab's two-step method. To confirm that shARNT was affecting only ARNT, and not the oxygen-regulated *HIF1α* subunit, I performed a western blot: although ARNT had diminished expression in shARNT-infected cells (Figure 5.10A), the HIF1α subunit was expressed in both scrambled control and shARNT-infected (Figure 5.10B).

I next determined whether the HIF complex is required for FCM-BMP4-based hESC induction toward the trophoblast lineage. Based on my findings that hypoxia does not affect trophoblast lineage specification, I hypothesized that disruption of the

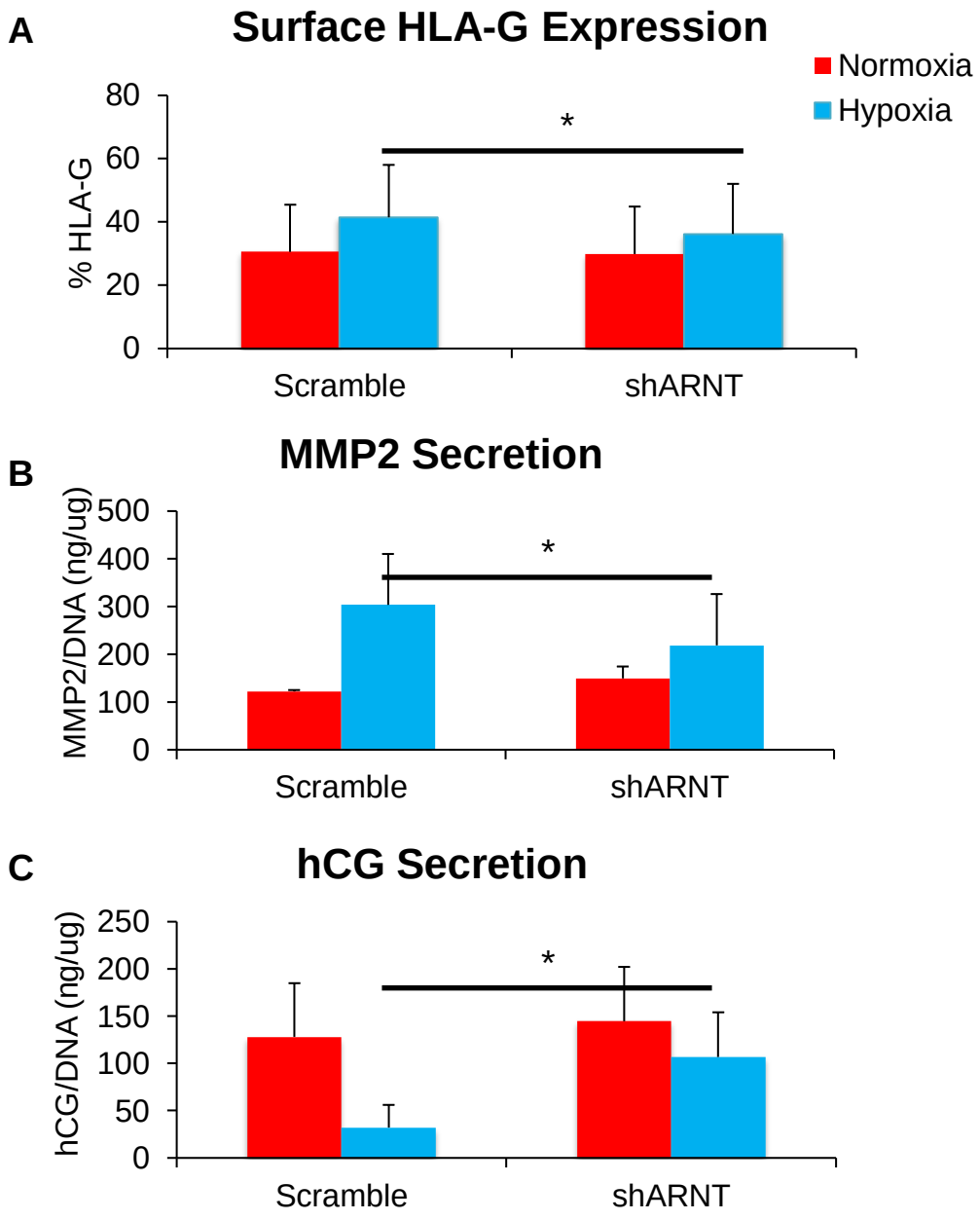

Figure 5.8. ARNT knockdown reduces EVT differentiation and increases STB differentiation in primary CTB.
(A) Surface HLA-G expression in scramble and shARNT-infected first trimester primary CTB measured by flow cytometry. n=5 **(B)** MMP2 secretion in scramble and shARNT-infected primary CTB measured by ELISA and normalized to DNA content. n=3 **(C)** hCG secretion in scramble and shARNT-infected primary CTB, measured by ELISA and normalized to DNA content . n=4 *p<0.05

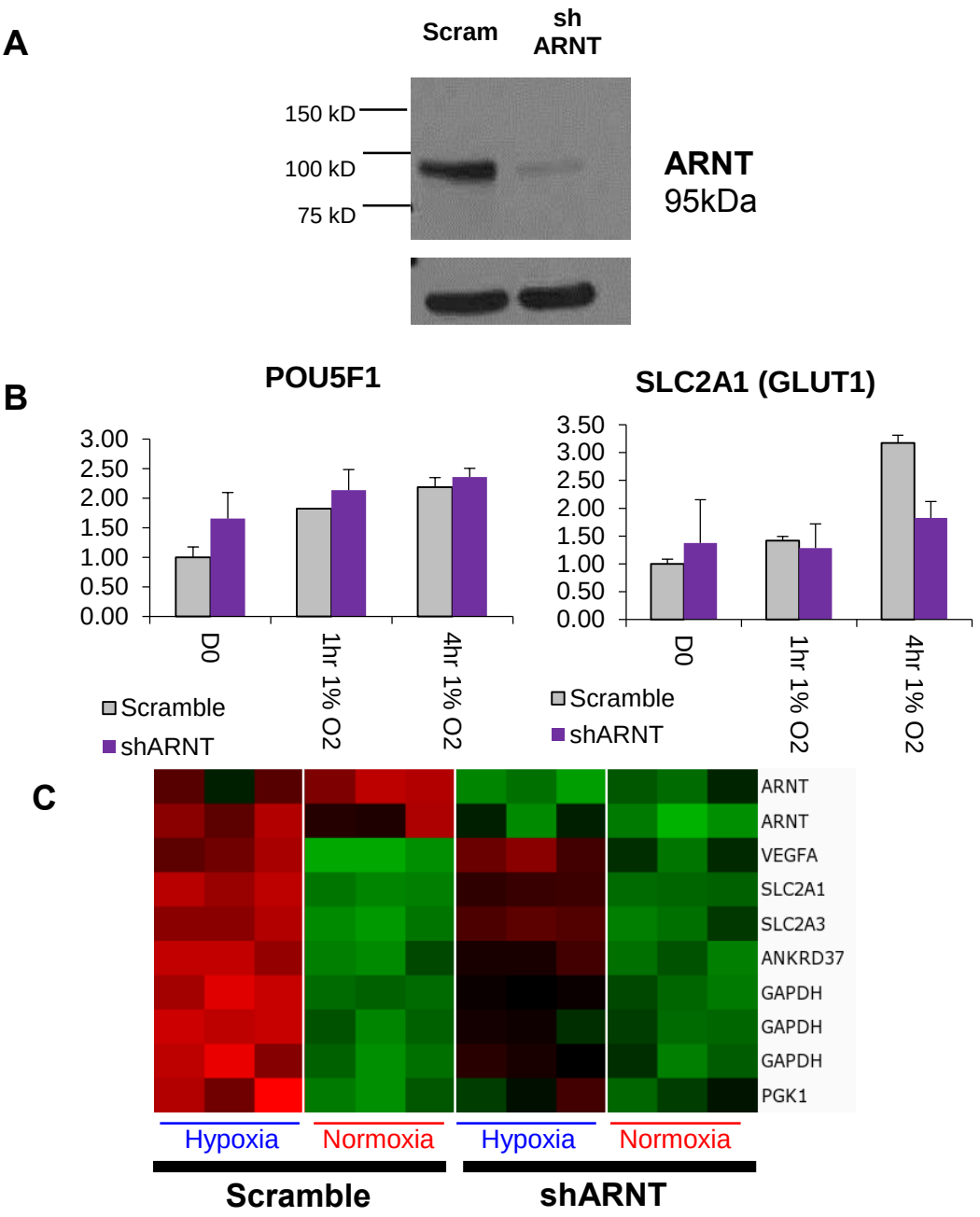

Figure 5.9. Knockdown of ARNT in hESC.
(A) Western blot for ARNT in undifferentiated hESC stably infected with lentivirus expressing either *ARNT*-specific or scrambled shRNA. **(B)** qRT-PCR analysis of pluirpotency marker (POU5F1) and downstream target of HIF complex (SLC2A1). Values adjusted to undifferentiated hESC and normalized to 18S ribosomal RNA. *p<0.05 **(C)** Gene expression of ARNT or HIF targets in scramble or shARNT hESC-derived CTB at day CTB+2 in hypoxia (2% O_2) or normoxia.

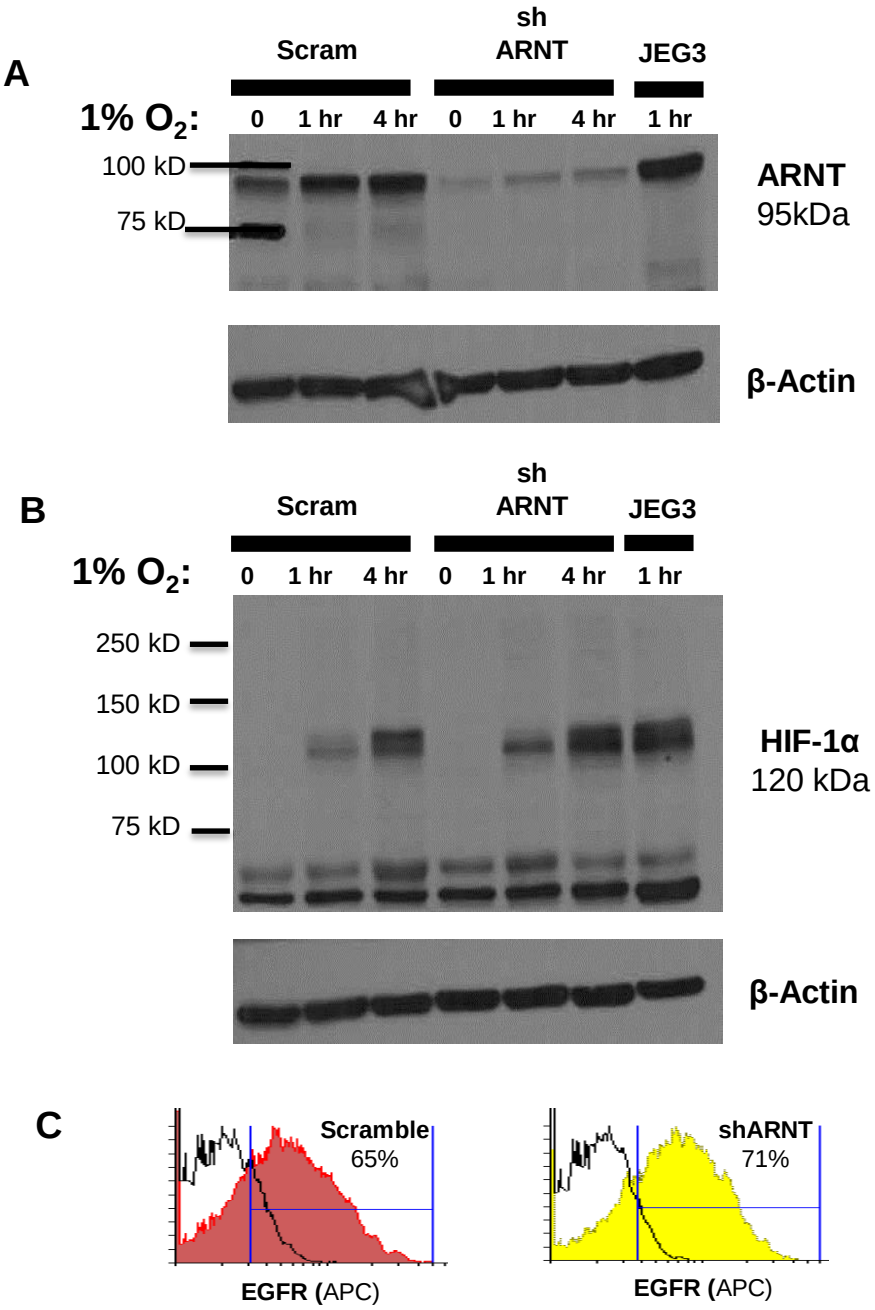

Figure 5.10. ARNT knockdown is specific and does not affect trophoblast lineage specification of hESC-derived CTB.
(A) Western blot for ARNT in scramble or shARNT-infected hESC and uninfected JEG3 as a control. **(B)** Western blot for HIF-1α in scramble or shARNT-infected hESC and uninfected JEG3 as a control. **(C)** Flow cytometric analysis of surface EGFR expression of CTB Day 4 scramble or shARNT-infected hESC differentiated using the two-step .

HIF complex would also not affect trophoblast lineage specification. As expected, hESC-derived CTB that were stably infected with shARNT constructs induced trophoblast-associated genes at the same time points and also had levels of EGFR expression similar to scrambled control-infected hESC-derived CTB (Figure 5.10C).

5.7 Comparative gene expression profiling of hESC-derived trophoblast differentiation and ARNT knockdown

I subjected the scrambled control or shARNT-infected hESC-derived trophoblast to microarray-based gene expression analysis. I evaluated the effect of shARNT in these cells by comparing the 429 gene probes previously found to be upregulated in hypoxia in the scrambled control (see Figure 4.18). The expression patterns of hypoxia-upregulated genes in shARNT-infected hESC-derived CTBs was clearly reduced compared to levels in scrambled control in hypoxia (Figure 5.11). Next, I determined the percentage of those genes which are significantly affected by the absence of ARNT by applying multigroup analysis between just shARNT normoxia and shARNT hypoxia samples. I found that, similar to primary CTB, ~37% of the 429 probes were significantly upregulated in hypoxia even in the absence of ARNT, suggesting these genes to be induced by hypoxia in a HIF-independent manner (Figure 5.12). The other 63% of genes were HIF complex-dependent, including the EVT marker HLA-G. CTB markers EGFR and ID2 were also on this list, but ITGA1 and ITGA5 were not. To further characterize these HIF-dependent genes, I subjected the list to ontology analysis using Metascape software, and found 10 groups of genes significantly enriched, including hypoxia, epithelial to mesenchymal transition, and integrin mediated signaling pathways and organ morphogenesis (Figure 5.13).

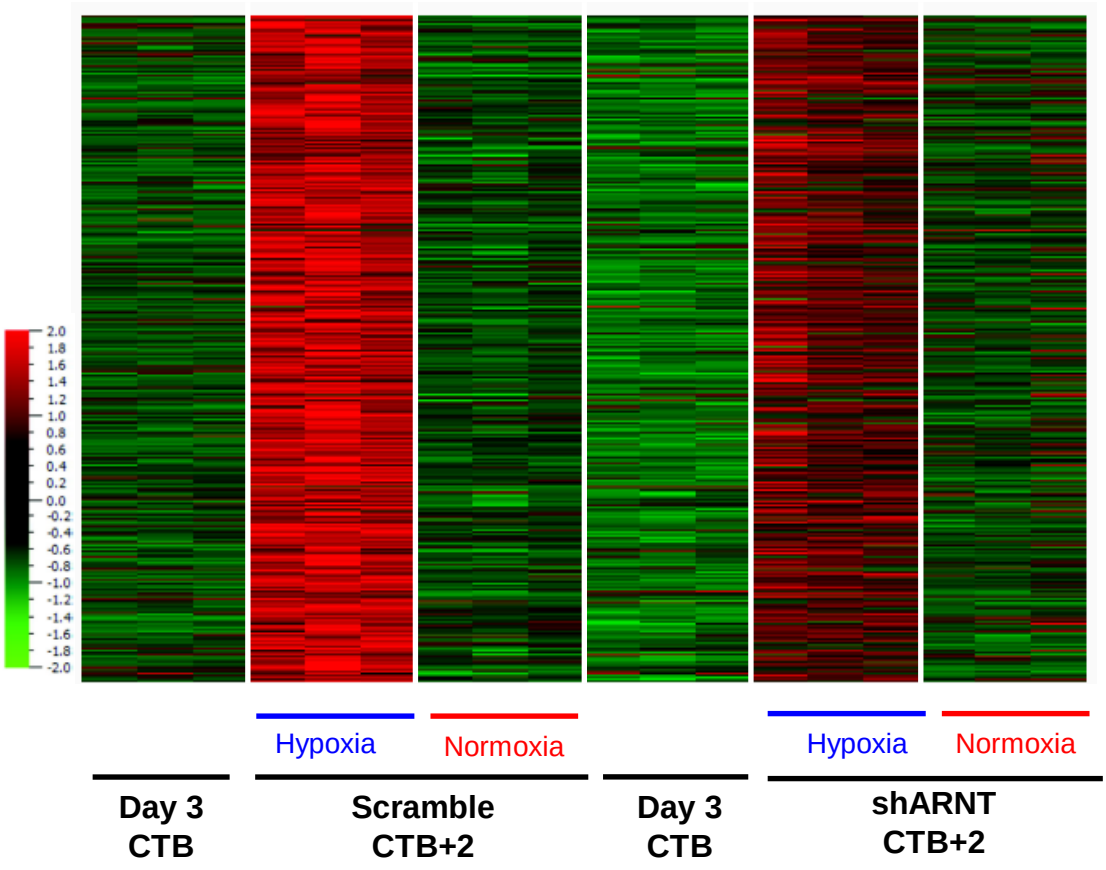

Figure 5.11. Effect of ARNT knockdown on gene expression of hypoxia-upregulated genes in hESC-derived CTB.
Expression patterns of genes significantly upregulated in scramble-infected hESC-derived CTB cultured in hypoxia compared to shARNT-infected cells.

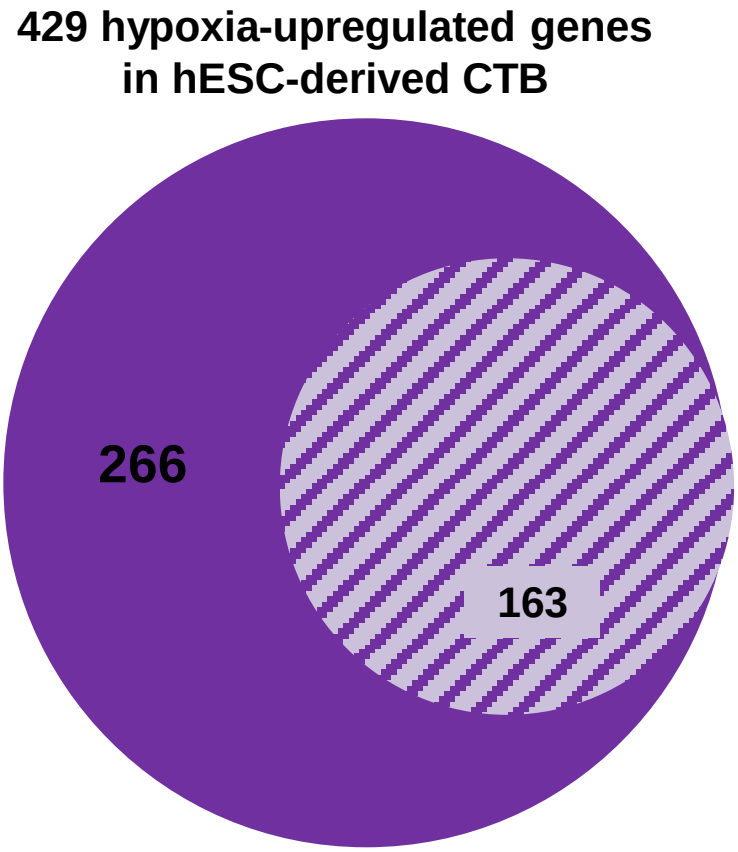

Figure 5.12. Graphic representation of potentially HIF-dependent and HIF-independent genes in shARNT hESC-derived CTB.
To identify HIF dependent genes in hypoxic conditions, I focused on the genes previously identified as significantly upregulated in hypoxia in scramble-infected hESC-derived CTB. I then identified which genes were still significantly upregulated in shARNT-infected primary CTB (163). Therefore, the genes that were unchanged (266) in shARNT-infected cells potentially are regulated by the HIF complex.

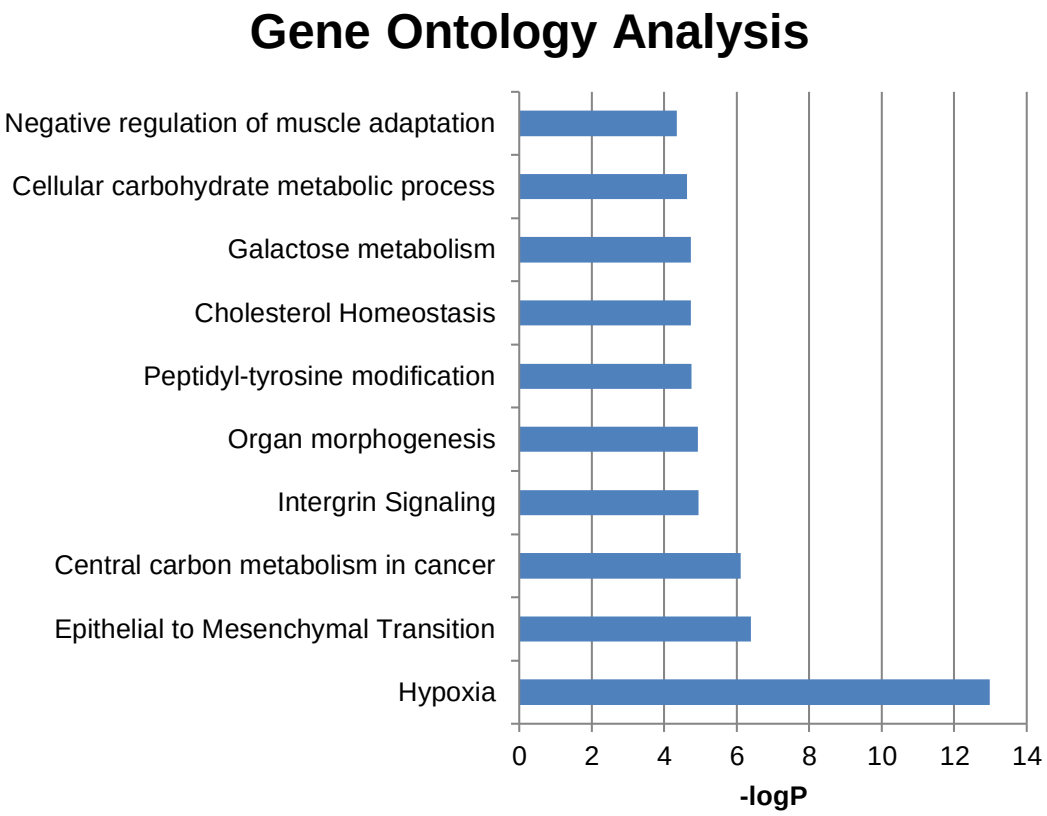

Figure 5.13. Gene ontology analysis of potentially HIF-dependent genes in hESC-derived CTB.
Gene ontology analysis of the genes not upregulated in hypoxia after ARNT knockdown in hESC-derived CTB. Some of the enriched groups can be associated with EVT functions.

5.8 Effect of ARNT knockdown on hESC-derived EVT differentiation

In order to further assess the effect of ARNT knockdown on EVT differentiation of hESC-derived CTB, I checked expression of surface HLA-G, a hallmark of EVT. I found that in scramble control, hypoxia increases the proportion of EGFR+/HLA-G+ expressing EVT, but in shARNT-infected hESC-derived CTBs, this population is decreased (Figures 5.14 and 5.15). When I looked at levels of MMP2 secretion, I found significantly reduced levels in shARNT-infected compared to scrambled control-infected cells (Figure 5.16A). Secretion of hCG, a hallmark of STB differentiation, was reduced by hypoxia as previously confirmed (as previously seen; see Figure 4.13B) However, unlike primary cells, this effect appeared to be independent of the HIF complex, as I noted the same reduction in hCG secretion in hypoxia in scrambled control as well as shARNT-infected cells (Figure 5.16B).

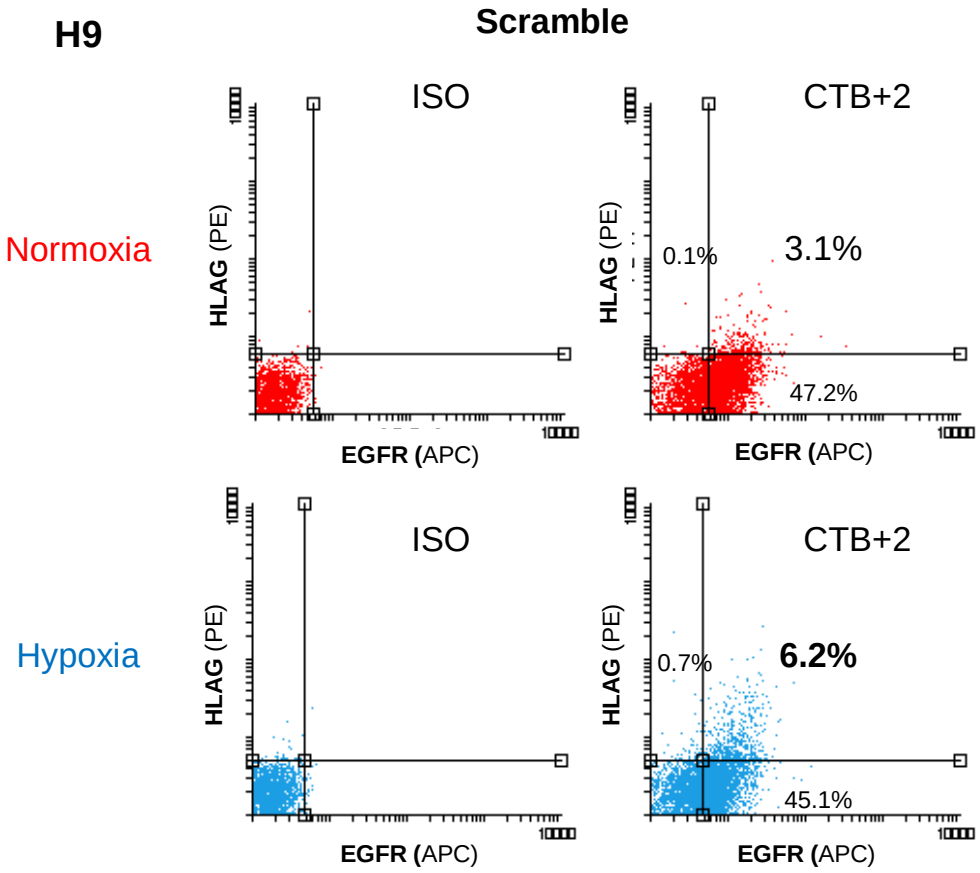

Figure 5.14. Hypoxia increases EVT differentiation of hESC-derived CTB. Scramble-infected hESC-derived CTB were differentiated using the two-step method to 2 days post-CTB and cultured in normoxia or hypoxia. Surface expression of EGFR (CTB marker) and HLA-G (EVT marker) was analyzed by flow cytometry.

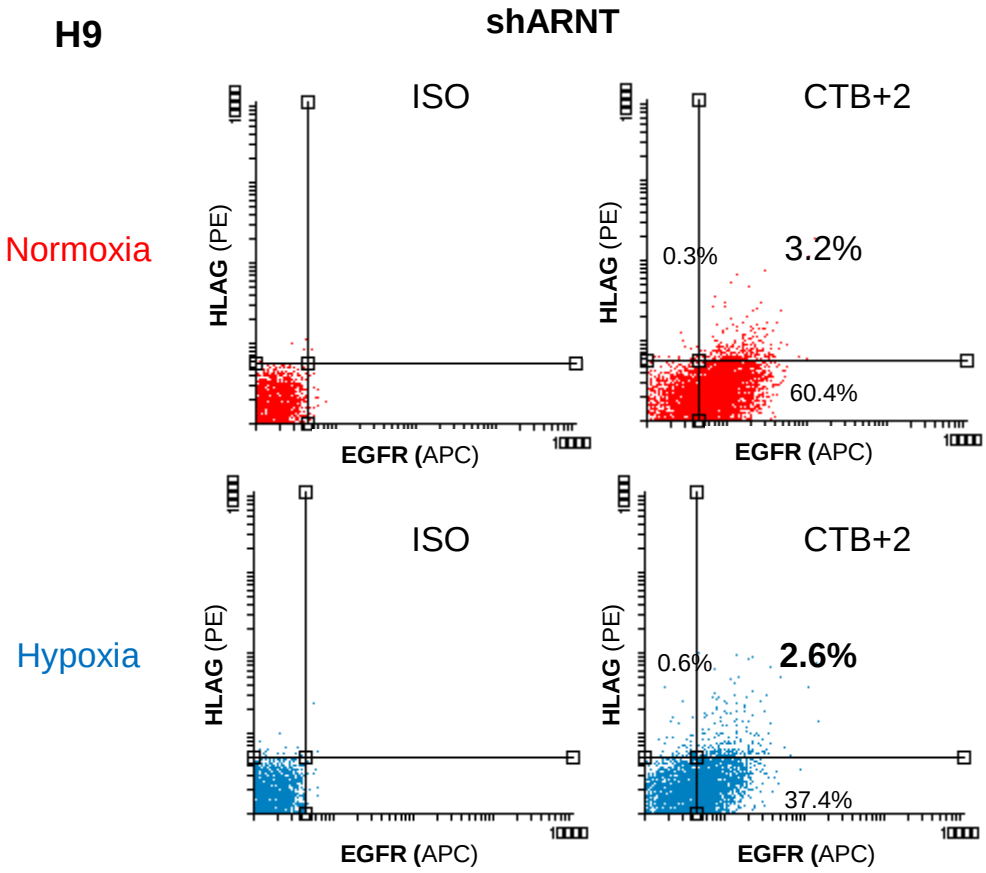

Figure 5.15. ARNT knockdown decreases EVT differentiation of hESC-derived CTB.
shARNT-infected hESC-derived CTB were differentiated using the two-step method to 2 days post-CTB and cultured in normoxia or hypoxia. Surface expression of EGFR (CTB marker) and HLA-G (EVT marker) was analyzed by flow cytometry.

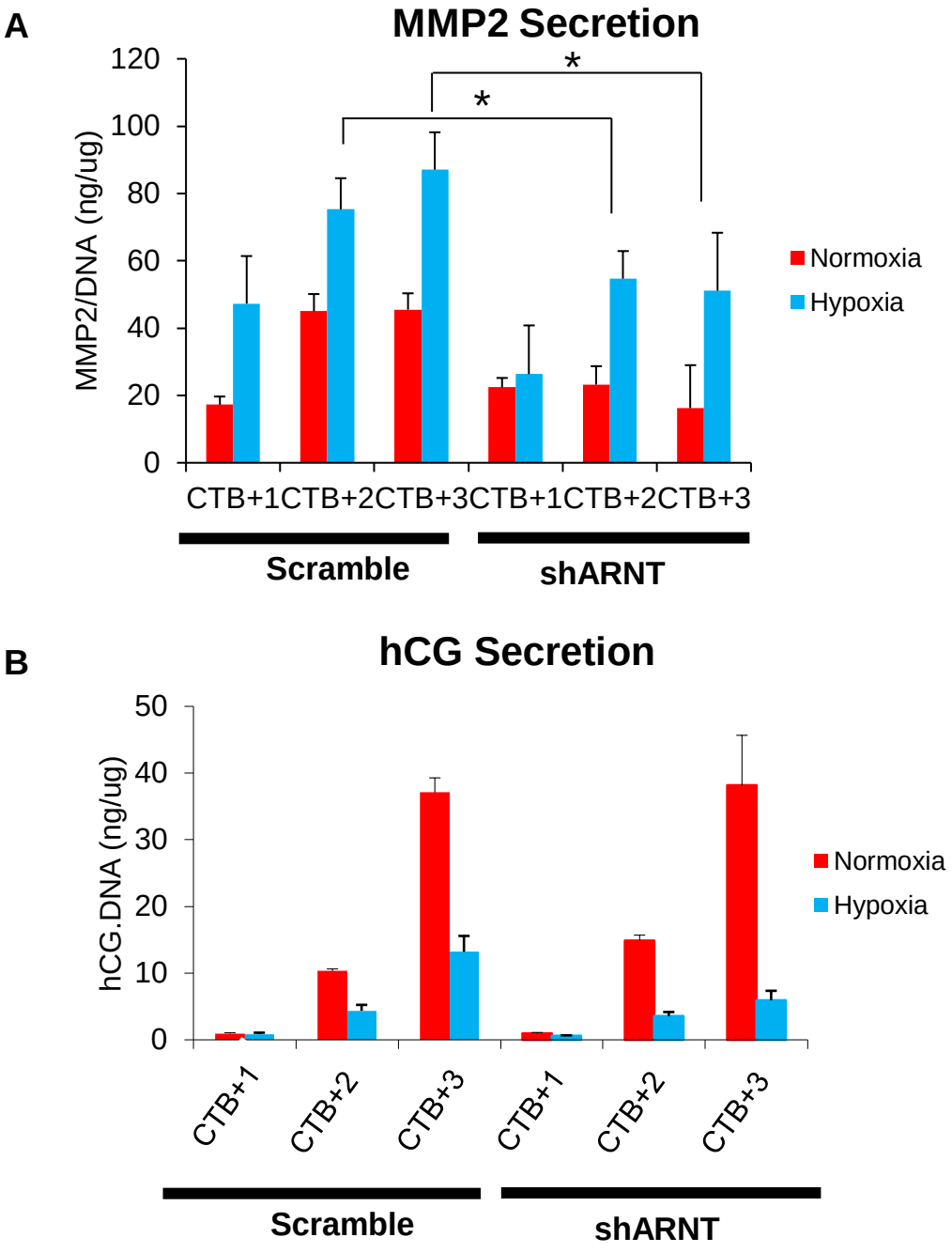

Figure 5.16. ARNT knockdown reduces EVT differentiation in hESC-derived CTB.
(A) MMP2 secretion in scramble and shARNT-infected hESC-derived CTB measured by ELISA and normalized to DNA content. **(B)** hCG secretion in scramble and shARNT-infected hESC-derived CTB, measured by ELISA and normalized to DNA content . *p<0.05

Chapter 6

Discussion of the Dissertation

In order to assess the role of BMP4 in mouse trophoblast differentiation, I determined that BMP4 and its receptors are expressed and BMP4 signaling is active in undifferentiated mTSC. I also found that in differentiating mTSC, sustained BMP4 treatment causes a reduction in spongiotrophoblast marker Tpbpa, a precursor to TGC differentiation. In addition, while inhibition of BMP4 signaling in undifferentiated mTSC resulted in an increase in Tpbpa expression, it did not affect expression of stem cell markers in these cells. Collectively, these results indicate that, in mTSCs, BMP4 helps to inhibit differentiation, but is not required for maintenance of the stem cell state.

In the context of human trophoblast, little is known about BMP4, except that it induces trophoblast lineage specification in hESC (Xu et al., 2002). I set out to determine the role of BMP4 in primary trophoblast, isolated from human placentas of varying gestational ages. I found that expression of BMP4 and BMP receptors in human first trimester CTB is similar to that in mTSC. In first trimester explants, BMP4 treatment had similar effects as the pro-differentiation factor EGF; there was a reduction in Ki67+ cells, compared to untreated explants. This indicates that, in presence of exogenous BMP4, CTB are unable to maintain their proliferative state. I further assessed the role of BMP4 in differentiation, but found, at least under current, likely suboptimal culture conditions, that there is no significant difference in expression of lineage-specific markers nor hCG secretion from differentiated CTB at any gestational age. Taken together, the results indicate that in cells that are already specified as trophoblast, BMP4 decreases the number of proliferative CTB as evidenced by reduced Ki67 expression but has little effect on functional differentiation into terminal lineages. However, BMP4 has a clear effect on induction of trophoblast lineage, as seen by the combined results from hESC-derived experiments using the traditional one-step (FCM

+ BMP4) method (Xu et al., 2002; Wu et al., 2008; Das et al., 2007; Yu et al., 2011; Marchand et al., 2011; Bai et al., 2012) and our lab's improved two-step method. Both methods clearly show that BMP4 induces both initial trophoblast lineage specification and further differentiation of hESC-derived CTB.

To study the role of hypoxia in human trophoblast differentiation, I first tried several human trophoblast cell lines. However, there were several inconsistencies with both cell lines used. In HTR-8 cells, which are a model of EVT, hypoxia significantly increased RNA expression of EVT marker HLA-G, but flow cytometry revealed no surface expression of this marker, the hallmark of primary EVT. In JEG3, choriocarcinoma cells with features of both EVT and STB, hypoxia reduced hCG secretion and increased surface expression of HLA-G. However, ARNT knockdown did not affect HLA-G expression in these cells. These results, together with the fact that neither HTR-8 nor JEG3 cells secrete MMP2, indicate these trophoblast cell lines do not fully recapitulate primary EVT.

I therefore turned to primary cells for the majority of these experiments, but also tested the effect of hypoxia on trophoblast differentiation of hESC in order to assess their utility in modeling EVT differentiation of primary CTB. To utilize isolated CTB, I first had to find optimal culture conditions, which included trying to find the best extracellular matrix (ECM) for the cells. The cells plated best on fibronectin, which is the matrix abundant in the cell column of anchoring villi; surprising, and despite widely-accepted previously published reports, the cells did not plate at all on laminin, or laminin-rich Matrigel, which is abundant in the basement membrane directly in contact with proliferative CTB (Damsky et al., 1992).

I used flow cytometry to analyze surface expression of CTB-associated marker EGFR and EVT-specific marker HLA-G. One interesting and repeatable inconsistency was between the surface expression of these two markers in isolated vs. cultured cells. In freshly isolated cells, there were only EGFR single-positive cells, by definition CTB, and $EGFR^{low}$, HLA-G+ cells, by definition EVT. Once the isolated cells were plated, this profile changed. While some cells stayed EGFR single-positive, there was always an increase in HLA-G+ cells, particularly in hypoxia; however, the latter cells always co-expressed EGFR, at a similar level as the initially-isolated CTB. This EGFR/HLAG double positive population was mononuclear, consistent with the EVT phenotype. Additionally, MMP2 secretion, another marker of EVT differentiation, was found to be higher in hypoxia compared to normoxia. Conversely, hCG secretion was always significantly and drastically reduced in hypoxia, as were the number of multinucleated cells based on morphology (data not shown). Finally, gene expression profiling also showed that CTB cultured in hypoxia expressed many more EVT- than CTB-associated genes (46% vs. 1.3%). Therefore, while these results overwhelmingly support the enhancement of EVT differentiation in hypoxia, they show subtle, but important differences between isolated and *in vitro* cultured EVT, indicating that the current culture conditions are still suboptimal for this process.

I also evaluated the effect of hypoxia on trophoblast differentiation using hESC-derived CTB. Surface HLA-G expression and MMP2 secretion were both increased in hypoxia, while hCG secretion was decreased. These results clearly demonstrate that hESC-derived CTB are superior to the current human trophoblast cell lines, as the former behave similarly to primary CTB under low oxygen tension, with an increase in EVT differentiation, based on both marker expression and secretory function. Given

the lack of widespread access to early gestational age samples, these data would support the use of hESC to model EVT differentiation.

Gene ontology analysis of genes upregulated in hypoxia also show similar results in primary and hESC-derived CTB, with hypoxia as the most enriched group of genes (Figure 4.19A and Figure 4.19). In primary CTB, other enriched groups include actin-filament based processes and focal adhesion-associated genes, both of which have important functions in the invasive properties of these cells (Zhou et al., 2014; Ilić et al., 2001; MacPhee et al., 2001). Other gene groups enriched in hypoxia-treated cells also relate to migration and invasion of EVT, including regulation of anatomical structure morphogenesis, epithelial to mesenchymal transition, and cell junction organization (Pollheimer and Knöfler, 2005; DaSilva-Arnold et al., 2015). Hypoxia is known to induce epithelial-to-mesenchymal transition, a prominent feature of certain cancer stem cells, including breast cancer (Chen et al., 2015). Interestingly, I found that many of the genes enriched in both primary and hESC-derived CTB cultured under hypoxia belong to pathways of EMT, actin reorganization, and cell migration. These results demonstrate similarities between hypoxia-induced responses of trophoblast and cancer cells. Some gene groups are related to other hypoxia-induced functions including blood vessel development. In hESC-derived CTB, one gene group, “negative regulation of developmental processes,” was enriched, and included many sub-groups of genes associated with regulation of neurogenesis and neural development; this is consistent with the known effect of BMP4 on inhibition of neural differentiation of hESC (Mehler et al., 1997).

One interesting discrepancy between hypoxia-induced responses of primary and hESC-derived CTB, based on genome-wide expression profiling, was the

maintenance of expression of *ID2*. In hESC-derived CTB, the analysis showed that hypoxia upregulates expression of EVT genes, including *HLA-G* and *ITGA1,* but it also upregulates *ID2*, which is a CTB stem cell associated gen. However, *ID2* is downregulated with differentiation in primary CTB. One possible reason for this discrepancy may be timing of analysis: a previous study showed that first trimester CTB cultured in hypoxia for 12 hours upregulated *ID2* mRNA (Janatpour et al., 2000); my primary CTB experiments involved culture in hypoxia for 4 days and failed to show a difference in *ID2* expression. Another reason may be a more suboptimal culture condition for maintenance of primary, compared to hESC-derived, CTB. While optimized conditions for continuous self-renewal of these cells has not been achieved in either system, culture conditions for hESC-derived CTB might be slightly better, such that hypoxia may actually help to maintain the CTB stem cell state, as well as promote EVT differentiation, while primary isolated CTB immediately begin to terminally differentiate after plating. Our lab is currently working to optimize conditions for continuous self-renewal of both primary and hESC-derived CTB, and hypoxia will likely play a major role.

Most importantly, however, was the determination that hypoxia-mediated EVT differentiation was HIF-dependent. EVT are characterized by surface expression of HLA-G, and functionally, by their secretion of MMPs. Both these parameters (surface HLA-G expression and MMP2 secretion) were significantly reduced in hypoxia when HIF complex formation was disrupted, in both primary and hESC-derived CTB. Results of genome-wide expression profiling in scramble vs. shARNT between the two models were more variable. Overall, in both primary and hESC-derived CTB, 63-70% of hypoxia-induced genes were determined to be HIF complex-dependent. In primary

CTB, EVT-associated genes ITGA1 and ITGA5 were among the HIF complex-dependent group of genes, while other EVT-associated genes, including HLA-G and ASCL2, were among the minority of hypoxia-induced, but HIF-independent genes; nevertheless, the mean raw values of these two genes in scramble (HLA-G=7847, ASCL2=4935) compared to shARNT (HLA-G=6777, ASCL2=2353) in hypoxia did show a trend toward reduction in the absence of (and hence a partial dependence on) ARNT. In hESC-derived CTB, as well, HLA-G was among the HIF-dependent group of genes. Taken together, the gene expression profiling results in both primary CTB and hESC-dervied CTB suggest that hypoxia-induced EVT differentiation is in fact HIF complex-dependent.

Interestingly, in primary CTB, the reduction in hCG secretion in hypoxia is abrogated in the absence of ARNT; in fact, without ARNT, the amount of hCG secretion is similar in normoxia and hypoxia. This suggests that hypoxia-mediated repression of STB differentiation is dependent on the HIF complex, which is a novel and exciting finding. While previous studies had found hypoxia to blunt secretion of hCG in choriocarcinoma cells and isolated primary CTB (Strohmer et al., 1997; Esterman et al., 1996), my results are the first to show this effect to be HIF-dependent. It is well reported that HIF acts as a transcription factor to activate expression of target genes, however there is less known about possible repressive functions of HIF for target gene expression. A recent ChIP–chip study did not find an association between HIF binding and transcriptional downregulation (Mole et al., 2009). However, some exceptions have been reported, including one study which reported that HIF1α represses transcription of Estrogen Receptor 1 (ESR1) (Ryu et al., 2011). Additionally, HIF1α was found to

bind to and repress expression of CAD, a gene important in the first three steps of *de novo* pyrimidine biosynthesis (Chen et al., 2005).

Some possible mechanisms of HIF serving as a repressor could be that HIF indirectly promotes transcriptional repression of specific genes by controlling the expression of co-repressors. For example, one study found a novel HIF target, RCOR2, which is a known transcriptional repressor (Ortiz-Barahona et al., 2010). Another possible mechanism could be induction of microRNAs by hypoxia and HIF, resulting in downregulation of specific groups of genes, which has been reported (Kulshreshtha et al., 2007). Unlike primary CTB, hESC-derived CTB do not show hypoxia-induced repression of hCG secretion to be dependent on ARNT. While the etiology behind this discrepancy is unclear, the data show that the novel finding of HIF-dependent reduction of hCG secretion is best studied using primary CTB.

Gene ontology analysis of HIF-dependent genes showed that, in both primary and hESC-derived CTB, the hypoxia-associated gene group was most significantly enriched. Other significantly enriched groups present in both primary CTB and hESC-derived CTB included integrin signaling and EMT. This is similar to mouse trophoblast stem cells, which, in the absence of ARNT, show reduced adhesion and migration, along with altered expression of integrins in focal adhesions (Cowden Dahl et al., 2005).

In summary, my work has shown that hypoxia mediates differentiation of CTB into EVT and reduces differentiation into STB. This conclusion is based on gene expression analysis, as well as functional assays, including increased surface HLA-G expression, and increased MMP2 and reduced hCG secretion in hypoxia. The results were, for the most part, consistent between primary and hESC-derived CTB, while trophoblast cell lines did not show the same response to hypoxia. Finally, hypoxia-

directed increase in EVT differentiation was dependent on the ability to form an intact HIF complex; when this was disrupted by knockdown of the ARNT subunit, hypoxia did not induce EVT differentiation.

Future directions of this research will be to use the findings from the microarray-based gene expression analysis to find novel pathways of EVT differentiation. Currently, little is known about these pathways, as access to such primary tissue is highly limited. Further study of the list of HIF-dependent genes will be very useful in determining regulatory pathways in this important cell population. Specifically, the effect of ARNT knockdown on the invasive ability of EVT deserves further study, as the gene ontology analysis points to changes in focal adhesion and actin filament-based processes as being HIF-dependent.

Appendix A

Probe lists with fold change values

CTB HIF Dependent		
Probe_ID	**SYMBOL**	**Fold Change**
ILMN_1694589	PAQR8	2.93
ILMN_2128931	FAT2	2.79
ILMN_1767842	SLC17A8	2.78
ILMN_1807016	LHX2	2.55
ILMN_1801307	TNFSF10	2.07
ILMN_1778087	ANXA8	1.94
ILMN_1752478	DHRS3	1.89
ILMN_2228035	HS3ST1	1.87
ILMN_1664861	ID1	1.81
ILMN_1651717	ADAMTS20	1.78
ILMN_1670532	GMCL1	1.73
ILMN_1669928	ARHGEF16	1.72
ILMN_1702127	SPRR2G	1.72
ILMN_1750097	CLDN19	1.69
ILMN_1778226	EXTL3	1.68
ILMN_1713934	LITAF	1.67
ILMN_1746646	CHRM5	1.67
ILMN_1813386	CORO6	1.67
ILMN_2173004	RAB8B	1.67
ILMN_2194627	GMCL1	1.66
ILMN_1807106	LDHA	1.64
ILMN_3292163	LOC391532	1.63
ILMN_1694432	CRIP2	1.62
ILMN_1724495	SESTD1	1.62
ILMN_3242038	GPX8	1.62
ILMN_1799098	LOC652846	1.61
ILMN_2366463	FN1	1.61
ILMN_1746578	SLC23A2	1.6
ILMN_2095610	ANXA8	1.6
ILMN_2330341	TCEAL4	1.59
ILMN_1716815	CEACAM1	1.58
ILMN_1912083	HS.559604	1.58
ILMN_2109708	ECGF1	1.58
ILMN_1662741	EDG4	1.57
ILMN_1697268	EMILIN2	1.57
ILMN_2357062	IL1RAP	1.57
ILMN_1666078	HLA-H	1.56
ILMN_1748124	TSC22D3	1.56
ILMN_2079786	NUAK1	1.56
ILMN_2081682	SMAP2	1.56
ILMN_2178587	ANKRD6	1.56
ILMN_1804396	C14ORF4	1.55
ILMN_1668417	WASPIP	1.54
ILMN_1748625	TCEAL4	1.54
ILMN_1667626	EGLN3	1.53
ILMN_1813746	CORO2A	1.53
ILMN_1741755	TRIM29	1.52
ILMN_1743205	ABCA7	1.52
ILMN_1763382	NPPB	1.52
ILMN_1660871	NEK6	1.5
ILMN_1770290	CNN2	1.5
ILMN_1781155	LYN	1.5
ILMN_1689318	NUAK1	1.49
ILMN_1767665	LOC493869	1.49
ILMN_1771599	PLOD2	1.49
ILMN_1796013	PYCR1	1.49
ILMN_3240389	CPOX	1.49
ILMN_1748797	GRB2	1.48
ILMN_2148913	TMEM45A	1.48
ILMN_1732410	SLC16A9	1.47
ILMN_1743103	SH3PXD2A	1.47
ILMN_1798360	CXCR7	1.47
ILMN_2166457	HPGD	1.47
ILMN_2354381	PON2	1.47
ILMN_1707720	SLC1A5	1.46
ILMN_1730794	SERTAD4	1.46
ILMN_1762106	MMP2	1.46
ILMN_1767651	TECPR1	1.46
ILMN_1802411	ITGA1	1.46
ILMN_1675646	FN1	1.45
ILMN_1666845	KRT17	1.44
ILMN_1746673	3-Sep	1.44
ILMN_1779171	SGSM2	1.43
ILMN_1781386	WIPI1	1.43
ILMN_2371724	CEACAM1	1.43
ILMN_1703433	PLSCR3	1.42
ILMN_1752526	RNF144B	1.42
ILMN_1768577	PCSK6	1.42
ILMN_1776464	PARP4	1.42
ILMN_1836550	HS.440518	1.42
ILMN_1874689	HS.554507	1.42
ILMN_1733415	MFAP5	1.41
ILMN_1812392	TMSB10	1.41
ILMN_1713952	C1ORF106	1.4
ILMN_1716687	TPM1	1.4
ILMN_1781819	PAPSS1	1.4
ILMN_1803194	GALK1	1.4
ILMN_2360710	TPM1	1.4
ILMN_1739576	CYB5R2	1.39
ILMN_1764723	SH3PXD2B	1.39
ILMN_1798081	PTPRF	1.39
ILMN_1803819	IQGAP1	1.39
ILMN_2055156	PAG1	1.39
ILMN_2365307	CD276	1.39
ILMN_2386973	PKP2	1.39
ILMN_1676595	PCSK6	1.38
ILMN_1714567	AHNAK	1.38
ILMN_1735220	CAV2	1.38
ILMN_1859127	HS.190748	1.38
ILMN_2376403	TSC22D3	1.38
ILMN_1661589	CD151	1.37

ILMN_1668865	SLC2A14	1.37
ILMN_1707464	MST1	1.37
ILMN_1724994	COL4A2	1.37
ILMN_1735155	GLB1	1.37
ILMN_1740512	MGC39900	1.37
ILMN_1751656	KLF11	1.37
ILMN_1809931	NDRG1	1.37
ILMN_1815500	ITPR3	1.37
ILMN_3242004	ANXA8L1	1.37
ILMN_1653856	STS-1	1.36
ILMN_1707727	ANGPTL4	1.36
ILMN_1716382	LOC387882	1.36
ILMN_1758164	STC1	1.36
ILMN_1816244	HS.4988	1.36
ILMN_1838313	HS.538259	1.36
ILMN_3253456	FNDC3B	1.36
ILMN_2038775	TUBB2A	1.35
ILMN_2218935	GPR37	1.35
ILMN_2397721	GLB1	1.35
ILMN_2402341	MAPK3	1.35
ILMN_3273229	LOC100129781	1.35
ILMN_1665909	LASP1	1.34
ILMN_1667260	MAPK3	1.34
ILMN_1673820	HLTF	1.34
ILMN_1676891	CDC2L6	1.34
ILMN_1763447	PLXNB2	1.34
ILMN_1799139	PLOD2	1.34
ILMN_1807042	MARCKS	1.34
ILMN_2151541	DNAJC10	1.34
ILMN_2201678	FSTL1	1.34
ILMN_1741727	QPCT	1.33
ILMN_1749834	LOC388588	1.33
ILMN_1771019	MTMR4	1.33
ILMN_2070896	BMPR2	1.33
ILMN_2342240	MGAT2	1.33
ILMN_3243831	CAPN6	1.33
ILMN_1693334	P4HA1	1.32
ILMN_1697733	CST6	1.32
ILMN_1706426	DSTN	1.32
ILMN_1720858	C6ORF115	1.32
ILMN_1764927	CDC42EP1	1.32
ILMN_2153332	ATXN1	1.32
ILMN_2340052	NCOR2	1.32
ILMN_2350574	MYADM	1.32
ILMN_2374159	HERPUD1	1.32
ILMN_3246401	AIF1L	1.32
ILMN_1677404	RAP2A	1.31
ILMN_1677574	GALNT6	1.31
ILMN_1679391	MAMDC2	1.31
ILMN_1777261	FAM3C	1.31
ILMN_2180239	DOPEY2	1.31
ILMN_3300353	LOC729920	1.31
ILMN_1658835	CAV2	1.3
ILMN_1659990	C7ORF68	1.3
ILMN_1695276	MAPRE2	1.3
ILMN_1722753	GJA5	1.3
ILMN_1739423	RN7SK	1.3
ILMN_1781290	RHOA	1.3
ILMN_2374164	HERPUD1	1.3
ILMN_3178302	FNDC3B	1.3
ILMN_1681249	KIF21A	1.29
ILMN_1729288	C1QTNF6	1.29
ILMN_1781479	SUV39H1	1.29
ILMN_1787718	SLC27A1	1.29
ILMN_1799744	GALC	1.29
ILMN_1802252	GAPDH	1.29
ILMN_2278152	TPM1	1.29
ILMN_3241091	LOC100130886	1.29
ILMN_1652797	FAM174B	1.28
ILMN_1670305	SERPING1	1.28
ILMN_1685339	TPM1	1.28
ILMN_1703593	BAIAP2L1	1.28
ILMN_1732060	ARHGAP1	1.28
ILMN_1814917	TLE2	1.28
ILMN_2087702	MYH9	1.28
ILMN_2393450	C14ORF173	1.28
ILMN_3237946	LOC100134134	1.28
ILMN_3238058	LOC151162	1.28
ILMN_1653466	HES4	1.27
ILMN_1658044	LOC648814	1.27
ILMN_1673521	KISS1R	1.27
ILMN_1714586	VGLL3	1.27
ILMN_1722872	MYH9	1.27
ILMN_1733811	JUP	1.27
ILMN_1768534	BHLHB2	1.27
ILMN_1782050	CEBPD	1.27
ILMN_2405521	MTHFD2	1.27
ILMN_3249435	UBASH3B	1.27
ILMN_1682864	SPSB3	1.26
ILMN_1708095	PANK2	1.26
ILMN_1768505	IL13RA1	1.26
ILMN_1774982	CDC42EP5	1.26
ILMN_1785191	TMEM14A	1.26
ILMN_1805737	PFKP	1.26
ILMN_1652287	NOG	1.25
ILMN_1672589	SEMA4B	1.25
ILMN_1747223	FRYL	1.25
ILMN_2050911	SLC22A4	1.25
ILMN_2368773	FAM3C	1.25
ILMN_2414325	TNFAIP8	1.25
ILMN_3283772	LOC644237	1.25
ILMN_1677305	PVR	1.24
ILMN_1701461	TIMP3	1.24
ILMN_1703477	ARHGEF2	1.24

ILMN_1741176	CHMP2B	1.24
ILMN_1785330	SH3BP4	1.24
ILMN_1787885	NUDT18	1.24
ILMN_2090105	TAGLN2	1.24
ILMN_2128639	C10ORF47	1.24
ILMN_2149226	CAV1	1.24
ILMN_2323508	C9ORF58	1.24
ILMN_2342033	F11R	1.24
ILMN_2399896	SEC31A	1.24
ILMN_3244521	LOC283267	1.24
ILMN_3301749	SPNS2	1.24
ILMN_1713174	TCP11L1	1.23
ILMN_1751097	CREB3L2	1.23
ILMN_1752591	LEPROTL1	1.23
ILMN_1770922	TMEM45A	1.23
ILMN_1776522	RAG1AP1	1.23
ILMN_1780036	WDR1	1.23
ILMN_1784352	CCM2	1.23
ILMN_1814213	PQLC3	1.23
ILMN_1814998	FKSG30	1.23
ILMN_2069632	GTSF1	1.23
ILMN_2174612	CNOT8	1.23
ILMN_2195482	CACNB3	1.23
ILMN_2364022	SLC16A3	1.23
ILMN_3205656	LOC391075	1.23
ILMN_1659462	DUSP23	1.22
ILMN_1661599	DDIT4	1.22
ILMN_1664010	ELF1	1.22
ILMN_1683146	FTH1	1.22
ILMN_1691892	TAGLN2	1.22
ILMN_1768867	AP3B1	1.22
ILMN_1771026	GARS	1.22
ILMN_1815319	CMTM4	1.22
ILMN_1865764	HS.371609	1.22
ILMN_2094952	NUAK2	1.22
ILMN_2121282	MRPS18B	1.22
ILMN_1655163	STK24	1.21
ILMN_1656826	SH3RF1	1.21
ILMN_1667162	NKX3-1	1.21
ILMN_1689908	ANKRD13A	1.21
ILMN_1718961	BNIP3L	1.21
ILMN_1723467	ITGB1	1.21
ILMN_1728907	SCAMP1	1.21
ILMN_1731107	CCDC92	1.21
ILMN_1750158	ACOX1	1.21
ILMN_1755727	KDM5B	1.21
ILMN_1774836	PLOD3	1.21
ILMN_1801068	DACT1	1.21
ILMN_1803211	FBXO2	1.21
ILMN_1804663	THBS3	1.21
ILMN_1804929	OXTR	1.21
ILMN_1807662	IGF2R	1.21
ILMN_2045419	BNIP3L	1.21
ILMN_2143487	TAF1B	1.21
ILMN_2363658	PXDN	1.21
ILMN_2380163	PTPRF	1.21
ILMN_2404688	NUPR1	1.21
ILMN_1691410	BAMBI	1.2
ILMN_1696187	PYGL	1.2
ILMN_1700690	VAT1	1.2
ILMN_1755234	SSH3	1.2
ILMN_1760320	GNB1	1.2
ILMN_1762718	CMTM4	1.2
ILMN_1785265	PLS3	1.2
ILMN_1793672	SIX5	1.2
ILMN_2220739	TMCO3	1.2
ILMN_2224907	C4ORF34	1.2
ILMN_3253304	BRI3P1	1.2
ILMN_1343295	GAPDH	1.19
ILMN_1662340	ZNF358	1.19
ILMN_1671265	ING2	1.19
ILMN_1710216	AVEN	1.19
ILMN_1727043	GLT25D1	1.19
ILMN_2139761	LIMCH1	1.19
ILMN_2328094	DACT1	1.19
ILMN_2378952	GPX4	1.19
ILMN_2386444	ANGPTL4	1.19
ILMN_3228585	LOC728661	1.19
ILMN_1686750	MGEA5	1.18
ILMN_1690122	CRKL	1.18
ILMN_1698419	NCOR2	1.18
ILMN_1714820	ITGB1	1.18
ILMN_1738816	FOXO1	1.18
ILMN_1745954	CORO1C	1.18
ILMN_1786976	RAB22A	1.18
ILMN_1792679	ITGA5	1.18
ILMN_1793616	RNF38	1.18
ILMN_1797604	CAP1	1.18
ILMN_2364131	TTPAL	1.18
ILMN_2364674	TRPT1	1.18
ILMN_3241441	MEGF6	1.18
ILMN_1664068	ERGIC1	1.17
ILMN_1674650	C9ORF95	1.17
ILMN_1701875	ZYX	1.17
ILMN_1721204	CSF2RA	1.17
ILMN_1721344	MOBKL2A	1.17
ILMN_1725534	ACTN4	1.17
ILMN_1727479	TPRG1L	1.17
ILMN_1727524	ADAM9	1.17
ILMN_1730491	FMNL2	1.17
ILMN_1738759	PIGT	1.17
ILMN_1745962	FBXO7	1.17
ILMN_1750144	C3ORF19	1.17
ILMN_1753101	VTCN1	1.17

ILMN_1769546	RIN2	1.17
ILMN_1770803	BNIP2	1.17
ILMN_1806432	NT5C	1.17
ILMN_1808501	SH3KBP1	1.17
ILMN_2038777	ACTB	1.17
ILMN_2038778	GAPDH	1.17
ILMN_2041788	PLS3	1.17
ILMN_2197519	ZNF627	1.17
ILMN_1698605	TMEM43	1.16
ILMN_1743711	LOC650215	1.16
ILMN_1750101	S100A11	1.16
ILMN_1810782	SH3KBP1	1.16
ILMN_2205896	MEIS3P1	1.16
ILMN_2390162	PHF11	1.16
ILMN_3238859	FAM120AOS	1.16
ILMN_1669617	GRB10	1.15
ILMN_1701514	TRAF3IP2	1.15
ILMN_1740171	DUSP11	1.15
ILMN_1765880	C16ORF57	1.15
ILMN_1766054	ABCA1	1.15
ILMN_1802456	DCTD	1.15
ILMN_1810387	PLAA	1.15
ILMN_1811592	ARHGAP21	1.15
ILMN_1811909	LOC402221	1.15
ILMN_1813669	ANKS1A	1.15
ILMN_1815303	LOC642197	1.15
ILMN_3226045	LOC728533	1.15
ILMN_3241218	ANKIB1	1.15
ILMN_3284114	LOC399748	1.15
ILMN_1658182	MEX3C	1.14
ILMN_1675124	DDX17	1.14
ILMN_1703335	LACTB	1.14
ILMN_1710326	CLDND1	1.14
ILMN_1713290	GLT8D1	1.14
ILMN_1739840	LRRC8A	1.14
ILMN_1763694	RSPRY1	1.14
ILMN_1776723	PHF11	1.14
ILMN_1811702	GRN	1.14
ILMN_2074860	RN7SK	1.14
ILMN_2170949	SNX10	1.14
ILMN_2381697	P4HA2	1.14
ILMN_2383934	ITGB1	1.14
ILMN_1653180	TPM4	1.13
ILMN_1653429	SLC35A3	1.13
ILMN_1673682	GATAD2A	1.13
ILMN_1678075	CDYL	1.13
ILMN_1691499	TJP1	1.13
ILMN_1702636	TUBB6	1.13
ILMN_1712400	SERPINB6	1.13
ILMN_1732967	KIAA1949	1.13
ILMN_1734895	SFT2D1	1.13
ILMN_1735347	MCEE	1.13
ILMN_1739050	PIPOX	1.13
ILMN_1750969	C9ORF10OS	1.13
ILMN_1765109	TNFRSF25	1.13
ILMN_1804854	CTNNA1	1.13
ILMN_1811574	MAPK8IP3	1.13
ILMN_2085722	ING2	1.13
ILMN_2364376	ILK	1.13
ILMN_1667519	RRAS2	1.12
ILMN_1673566	ADAMTS1	1.12
ILMN_1674706	MTHFD2	1.12
ILMN_1677396	NDFIP2	1.12
ILMN_1680314	TXN	1.12
ILMN_1723486	HK2	1.12
ILMN_1729237	CYB5R1	1.12
ILMN_1752923	IFNAR1	1.12
ILMN_1756982	CLIC1	1.12
ILMN_1761159	ESYT1	1.12
ILMN_1803277	MVP	1.12
ILMN_2177090	LOC200030	1.12
ILMN_2339627	COPE	1.12
ILMN_2352563	CLDND1	1.12
ILMN_3241758	POTEF	1.12
ILMN_3256325	CYB561D1	1.12
ILMN_1651719	MBTPS1	1.11
ILMN_1654262	ZMAT3	1.11
ILMN_1665049	SPG11	1.11
ILMN_1665428	GSDMD	1.11
ILMN_1685480	TARS	1.11
ILMN_1740351	KIAA0174	1.11
ILMN_1760676	MORF4L1	1.11
ILMN_1771957	MAN1B1	1.11
ILMN_1778240	GFOD1	1.11
ILMN_1810560	P8	1.11
ILMN_1813836	DARS	1.11
ILMN_2174394	MMS19L	1.11
ILMN_2376458	CSF2RA	1.11
ILMN_1684594	USP24	1.1
ILMN_1684771	PGRMC1	1.1
ILMN_1729563	UGDH	1.1
ILMN_1743432	DGUOK	1.1
ILMN_1752837	ARL8B	1.1
ILMN_1754738	AP1M1	1.1
ILMN_1781580	BRI3	1.1
ILMN_1783695	EPRS	1.1
ILMN_1787808	CEP63	1.1
ILMN_2188722	GLS	1.1
ILMN_2326071	MYL6	1.1
ILMN_2367469	CARS	1.1
ILMN_1685005	TNFRSF1A	1.09
ILMN_1691432	PRDM4	1.09
ILMN_1699489	TUBB6	1.09
ILMN_1720708	CSNK1D	1.09

ILMN_1772981	EPN1	1.09
ILMN_2076463	SLC15A4	1.09
ILMN_2096719	GRK5	1.09
ILMN_2152131	ACTB	1.09
ILMN_2186983	ANXA8L2	1.09
ILMN_2315979	LBH	1.09
ILMN_2361695	BAG5	1.09
ILMN_2412807	DCTN1	1.09
ILMN_3225300	LOC728532	1.09
ILMN_1671791	PCK2	1.08
ILMN_1682449	ZNF518B	1.08
ILMN_1691884	STC2	1.08
ILMN_1693338	CYP1B1	1.08
ILMN_1699496	PHF21A	1.08
ILMN_1727023	AMMECR1L	1.08
ILMN_1759252	ADD1	1.08
ILMN_1766024	PDCD10	1.08
ILMN_1796245	DNASE2	1.08
ILMN_1807994	PCNP	1.08
ILMN_1814113	ZFR	1.08
ILMN_2038776	TXN	1.08
ILMN_2163723	KRT7	1.08
ILMN_2386008	MPZL1	1.08
ILMN_2403237	CHN2	1.08
ILMN_1651735	TGOLN2	1.07
ILMN_1668507	DDAH1	1.07
ILMN_1671583	MKRN1	1.07
ILMN_1679919	ASCC2	1.07
ILMN_1714364	PTK2	1.07
ILMN_1772521	MTHFD1L	1.07
ILMN_1777881	TSPAN17	1.07
ILMN_1777906	RPRC1	1.07
ILMN_1778557	CDC2L5	1.07
ILMN_1789492	ZDHHC8	1.07
ILMN_1812297	CYP26B1	1.07
ILMN_2222074	PTPN12	1.07
ILMN_2353033	FUBP3	1.07
ILMN_2356031	RNF121	1.07
ILMN_2386818	URG4	1.07
ILMN_3282768	LOC644879	1.07
ILMN_1655922	SAPS2	1.06
ILMN_1666976	PLD3	1.06
ILMN_1697420	TINF2	1.06
ILMN_1699226	UBR4	1.06
ILMN_1705310	VEZF1	1.06
ILMN_1708604	C7ORF28A	1.06
ILMN_1718866	C5ORF46	1.06
ILMN_1731181	TEX2	1.06
ILMN_1750079	PURB	1.06
ILMN_1786388	RNF113A	1.06
ILMN_3200414	LOC441131	1.06
ILMN_1665877	RNF149	1.05
ILMN_1689378	CCRN4L	1.05
ILMN_1706706	WDR68	1.05
ILMN_1740010	PCNX	1.05
ILMN_1757781	SAP30L	1.05
ILMN_1795778	P4HA2	1.05
ILMN_2175465	RSL24D1	1.05
ILMN_1661264	SHMT2	1.04
ILMN_1669657	LOC440345	1.04
ILMN_1687519	SNAP23	1.04
ILMN_1747673	RASL10A	1.04
ILMN_1766539	LOC643319	1.04
ILMN_1786972	SARS	1.04
ILMN_1798061	ZFYVE26	1.04
ILMN_1659888	PPP1R14B	1.03
ILMN_1683859	SLC7A1	1.03
ILMN_1687583	CAV1	1.03
ILMN_1694742	RPS29	1.03
ILMN_1706505	COL5A1	1.03
ILMN_1707312	NFIL3	1.03
ILMN_1712678	RPS27L	1.03
ILMN_1715693	LOC440160	1.03
ILMN_1718863	KCNK1	1.03
ILMN_1726565	PIK3R2	1.03
ILMN_1793371	KIAA0430	1.03
ILMN_1801383	SMG1	1.03
ILMN_2390227	TBC1D9B	1.03
ILMN_2409167	ANXA2	1.03
ILMN_3241870	FRMD8	1.03
ILMN_1659845	KIAA0355	1.02
ILMN_1661650	SMEK2	1.02
ILMN_1711227	GMDS	1.02
ILMN_1733538	RGS10	1.02
ILMN_1790807	XPC	1.02
ILMN_2232177	ACTN1	1.02
ILMN_2352023	RIPK5	1.02
ILMN_3299365	LOC729406	1.02
ILMN_1655418	CAPNS1	1.01
ILMN_1664016	ARHGEF18	1.01
ILMN_1683127	ZNF281	1.01
ILMN_1713322	C7ORF28B	1.01
ILMN_1778236	PTPN11	1.01
ILMN_1778668	TAGLN	1.01
ILMN_1803392	TAX1BP3	1.01
ILMN_1808404	RHBDF1	1.01
ILMN_2337655	WARS	1.01
ILMN_2401978	STAT3	1.01
ILMN_3240117	AIDA	1.01
ILMN_1804673	SLC16A4	1
ILMN_2195236	PGRMC2	1
ILMN_2400935	TAGLN	1
ILMN_1657797	FIBP	-1
ILMN_1777811	URG4	-1

ILMN_1815445	IDS	-1
ILMN_1661628	LOC653110	-1.01
ILMN_1672128	ATF4	-1.01
ILMN_1673363	CD97	-1.01
ILMN_1678766	DYNLT1	-1.01
ILMN_1692938	PSAT1	-1.01
ILMN_1770977	TMEM134	-1.01
ILMN_1778673	GOLGA7	-1.01
ILMN_1799614	PNPLA6	-1.01
ILMN_2071641	KCNK1	-1.01
ILMN_1715994	HGS	-1.02
ILMN_1739876	RAB3GAP1	-1.02
ILMN_1767816	APH1B	-1.02
ILMN_1801822	C18ORF25	-1.02
ILMN_2047511	CENTA1	-1.02
ILMN_3297577	LOC729841	-1.02
ILMN_1659027	SLC2A1	-1.03
ILMN_1678140	TTC4	-1.03
ILMN_1678961	FRMD4A	-1.03
ILMN_1694671	ZFAND2A	-1.03
ILMN_1664956	SSU72	-1.04
ILMN_1720270	CDR2	-1.04
ILMN_2085236	SNX24	-1.04
ILMN_2311761	AP3S1	-1.04
ILMN_3230880	BEND7	-1.04
ILMN_1726981	VEGFB	-1.05
ILMN_1799890	ZFYVE20	-1.05
ILMN_2146418	CRIM1	-1.05
ILMN_2318643	TGIF1	-1.05
ILMN_3206390	LOC727808	-1.05
ILMN_3305273	LOC729779	-1.05
ILMN_1659415	MAP2K1IP1	-1.06
ILMN_1705231	SLCO2A1	-1.06
ILMN_1726169	EDF1	-1.06
ILMN_1745620	KRCC1	-1.06
ILMN_1758398	GUK1	-1.06
ILMN_1766851	TMEM126B	-1.06
ILMN_2397750	IVNS1ABP	-1.06
ILMN_3288587	LOC100131785	-1.06
ILMN_1741954	SMYD3	-1.08
ILMN_1757074	GNG10	-1.08
ILMN_1655429	TNFAIP1	-1.09
ILMN_1717877	IVNS1ABP	-1.09
ILMN_1805161	LZTR1	-1.09
ILMN_2398107	ASNS	-1.09
ILMN_1736939	UGCG	-1.1
ILMN_1733746	REEP1	-1.11
ILMN_2077905	PTGFRN	-1.11
ILMN_1743130	PTGFRN	-1.12
ILMN_1796417	ASNS	-1.13
ILMN_1666178	TP53I13	-1.14
ILMN_1730568	ZDHHC7	-1.15
ILMN_1772286	OCIAD2	-1.15
ILMN_1656369	C8ORF4	-1.16
ILMN_1774604	PNKD	-1.17
ILMN_1787815	TRIB3	-1.22
ILMN_2394250	PLEKHA1	-1.23
ILMN_1752249	FAM38A	-1.25
ILMN_1661733	FOLR1	-1.3
ILMN_2346339	FOLR1	-1.32
ILMN_1699265	TNFRSF10B	-1.34
ILMN_1700306	OCIAD2	-1.45
ILMN_1667295	VASN	-1.74
ILMN_1665792	ITGA2	-1.87

CTB HIF Independent		
Probe_ID	**SYMBOL**	**Fold Change**
ILMN_1711988	KCNK12	5.58
ILMN_1723412	ASCL2	4.31
ILMN_1651282	COL17A1	3.72
ILMN_1678833	CCR1	3.01
ILMN_2396875	IGFBP3	2.98
ILMN_2149164	SFRP1	2.94
ILMN_1662795	CA2	2.87
ILMN_1744455	NOTUM	2.87
ILMN_2166275	NOTUM	2.85
ILMN_1746085	IGFBP3	2.65
ILMN_1718629	NRIP1	2.56
ILMN_1760315	VWCE	2.56
ILMN_1697189	PNCK	2.54
ILMN_1656670	HLA-G	2.53
ILMN_1827736	HS.296031	2.52
ILMN_1685441	ASAP3	2.5
ILMN_1788538	NCALD	2.5
ILMN_2199439	CA2	2.47
ILMN_1653026	PLAC8	2.44
ILMN_1685580	CBLB	2.38
ILMN_1712673	SASH1	2.38
ILMN_1730777	KRT19	2.37
ILMN_1745785	NR2F2	2.34
ILMN_1767448	LHFP	2.31
ILMN_1675656	PPFIBP2	2.28
ILMN_1753312	PLXDC2	2.28
ILMN_2093343	PLAC8	2.27
ILMN_1773002	LOC730417	2.24
ILMN_1705442	CMTM3	2.22
ILMN_1730670	FSTL3	2.22
ILMN_2400219	SRI	2.22
ILMN_2413956	IGF2	2.2
ILMN_1791840	RALBP1	2.19
ILMN_2250521	INS-IGF2	2.15
ILMN_2371053	EFNA1	2.15
ILMN_2371055	EFNA1	2.14
ILMN_1775708	SLC2A3	2.13
ILMN_2185984	SASH1	2.1
ILMN_1699525	SRI	2.06
ILMN_1699867	IGF2	2.05
ILMN_1762561	PLA2G10	2.05
ILMN_1658015	MBNL2	2.03
ILMN_1753823	IL17D	2.03
ILMN_1849013	HS.570988	2.03
ILMN_2226304	ANKRD50	2.03
ILMN_1724040	ANKRD57	2.02
ILMN_1735445	SLC7A9	2.02
ILMN_1764964	IFNGR2	2.02
ILMN_1682054	SRI	2.01
ILMN_2323944	FAM110A	1.98
ILMN_1811272	GPR81	1.97
ILMN_2115669	SEMA4C	1.96
ILMN_1708167	CDCP1	1.92
ILMN_1701998	AFAP1	1.91
ILMN_1799105	COL17A1	1.91
ILMN_1652082	ELF4	1.89
ILMN_1838655	HS.151692	1.88
ILMN_2364272	MBNL2	1.88
ILMN_1815745	SOX4	1.87
ILMN_1673177	THSD3	1.86
ILMN_1726928	TCEA3	1.86
ILMN_1748105	DDB1	1.84
ILMN_1761463	EFHD2	1.84
ILMN_3269849	ISM2	1.83
ILMN_1678143	ARHGDIB	1.82
ILMN_1751227	LOC401321	1.81
ILMN_1776582	PDK3	1.79
ILMN_1709683	RASSF2	1.78
ILMN_1668411	FHL2	1.77
ILMN_2361862	VLDLR	1.77
ILMN_3233179	LOC728969	1.77
ILMN_3261938	LOC100130154	1.77
ILMN_1669033	NCOA1	1.75
ILMN_1654563	EFNB1	1.74
ILMN_1756920	ADAM15	1.74
ILMN_1671404	SVIL	1.73
ILMN_1695763	PDIA5	1.73
ILMN_1747281	EVI5L	1.73
ILMN_1782095	C20ORF55	1.72
ILMN_2405264	THSD3	1.72
ILMN_3243366	C2ORF55	1.72
ILMN_1812666	DNAJC15	1.71
ILMN_2228732	CCNG2	1.71
ILMN_1686884	IL1RAP	1.68
ILMN_1813753	PTN	1.68
ILMN_1660749	ASPSCR1	1.67
ILMN_1674640	CXCR6	1.67
ILMN_1714158	PON2	1.67
ILMN_1776121	MGC42367	1.67
ILMN_1796339	PLEKHA2	1.67
ILMN_1704353	IGSF3	1.66
ILMN_1768197	ROD1	1.66
ILMN_3249748	LDHA	1.66
ILMN_1752455	DOCK5	1.64
ILMN_1672834	SSH2	1.63
ILMN_1745130	RBM9	1.63
ILMN_3307892	PARVA	1.63
ILMN_1703374	NAV1	1.62
ILMN_1727315	DENND1A	1.62
ILMN_2099301	UNC84B	1.62
ILMN_1669268	MEX3D	1.61

ILMN_1713751	ADAM19	1.61
ILMN_1778237	FN1	1.61
ILMN_1658706	ST6GALNAC2	1.6
ILMN_1674941	ANO6	1.59
ILMN_1664922	FLNB	1.58
ILMN_1666156	MORF4L2	1.58
ILMN_1669497	OSBPL10	1.58
ILMN_1862070	HS.189987	1.58
ILMN_1661299	TLE6	1.57
ILMN_2355831	FHL2	1.57
ILMN_1802808	LOC654103	1.56
ILMN_1808299	IQSEC1	1.55
ILMN_2398403	TCEAL1	1.55
ILMN_3195198	KRT17P3	1.55
ILMN_1684227	GPR146	1.54
ILMN_1759023	WFS1	1.54
ILMN_1766045	SH3GLB1	1.54
ILMN_2313926	CDC42SE2	1.53
ILMN_1678962	DFFB	1.52
ILMN_1755643	MGAT4A	1.52
ILMN_1806015	LOC391045	1.52
ILMN_1719661	SEPX1	1.51
ILMN_1796912	ARHGEF7	1.51
ILMN_3294365	LOC646993	1.51
ILMN_1698732	PALLD	1.5
ILMN_2226324	BRP44L	1.5
ILMN_1659953	3-Sep	1.49
ILMN_2128668	FOXJ3	1.49
ILMN_1683817	UBE2Q2	1.48
ILMN_1793384	JAK1	1.48
ILMN_1715969	SLC25A37	1.47
ILMN_1815023	PIM1	1.47
ILMN_1656934	REPS2	1.46
ILMN_1671891	PID1	1.46
ILMN_1676563	HTRA1	1.46
ILMN_1684440	PXN	1.46
ILMN_1707434	LOC653778	1.46
ILMN_1761858	MID1	1.46
ILMN_1663541	B4GALT7	1.45
ILMN_2402600	GLIS3	1.45
ILMN_1687592	WWC3	1.44
ILMN_1728083	EIF4EBP2	1.44
ILMN_1741148	ALDOA	1.44
ILMN_2396546	IGSF3	1.44
ILMN_1786021	PRKAB2	1.43
ILMN_1810729	UBL3	1.43
ILMN_3247223	TPBG	1.43
ILMN_1661500	B4GALT4	1.42
ILMN_1696127	KIAA0240	1.42
ILMN_1704369	LIMA1	1.42
ILMN_3176090	LOC100130919	1.42
ILMN_1653028	COL4A1	1.41
ILMN_1698666	CST6	1.41
ILMN_1754600	FNBP1L	1.4
ILMN_1810584	IL1R1	1.4
ILMN_3202863	LOC389662	1.4
ILMN_3236259	PPIAL4A	1.4
ILMN_1766185	AXIN1	1.39
ILMN_1672547	MYO9B	1.38
ILMN_1737314	BCL6	1.38
ILMN_1747119	FBXO46	1.38
ILMN_2089977	FKBP9L	1.38
ILMN_1704446	SLC6A10P	1.37
ILMN_1749109	PSAP	1.37
ILMN_1862217	HS.532698	1.37
ILMN_3220861	LOC729952	1.37
ILMN_1658425	DAG1	1.36
ILMN_1790518	PHF16	1.36
ILMN_2308849	MYADM	1.35
ILMN_3260715	CRTC3	1.35
ILMN_1653828	CHFR	1.34
ILMN_1678671	KLHL24	1.34
ILMN_1670130	ARID3A	1.33
ILMN_1688127	LOC341457	1.33
ILMN_1792508	TMEM59	1.33
ILMN_2360784	RRBP1	1.33
ILMN_1653134	TMEM188	1.32
ILMN_1683664	LOC650369	1.32
ILMN_3213792	LOC439953	1.32
ILMN_1717706	PLK2	1.31
ILMN_1763347	PIK3CB	1.31
ILMN_1787919	PARVB	1.31
ILMN_2355559	PSAP	1.31
ILMN_2373177	PANK2	1.31
ILMN_1709880	RPLP0	1.3
ILMN_1731648	FOXJ2	1.3
ILMN_2388466	TIA1	1.3
ILMN_1733931	PDCD6	1.29
ILMN_1769412	RAPGEF1	1.29
ILMN_1786211	HERC1	1.29
ILMN_1812721	LOC728014	1.29
ILMN_2393994	CSPP1	1.29
ILMN_1758214	RARS2	1.28
ILMN_1734316	YME1L1	1.27
ILMN_1755749	PGK1	1.27
ILMN_1763127	CCBP2	1.27
ILMN_1771987	SLC44A2	1.27
ILMN_1782954	HIP2	1.27
ILMN_1810037	RUSC2	1.27
ILMN_3272603	FAM60A	1.27
ILMN_1666924	PINK1	1.26
ILMN_1807455	DHRS7	1.26
ILMN_1678629	DOCK7	1.25
ILMN_1811615	COPA	1.25

ILMN_2304624	EIF4H	1.25
ILMN_3251341	TUBA1C	1.25
ILMN_1734312	GCN1L1	1.24
ILMN_1779258	LOC644774	1.24
ILMN_1722276	PAFAH1B1	1.23
ILMN_1768449	PRPSAP1	1.23
ILMN_1792489	ARPC2	1.23
ILMN_1713892	C4ORF34	1.22
ILMN_1779828	EDEM1	1.22
ILMN_3199780	LOC401076	1.22
ILMN_1661002	RFWD2	1.21
ILMN_1676548	BZW2	1.21
ILMN_1724700	RIOK3	1.21
ILMN_1737146	TRAM1	1.21
ILMN_3241234	LOC730278	1.21
ILMN_1654939	TMED2	1.2
ILMN_1705064	NDEL1	1.2
ILMN_2329958	ABI1	1.2
ILMN_1678922	HERC4	1.19
ILMN_1705617	CFL1	1.19
ILMN_1719039	UBE2G1	1.19
ILMN_1745076	CLINT1	1.19
ILMN_1773847	DYNC1I2	1.19
ILMN_2344204	PRR13	1.19
ILMN_1714527	VAMP3	1.18
ILMN_1734486	C1ORF19	1.18
ILMN_2408001	RFWD2	1.18
ILMN_1653266	DNAJB14	1.17
ILMN_1666893	TRIML2	1.17
ILMN_1673944	MANBAL	1.17
ILMN_1774547	MPRIP	1.17
ILMN_1788062	SH3GL1	1.17
ILMN_1733511	GOLGA3	1.16
ILMN_1758906	GNA13	1.16
ILMN_2321416	DIAPH1	1.15
ILMN_2230902	CTNNA1	1.11
ILMN_1706521	CSNK1G2	1.09
ILMN_1689004	TNFRSF12A	-1.63
ILMN_1744381	SERPINE1	-1.73

hESC-derived HIF Dependent		
Probe_ID	**SYMBOL**	**Fold Change**
ILMN_2099277	HTRA4	2.58
ILMN_2206746	BGN	1.64
ILMN_1656670	HLA-G	1.63
ILMN_1747759	WSB1	1.57
ILMN_1786021	PRKAB2	1.54
ILMN_1706643	COL6A3	1.51
ILMN_1735347	MCEE	1.5
ILMN_3287996	LOC400446	1.41
ILMN_1757877	HCFC1R1	1.39
ILMN_1798975	EGFR	1.37
ILMN_1806320	PPFIBP1	1.37
ILMN_2336595	ACSS2	1.37
ILMN_1786388	RNF113A	1.36
ILMN_1793990	ID2	1.36
ILMN_2063584	CLIC4	1.35
ILMN_1697448	TXNIP	1.34
ILMN_2132982	IGFBP5	1.34
ILMN_1654915	LOC646786	1.33
ILMN_1675612	BLCAP	1.33
ILMN_1736700	ALDOA	1.33
ILMN_1803686	ADA	1.33
ILMN_1775823	POFUT2	1.3
ILMN_1756326	CKS2	1.29
ILMN_1760556	C1ORF63	1.29
ILMN_2198515	ARRDC3	1.29
ILMN_2404049	RBM38	1.29
ILMN_1706051	PLD5	1.28
ILMN_1725193	IGFBP2	1.28
ILMN_1793474	INSIG1	1.28
ILMN_2224907	C4ORF34	1.28
ILMN_2232712	MYO10	1.28
ILMN_2307861	COL6A3	1.28
ILMN_1734190	TCEAL3	1.27
ILMN_1755392	HERV-FRD	1.27
ILMN_1779258	LOC644774	1.27
ILMN_2097410	DAPP1	1.27
ILMN_1664802	WSB1	1.26
ILMN_1794863	CAMK2N1	1.26
ILMN_1722218	MBOAT7	1.25
ILMN_1773459	SOX11	1.25
ILMN_1791097	RSBN1	1.25
ILMN_2190414	ZNF83	1.25
ILMN_3299558	SFRS18	1.25
ILMN_1680132	CADM1	1.24
ILMN_1694219	ARIH1	1.24
ILMN_1767665	LOC493869	1.24
ILMN_1774074	RXRB	1.24
ILMN_2320336	CLK3	1.24
ILMN_2347068	MKNK2	1.24
ILMN_2366634	PKM2	1.24
ILMN_1343295	GAPDH	1.23
ILMN_1652753	PAAF1	1.23
ILMN_1672503	DPYSL2	1.23
ILMN_1672843	FBXO8	1.23
ILMN_1713449	TBX3	1.23
ILMN_1757467	H1F0	1.23
ILMN_1797342	FNBP1	1.23
ILMN_1814204	C21ORF55	1.23
ILMN_1879482	HS.560732	1.23
ILMN_2371053	EFNA1	1.23
ILMN_1678842	THBS2	1.22
ILMN_1685289	C16ORF58	1.22
ILMN_1686750	MGEA5	1.22
ILMN_1722713	FBLN1	1.22
ILMN_1775111	SND1	1.22
ILMN_1788184	CIDEA	1.22
ILMN_2062381	LCOR	1.22
ILMN_1671583	MKRN1	1.21
ILMN_1672536	FBLN1	1.21
ILMN_1676611	PHPT1	1.21
ILMN_2404063	APP	1.21
ILMN_1656482	OSBPL2	1.2
ILMN_1661366	PGAM1	1.2
ILMN_1700268	QPRT	1.2
ILMN_1706376	OSBP	1.2
ILMN_1715175	MET	1.2
ILMN_1789186	OBFC1	1.2
ILMN_1800659	PGM1	1.2
ILMN_2116127	NPEPPS	1.2
ILMN_1682953	PGAM4	1.19
ILMN_1688702	PJA2	1.19
ILMN_1699856	RALGDS	1.19
ILMN_1741942	STX16	1.19
ILMN_1755749	PGK1	1.19
ILMN_1787378	ADD3	1.19
ILMN_2056032	CD99	1.19
ILMN_3200921	LOC642590	1.19
ILMN_3244110	FAM156B	1.19
ILMN_1651498	GADD45G	1.18
ILMN_1682054	SRI	1.18
ILMN_1684114	LOC286016	1.18
ILMN_1692962	CTDSP2	1.18
ILMN_1728180	CROP	1.18
ILMN_1763390	ISL1	1.18
ILMN_1775327	PKM2	1.18
ILMN_1799139	PLOD2	1.18
ILMN_2165867	DHCR7	1.18
ILMN_2357386	FKTN	1.18
ILMN_3247895	LOC728188	1.18
ILMN_1655952	FAM39E	1.17
ILMN_1670134	FADS1	1.17

ILMN_1741613	SERINC1	1.17
ILMN_1745415	BBX	1.17
ILMN_1749915	C1ORF63	1.17
ILMN_1781942	HMMR	1.17
ILMN_1792305	ZNF318	1.17
ILMN_2376458	CSF2RA	1.17
ILMN_2406132	LILRB3	1.17
ILMN_1699071	C21ORF7	1.16
ILMN_1700025	LOC732007	1.16
ILMN_1741204	KLHDC2	1.16
ILMN_1803647	FAM162A	1.16
ILMN_1807074	MIF	1.16
ILMN_2041293	SQLE	1.16
ILMN_2175075	SFRS4	1.16
ILMN_2399896	SEC31A	1.16
ILMN_3244019	LOC647886	1.16
ILMN_1665510	ERRFI1	1.15
ILMN_1672611	CDH11	1.15
ILMN_1699703	ARCN1	1.15
ILMN_1702447	IGF2BP2	1.15
ILMN_1708805	NCOA3	1.15
ILMN_1711270	SFRS14	1.15
ILMN_1712975	YIF1A	1.15
ILMN_1725862	USP3	1.15
ILMN_1752631	CGGBP1	1.15
ILMN_1770936	COQ5	1.15
ILMN_1772261	GLG1	1.15
ILMN_1784540	KBTBD2	1.15
ILMN_2053103	SLC40A1	1.15
ILMN_1672878	ABR	1.14
ILMN_1748840	CALB2	1.14
ILMN_1773741	GOLGA5	1.14
ILMN_1803194	GALK1	1.14
ILMN_1815745	SOX4	1.14
ILMN_2050023	CCDC23	1.14
ILMN_2118472	C10ORF58	1.14
ILMN_2306189	MAGED1	1.14
ILMN_3214893	LOC100132761	1.14
ILMN_3246805	LOC100134364	1.14
ILMN_3292551	LOC286157	1.14
ILMN_1663042	SDC4	1.13
ILMN_1713037	PFKL	1.13
ILMN_1724959	SEC31A	1.13
ILMN_1788538	NCALD	1.13
ILMN_2117716	SFRS17A	1.13
ILMN_2195482	CACNB3	1.13
ILMN_2376263	SMARCA1	1.13
ILMN_3235379	LOC100134265	1.13
ILMN_3292163	LOC391532	1.13
ILMN_3305475	LOC729708	1.13
ILMN_1668861	LOC732165	1.12
ILMN_1670130	ARID3A	1.12
ILMN_1684628	ZFP90	1.12
ILMN_1739441	GANAB	1.12
ILMN_1749345	STX5	1.12
ILMN_2181191	TPI1	1.12
ILMN_1674421	TM9SF4	1.11
ILMN_1699112	COPB1	1.11
ILMN_1714108	TP53INP1	1.11
ILMN_1773427	KANK1	1.11
ILMN_2232166	CCDC90B	1.11
ILMN_3302919	MYOF	1.11
ILMN_1694539	MAP3K6	1.1
ILMN_1724040	ANKRD57	1.1
ILMN_1784113	NAT14	1.1
ILMN_1655340	RNF181	1.09
ILMN_1661636	ZMYM2	1.09
ILMN_1671731	AVPI1	1.09
ILMN_1684446	SPAG7	1.09
ILMN_1700541	FBLN1	1.09
ILMN_1717219	C7ORF70	1.09
ILMN_1724504	SETD3	1.09
ILMN_1725090	CTHRC1	1.09
ILMN_1733110	RASSF7	1.09
ILMN_1763694	RSPRY1	1.09
ILMN_1769091	PRCP	1.09
ILMN_1777740	C8ORF55	1.09
ILMN_2112417	PGAM1	1.09
ILMN_2355665	MTP18	1.09
ILMN_1654545	CPSF1	1.08
ILMN_1657283	ALKBH5	1.08
ILMN_1710815	FBLN1	1.08
ILMN_1717990	CALD1	1.08
ILMN_1738866	DEXI	1.08
ILMN_1758918	BRD2	1.08
ILMN_1773567	LAMA5	1.08
ILMN_2286870	CSNK1D	1.08
ILMN_3201115	LOC440043	1.08
ILMN_1657977	MSRB2	1.07
ILMN_1658709	LAMB1	1.07
ILMN_1675124	DDX17	1.07
ILMN_1686748	TMEM9	1.07
ILMN_1761560	PHF13	1.07
ILMN_1769191	GNAS	1.07
ILMN_1812995	CTSL1	1.07
ILMN_2191568	TUSC4	1.07
ILMN_3182171	FGGY	1.07
ILMN_1670000	DCAF6	1.06
ILMN_1691188	UIMC1	1.06
ILMN_1693045	TMED1	1.06
ILMN_1784286	NDUFA1	1.06
ILMN_2201533	C17ORF61	1.06
ILMN_2352131	ERBB2	1.06
ILMN_1662340	ZNF358	1.05

ILMN_1667711	HRASLS3	1.05
ILMN_1683576	MAGED2	1.05
ILMN_1684108	IRX4	1.05
ILMN_1691942	CCNI	1.05
ILMN_1703123	AXUD1	1.05
ILMN_1703477	ARHGEF2	1.05
ILMN_1711909	EDEM2	1.05
ILMN_1724194	NPEPL1	1.05
ILMN_1756942	SP3	1.05
ILMN_1782439	CNN3	1.05
ILMN_1788961	PPP2R2A	1.05
ILMN_1792508	TMEM59	1.05
ILMN_1810289	FER1L3	1.05
ILMN_2053415	LDLR	1.05
ILMN_2115218	ANKRD10	1.05
ILMN_2203950	HLA-A	1.05
ILMN_2329679	TPST2	1.05
ILMN_1661917	LOC644039	1.04
ILMN_1685722	EIF4A2	1.04
ILMN_1719303	P4HB	1.04
ILMN_1814526	ADD3	1.04
ILMN_2130411	KDELR1	1.04
ILMN_2386982	PRKCZ	1.04
ILMN_1710756	ENO1	1.03
ILMN_1732534	CHMP5	1.03
ILMN_1806023	JUN	1.03
ILMN_2382990	HK1	1.03
ILMN_2389151	UGP2	1.03
ILMN_3303965	ZC3H11B	1.03
ILMN_1674874	MFSD10	1.02
ILMN_1686194	SDCCAG10	1.02
ILMN_1775522	MAGED1	1.02
ILMN_1804854	CTNNA1	1.02
ILMN_1811551	DERA	1.02
ILMN_2117508	CTHRC1	1.02
ILMN_2148012	EPR1	1.02
ILMN_2400874	SCYL1	1.02
ILMN_1815319	CMTM4	1.01
ILMN_2370976	FER1L3	1.01
ILMN_1697548	LPHN2	-1
ILMN_1757644	UBE2H	-1.01
ILMN_1781097	UBXN4	-1.01
ILMN_1792997	NPTN	-1.01
ILMN_1745130	RBM9	-1.02
ILMN_1761463	EFHD2	-1.02
ILMN_1666976	PLD3	-1.03
ILMN_1735180	NCSTN	-1.03
ILMN_1783709	RRAGA	-1.03
ILMN_1790136	C20ORF20	-1.04
ILMN_2389590	PRKAR1A	-1.04
ILMN_1693394	BCKDK	-1.05
ILMN_1731374	CPE	-1.05
ILMN_1749109	PSAP	-1.05
ILMN_1800733	MANBA	-1.05
ILMN_1673282	LAMP2	-1.06
ILMN_3243381	MLEC	-1.06
ILMN_1675325	ENPEP	-1.09
ILMN_1671568	ECHDC2	-1.1
ILMN_1680453	ITM2C	-1.1
ILMN_1796461	PRSS8	-1.13
ILMN_1715715	CEBPA	-1.24

hESC-derived HIF independent		
Probe_ID	**SYMBOL**	**Fold Change**
ILMN_1651282	COL17A1	2.2
ILMN_1653026	PLAC8	2.14
ILMN_1653292	PFKFB4	1.92
ILMN_1658289	WDR54	1.79
ILMN_1658485	LOC644612	2.18
ILMN_1658926	NOTCH3	1.66
ILMN_1659027	SLC2A1	2.16
ILMN_1659047	HIST2H2AA3	1.68
ILMN_1659463	APAF1	1.36
ILMN_1659990	C7ORF68	1.31
ILMN_1661599	DDIT4	3.84
ILMN_1662839	PLEKHA1	1.29
ILMN_1664294	LEPRE1	1.22
ILMN_1665526	TCEA2	1.26
ILMN_1666503	DENND2A	1.73
ILMN_1670306	SCGB3A2	1.7
ILMN_1671992	LOC650128	1.62
ILMN_1672589	SEMA4B	1.45
ILMN_1674941	ANO6	1.17
ILMN_1676563	HTRA1	2.21
ILMN_1676629	INSIG2	1.39
ILMN_1678781	SNX26	1.33
ILMN_1679428	CHIC2	1.18
ILMN_1679641	FAM120B	1.16
ILMN_1679727	CLK1	1.64
ILMN_1680874	TUBB2B	1.29
ILMN_1683980	PLEKHM2	1.08
ILMN_1686664	MT2A	4.1
ILMN_1689123	CCNK	1.24
ILMN_1689378	CCRN4L	1.56
ILMN_1689400	CLK1	1.54
ILMN_1691104	PGAM4	1.2
ILMN_1691156	MT1A	4.17
ILMN_1693334	P4HA1	2.31
ILMN_1695880	LOX	2.79
ILMN_1703316	LOC255783	1.29
ILMN_1703695	C19ORF12	-1.18
ILMN_1704154	TNFRSF19	-1.16
ILMN_1705144	ULK1	1.33
ILMN_1705384	PPFIBP1	1.35
ILMN_1706015	FAM43A	1.36
ILMN_1706841	PGAM4	1.16
ILMN_1706960	KIAA1217	1.36
ILMN_1707627	TPI1	1.33
ILMN_1707727	ANGPTL4	1.98
ILMN_1709307	GPSM1	1.25
ILMN_1712673	SASH1	1.43
ILMN_1714197	ACSS2	1.34
ILMN_1715169	HLA-DRB1	1.64
ILMN_1715401	MT1G	7.44
ILMN_1718766	MT1F	2.15
ILMN_1718961	BNIP3L	1.99
ILMN_1720708	CSNK1D	1.16
ILMN_1722156	RWDD2A	1.28
ILMN_1722898	SFRP2	1.34
ILMN_1724658	BNIP3	1.74
ILMN_1730670	FSTL3	1.34
ILMN_1731648	FOXJ2	1.46
ILMN_1733851	DACT3	1.6
ILMN_1735052	ULK1	1.26
ILMN_1735552	KIF1B	1.37
ILMN_1737426	PCMTD1	1.35
ILMN_1739558	CRELD1	1.21
ILMN_1739946	VKORC1	1.13
ILMN_1740996	CA3	1.57
ILMN_1741148	ALDOA	1.53
ILMN_1743205	ABCA7	1.29
ILMN_1744963	ERO1L	1.29
ILMN_1747968	RBM33	1.58
ILMN_1748124	TSC22D3	1.62
ILMN_1750324	IGFBP5	1.68
ILMN_1750338	C10ORF47	1.42
ILMN_1751656	KLF11	1.24
ILMN_1751753	IDH2	1.6
ILMN_1752592	HLA-DRB4	1.38
ILMN_1755822	SYDE1	1.47
ILMN_1755974	ALDOC	2.47
ILMN_1756071	MFGE8	1.18
ILMN_1756541	MXD4	1.33
ILMN_1758731	CYP2J2	1.32
ILMN_1759419	ILVBL	1.53
ILMN_1760727	ANG	1.48
ILMN_1764090	AK3L1	1.72
ILMN_1765796	ENO2	1.49
ILMN_1769451	ILVBL	1.46
ILMN_1771599	PLOD2	1.48
ILMN_1772821	KIAA1671	1.54
ILMN_1772876	ZNF395	1.38
ILMN_1774982	CDC42EP5	1.6
ILMN_1775170	MT1X	4.7
ILMN_1780255	KLK6	1.52
ILMN_1780825	RRAS	1.59
ILMN_1782538	VIM	1.3
ILMN_1784217	SOX15	1.28
ILMN_1785252	SLC26A6	1.13
ILMN_1786893	RBM5	1.21
ILMN_1789733	CLIP3	1.4
ILMN_1795026	FAM189B	1.13
ILMN_1795298	GPER	1.51
ILMN_1795639	MGMT	1.14
ILMN_1795778	P4HA2	1.54

ILMN_1796339	PLEKHA2	1.52
ILMN_1796423	CLIC3	1.48
ILMN_1801068	DACT1	1.25
ILMN_1801077	PLIN2	1.48
ILMN_1802252	GAPDH	1.33
ILMN_1804248	FDPS	1.18
ILMN_1807106	LDHA	1.58
ILMN_1808824	NEBL	1.41
ILMN_1809931	NDRG1	3.46
ILMN_1810844	RARRES2	1.45
ILMN_1811489	OXSR1	1.16
ILMN_1811615	COPA	1.26
ILMN_1812031	PALM	1.69
ILMN_1812297	CYP26B1	1.73
ILMN_1813669	ANKS1A	1.43
ILMN_1813746	CORO2A	1.41
ILMN_1831106	HS.19193	1.86
ILMN_1843198	HS.10862	2
ILMN_1849013	HS.570988	1.29
ILMN_2038778	GAPDH	1.22
ILMN_2045419	BNIP3L	1.44
ILMN_2058251	VIM	1.44
ILMN_2086095	ID2	1.37
ILMN_2104295	TMEM178	1.28
ILMN_2106902	CHES1	1.41
ILMN_2108735	EEF1A2	1.61
ILMN_2109708	ECGF1	1.46
ILMN_2128639	C10ORF47	1.83
ILMN_2138765	PLIN2	1.38
ILMN_2150654	ZSWIM4	1.41
ILMN_2173451	GPI	1.2
ILMN_2173611	MT1E	3.72
ILMN_2180239	DOPEY2	1.35
ILMN_2183409	SCARB1	1.39
ILMN_2185984	SASH1	1.41
ILMN_2207363	RABAC1	1.24
ILMN_2295518	TRO	1.13
ILMN_2299095	SIGLEC6	1.29
ILMN_2318568	HCFC1R1	1.38
ILMN_2328094	DACT1	1.25
ILMN_2334693	NARF	1.59
ILMN_2338038	AK3L1	1.67
ILMN_2352090	GPRC5C	1.86
ILMN_2364022	SLC16A3	2.39
ILMN_2371055	EFNA1	1.38
ILMN_2381697	P4HA2	1.6
ILMN_2384056	GPER	1.55
ILMN_2394250	PLEKHA1	1.31
ILMN_2394561	IRF2BP2	1.39
ILMN_2397750	IVNS1ABP	1.22
ILMN_2410924	PLOD2	1.42
ILMN_2414325	TNFAIP8	1.65
ILMN_2415748	WSB1	1.37
ILMN_3195198	KRT17P3	1.34
ILMN_3205656	LOC391075	1.2
ILMN_3223826	SPNS2	1.29
ILMN_3224934	SFRS18	1.23
ILMN_3248781	SDHAP2	1.38
ILMN_3249748	LDHA	1.55
ILMN_3267451	GAPDHL6	1.2
ILMN_3283772	LOC644237	1.4
ILMN_3301749	SPNS2	1.54

Appendix B

Gene ontology groups

Primary CTB Up in Hypoxia		
Groups	**logP**	**Genes**
Hypoxia	-18.351	ALDOA, ANXA2, BNIP3L, CAV1, CCNG2, COL5A1, EFNA1, GALK1, GAPDH, HK2, IDS, IGFBP3, LDHA, MYH9, NFIL3, P4HA1, SERPINE1, PDK3, PFKP, PGK1, PIM1, SLC2A1, SLC2A3, STC1, TPBG, VLDLR, BHLHE40, STC2, P4HA2, HS3ST1, NDRG1, NOCT, ANGPTL4, PLAC8, DDIT4, KLHL24, TMEM45A, ACKR3
Actin filament-based process	-17.240	ACTN4, ACTN1, ADD1, ALDOA, RHOA, ARHGDIB, BCL6, CFL1, CNN2, CTNNA1, DIAPH1, FLNB, GRB2, ID1, ILK, ITGB1, KRT19, MYH9, MYL6, MYO9B, PAFAH1B1, RAP2A, SFRP1, SRI, STC1, TNFAIP1, TPM1, TPM4, WIPF1, CORO2A, ZYX, TMSB10, ARHGEF2, IQSEC1, WDR1, ABI1, ARPC2, CAP1, DSTN, CDC42EP1, PDCD10, LIMCH1, PALLD, ARHGEF18, CORO1C, SUN2, PARVB, F11R, LIMA1, MSRB1, FNBP1L, SSH3, ASAP3, PARVA, BAIAP2L1, INF2, NUAK2, CORO6, SSH2, MYADM, FMNL2, CDC42EP5, FRYL, TMSB15B
Focal adhesion	-11.399	ACTB, ACTN4, ACTN1, RHOA, CAV1, CAV2, COL4A1, COL4A2, COL5A1, CRKL, DIAPH1, FLNB, FN1, GRB2, RAPGEF1, ILK, ITGA1, ITGA2, ITGA5, ITGB1, PIK3CB, PIK3R2, MAPK3, PTK2, PXN, THBS3, VEGFB, ZYX, PARVB, PARVA
Transmembrane receptor protein tyrosine kinase signaling pathway	-11.312	ACTB, RHOA, BMPR2, CAV1, CAV2, CFL1, AP3S1, CRKL, CSF2RA, CTNNA1, EFNA1, EFNB1, EIF4EBP2, FOXO1, GRB2, GRB10, RAPGEF1, IGF2, IGF2R, IGFBP3, ITGA1, ITGA5, ITPR3, JAK1, JUP, LYN, MMP2, MYH9, MYL6, NKX3-1, PCSK6, PIK3CB, PIK3R2, PRKAB2, MAPK3, PTK2, PTPN11, PXN, ATXN1, STAT3, VEGFB, LAMTOR3, IQGAP1, ARHGEF7, MPZL1, HGS, FIBP, ARHGEF2, REPS2, NOG, RASSF2, MVP, ABI1, PDCD6, ARPC2, PRDM4, ANKS1A, ARHGEF18, DSTYK, ARHGEF16, EPN1, SH3KBP1, CRIM1, DDIT4, PID1, PAG1, BAIAP2L1, TRIB3, PLEKHA1, RHBDF1, APH1B
Regulation of anatomical structure morphogenesis	-9.379	ACTN4, ALDOA, RHOA, BCL6, BMPR2, CFL1, COL4A2, COL5A1, CSNK1D, CSNK1G2, CYP1B1, DAG1, DIAPH1, EFNA1, FN1, ID1, ILK, MYH9, NPPB, PAFAH1B1, SERPINE1, PTK2, PTN, PXN, RAP2A, SFRP1, TGIF1, VEGFB, WARS, WIPF1, ADAM9, ARHGEF7, NOG, PDCD6, ARPC2, VAT1, GNA13, CDC42EP1, PDCD10, ANKRD6, TBC1D9B, SASH1, ARHGEF18, DDAH1, CORO1C, PLXNB2, BAMBI, PARVB, SH3KBP1, ANGPTL4, TNFRSF12A, DACT1, SSH3, PID1, PARVA, CDC42SE2, INF2, PINK1, NDEL1, SSH2, MYADM, FMNL2, VASN, EVI5L, CDC42EP5

Regulation of body fluid levels	-9.363	ACTB, ACTN4, ACTN1, ALDOA, ANXA2, RHOA, CEACAM1, SERPING1, CAV1, CFL1, CLIC1, COPA, FN1, GJA5, GNB1, GRB2, HK2, IGF2, ILK, ITGA1, ITGA2, ITGA5, ITGB1, ITPR3, LYN, MYH9, NPPB, OXTR, SERPINE1, PIK3CB, PIK3R2, MAPK3, PSAP, PTK2, PTPN11, SLC22A4, VEGFB, WFS1, AP3B1, NCOA1, SLC16A3, FIBP, VAMP3, WDR1, CAP1, GNA13, SLC7A9, F11R, PHF21A, CYP26B1, RBSN, LBH, UBASH3B, ANO6, POTEKP, ANXA8
Epithelial to Mesenchymal Transition	-8.914	COL4A1, COL4A2, COL5A1, COPA, FN1, IGFBP3, ITGA2, ITGA5, ITGB1, MMP2, OXTR, SERPINE1, PLOD2, HTRA1, SFRP1, TAGLN, TIMP3, TPM1, TPM4, WIPF1, MFAP5, PLOD3, FSTL3, FSTL1, TNFRSF12A, COLGALT1
Blood vessel development	-8.867	ANXA2, CEACAM1, BMPR2, CAV1, COL4A1, COL4A2, COL5A1, CRKL, CYP1B1, TYMP, EFNA1, FOXO1, FN1, FOLR1, GJA5, RAPGEF1, HPGD, ID1, ITGA5, ITGB1, MMP2, MYH9, NKX3-1, NPPB, SERPINE1, PIK3CB, PTK2, SFRP1, SOX4, NR2F2, VEGFB, WARS, VEZF1, ADAM15, PDCD6, GNA13, PNPLA6, TMED2, PDCD10, SASH1, DDAH1, ANGPTL4, TNFRSF12A, GATAD2A, PARVA, ACKR3, CCM2
Endomembrane system organization	-8.629	ABCA1, ANXA2, CAV1, CAV2, COL5A1, CSNK1D, ITGB1, JUP, PAFAH1B1, PKP2, MAPK3, RAP2A, TNFRSF1A, VAMP3, TMEM59, DOPEY2, ABCA7, NDRG1, NEK6, TMED2, PDCD10, RAB3GAP1, SUN2, CHMP2B, TSPAN17, ARHGEF16, SNX10, F11R, SH3GLB1, GOLGA7, RAB8B, FNBP1L, PID1, BAIAP2L1, PLSCR3, RAB22A, ARHGAP21, REEP1, TMEM43, NDEL1, MYADM, ANO6, CNEP1R1, ANXA8
Cell junction organization	-8.532	ACTB, ACTN4, ACTN1, RHOA, CAV1, CD151, COL17A1, CTNNA1, FN1, GJA5, RAPGEF1, ILK, ITGA5, ITGB1, JUP, PKP2, PTK2, PXN, SFRP1, TJP1, ARHGEF7, CORO1C, PARVB, F11R, RAB8B, PARVA, CCM2, MYADM, CLDN19

hESC-derived CTB Up in Hypoxia		
Groups	**logP**	**Genes**
Hypoxia	-31.770	PLIN2, AK4, ALDOA, ALDOC, BGN, BNIP3L, SCARB1, EFNA1, EGFR, ENO1, ENO2, GALK1, GAPDH, GPI, HK1, JUN, LDHA, LOX, MIF, MT1E, MT2A, P4HA1, PFKL, PGK1, PGM1, SDC4, SLC2A1, TPI1, UGP2, TPST2, P4HA2, NDRG1, ILVBL, NOCT, WSB1, FAM162A, ERO1A, ANGPTL4, PLAC8, ERRFI1, DDIT4
Epithelial to Mesenchymal Transition	-9.657	BGN, CALD1, CDH11, COL6A3, COPA, ENO2, FBLN1, ID2, IGFBP2, JUN, LOX, PLOD2, HTRA1, SDC4, THBS2, VIM, FSTL3, CADM1, P3H1, CTHRC1
Cellular response to zinc ion	-6.807	MT1A, MT1E, MT1F, MT1G, MT1X, MT2A
Cholesterol Homeostasis	-5.366	ALDOC, DHCR7, FDPS, LDLR, SQLE, STX5, ERRFI1, ACSS2, TP53INP1
Negative regulation of developmental process	-5.247	ABR, APP, BNIP3, CTNNA1, TSC22D3, EFNA1, ERBB2, FBLN1, GNAS, GPER1, HLA-G, ID2, IGFBP5, INSIG1, ISL1, MIF, NOTCH3, SFRP2, SOX11, SOX15, TBX3, THBS2, VIM, ARHGEF2, FSTL3, LILRB3, KANK1, NOCT, PLAC8, ITM2C, DACT3
Pentose phosphate pathway	-5.115	ALDOA, ALDOC, GPI, PFKL, PGM1, DERA
p53 pathway	-5.074	ADA, APAF1, APP, CEBPA, MKNK2, JUN, RALGDS, CCNK, NDRG1, MXD4, TXNIP, BLCAP, FAM162A, DDIT4
Growth	-5.002	APP, DHCR7, DPYSL2, ENO1, ERBB2, GNAS, IGFBP2, IGFBP5, MT1A, MT1E, MT1F, MT1G, MT1X, MT2A, OSBP, PKM, PRKAR1A, PRKCZ, KLK6, HTRA1, PSAP, RXRB, SFRP2, SOX15, TRO, NCOA3, ULK1, CADM1, CLIC4, PLAC8, MRGBP, PLEKHA1, P3H1, DACT3, HTRA4
Positive regulation of insulin secretion	-4.972	GPER1, HLA-DRB1, HLA-DRB4, ISL1, SOX4, SRI, MGEA5, PHPT1
Integrin Signaling	-4.946	COL17A1, EGFR, ERBB2, LAMA5, LAMB1, MET, RXRB

Primary CTB HIF Dependent		
Groups	**-logP**	**Genes**
Hypoxia	-11.282	ANXA2, BNIP3L, CAV1, COL5A1, GALK1, GAPDH, HK2, IDS, LDHA, MYH9, NFIL3, P4HA1, PFKP, SLC2A1, STC1, BHLHE40, STC2, P4HA2, HS3ST1, NDRG1, NOCT, ANGPTL4, DDIT4, TMEM45A, ACKR3
Actin filament-based process	-9.676	ACTN4, ACTN1, ADD1, RHOA, CNN2, CTNNA1, GRB2, ID1, ILK, ITGB1, MYH9, MYL6, RAP2A, STC1, TNFAIP1, TPM1, TPM4, WIPF1, CORO2A, ZYX, TMSB10, ARHGEF2, WDR1, CAP1, DSTN, CDC42EP1, PDCD10, LIMCH1, ARHGEF18, CORO1C, F11R, SSH3, BAIAP2L1, INF2, NUAK2, CORO6, MYADM, FMNL2, CDC42EP5, FRYL, TMSB15B
Transmembrane receptor protein tyrosine kinase signaling pathway	-9.234	ACTB, RHOA, BMPR2, CAV1, CAV2, AP3S1, CRKL, CSF2RA, CTNNA1, FOXO1, GRB2, GRB10, IGF2R, ITGA1, ITGA5, ITPR3, JUP, LYN, MMP2, MYH9, MYL6, NKX3-1, PCSK6, PIK3R2, MAPK3, PTK2, PTPN11, ATXN1, STAT3, VEGFB, LAMTOR3, IQGAP1, MPZL1, HGS, FIBP, ARHGEF2, NOG, MVP, PRDM4, ANKS1A, ARHGEF18, DSTYK, ARHGEF16, EPN1, SH3KBP1, CRIM1, DDIT4, PAG1, BAIAP2L1, TRIB3, PLEKHA1, RHBDF1, APH1B
Focal adhesion	-8.640	ACTB, ACTN4, ACTN1, RHOA, CAV1, CAV2, COL4A2, COL5A1, CRKL, FN1, GRB2, ILK, ITGA1, ITGA2, ITGA5, ITGB1, PIK3R2, MAPK3, PTK2, THBS3, VEGFB, ZYX
Regulation of body fluid levels	-8.209	ACTB, ACTN4, ACTN1, ANXA2, RHOA, CEACAM1, SERPING1, CAV1, CLIC1, FN1, GJA5, GNB1, GRB2, HK2, ILK, ITGA1, ITGA2, ITGA5, ITGB1, ITPR3, LYN, MYH9, NPPB, OXTR, PIK3R2, MAPK3, PTK2, PTPN11, SLC22A4, VEGFB, AP3B1, SLC16A3, FIBP, WDR1, CAP1, F11R, PHF21A, CYP26B1, RBSN, LBH, UBASH3B, POTEKP, ANXA8
Integrin-mediated signaling pathway	-7.877	CEACAM1, CTNNA1, ILK, ITGA1, ITGA2, ITGA5, ITGB1, MYH9, PTK2, PTPN11, ZYX, ADAM9, ADAMTS1, CCM2
Endomembrane system organization	-7.077	ABCA1, ANXA2, CAV1, CAV2, COL5A1, CSNK1D, ITGB1, JUP, PKP2, MAPK3, RAP2A, TNFRSF1A, DOPEY2, ABCA7, NDRG1, NEK6, PDCD10, RAB3GAP1, CHMP2B, TSPAN17, ARHGEF16, SNX10, F11R, GOLGA7, RAB8B, BAIAP2L1, PLSCR3, RAB22A, ARHGAP21, REEP1, TMEM43, MYADM, ANXA8
Cell junction organization	-7.018	ACTB, ACTN4, ACTN1, RHOA, CAV1, CD151, CTNNA1, FN1, GJA5, ILK, ITGA5, ITGB1, JUP, PKP2, PTK2, TJP1, CORO1C, F11R, RAB8B, CCM2, MYADM, CLDN19

Transmembrane receptor protein serine/threonine kinase signaling pathway	-6.658	RHOA, BMPR2, CAV1, CAV2, FOLR1, HPGD, ID1, ILK, ING2, ITGB1, PCSK6, MAPK3, PTK2, TGIF1, ZYX, ADAM9, MTMR4, NOG, NCOR2, FSTL1, ARHGEF18, BAMBI, F11R, DACT1, VASN
Epithelial to Mesenchymal Transition	-6.095	COL4A2, COL5A1, FN1, ITGA2, ITGA5, ITGB1, MMP2, OXTR, PLOD2, TAGLN, TIMP3, TPM1, TPM4, WIPF1, MFAP5, PLOD3, FSTL1, COLGALT1

hESC-derived CTB HIF Dependent		
Groups	**logP**	**Genes**
Hypoxia	-12.987	ALDOA, BGN, EFNA1, EGFR, ENO1, GALK1, GAPDH, HK1, JUN, MIF, PFKL, PGK1, PGM1, SDC4, TPI1, UGP2, TPST2, WSB1, FAM162A, ERRFI1
Epithelial to Mesenchymal Transition	-6.394	BGN, CALD1, CDH11, COL6A3, FBLN1, ID2, IGFBP2, JUN, PLOD2, SDC4, THBS2, CADM1, CTHRC1
Central carbon metabolism in cancer	-6.113	EGFR, ERBB2, HK1, MET, PFKL, PGAM1, PKM, PGAM4
Integrin Signaling	-4.941	EGFR, ERBB2, LAMA5, LAMB1, MET, RXRB
organ morphogenesis	-4.927	ABR, CPE, CTNNA1, EFNA1, EGFR, GLG1, GNAS, ID2, IGFBP5, INSIG1, ISL1, JUN, LAMA5, LAMB1, MET, SOX4, SOX11, SP3, TBX3, NCOA3, MAGED1, SLC40A1, IRX4, ERRFI1, CSRNP1, CTHRC1
peptidyl-tyrosine modification	-4.760	APP, CLK3, EFNA1, EGFR, ERBB2, ISL1, MET, MIF, PRKCZ, TPST2, ARHGEF2, NPTN, ERRFI1, SCYL1
Cholesterol Homeostasis	-4.736	DHCR7, LDLR, SQLE, STX5, ERRFI1, ACSS2, TP53INP1
Galactose metabolism	-4.733	GALK1, HK1, PFKL, PGM1, UGP2
cellular carbohydrate metabolic process	-4.624	FKTN, GALK1, HK1, IGFBP5, MANBA, PGAM1, PGM1, TPI1, UGP2, TMEM59, MGEA5, FGGY, PGAM4
negative regulation of muscle adaptation	-4.337	IGFBP5, MGEA5, ERRFI1

References

Adelman, D.M., Gertsenstein, M., Nagy, A., Simon, M.C., and Maltepe, E. (2000). Placental cell fates are regulated in vivo by HIF-mediated hypoxia responses. Genes Dev. *14*, 3191–3203.

Amita, M., Adachi, K., Alexenko, A.P., Sinha, S., Schust, D.J., Schulz, L.C., Roberts, R.M., and Ezashi, T. (2013). Complete and unidirectional conversion of human embryonic stem cells to trophoblast by BMP4. Proc. Natl. Acad. Sci. U. S. A. *110*, E1212–E1221.

Anson-Cartwright, L., Dawson, K., Holmyard, D., Fisher, S.J., Lazzarini, R.A., and Cross, J.C. (2000). The glial cells missing-1 protein is essential for branching morphogenesis in the chorioallantoic placenta. Nat. Genet. *25*, 311–314.

Arsham, A.M., Howell, J.J., and Simon, M.C. (2003). A novel hypoxia-inducible factor-independent hypoxic response regulating mammalian target of rapamycin and its targets. J. Biol. Chem. *278*, 29655–29660.

Bai, Q., Assou, S., Haouzi, D., Ramirez, J.-M., Monzo, C., Becker, F., Gerbal-Chaloin, S., Hamamah, S., and De Vos, J. (2012). Dissecting the first transcriptional divergence during human embryonic development. Stem Cell Rev. *8*, 150–162.

Berg, D.K., Smith, C.S., Pearton, D.J., Wells, D.N., Broadhurst, R., Donnison, M., and Pfeffer, P.L. (2011). Trophectoderm lineage determination in cattle. Dev. Cell *20*, 244–255.

Bernardo, A.S., Faial, T., Gardner, L., Niakan, K.K., Ortmann, D., Senner, C.E., Callery, E.M., Trotter, M.W., Hemberger, M., Smith, J.C., Bardwell, L., Moffett, A., Pedersen, R.A. (2011). BRACHYURY and CDX2 mediate BMP-induced differentiation of human and mouse pluripotent stem cells into embryonic and extraembryonic lineages. Cell Stem Cell *9*, 144–155.

Bruick, R.K. (2003). Oxygen sensing in the hypoxic response pathway: regulation of the hypoxia-inducible transcription factor. Genes Dev. *17*, 2614–2623.

Caniggia, I., and Winter, J.L. (2002). Adriana and Luisa Castellucci Award lecture 2001. Hypoxia inducible factor-1: oxygen regulation of trophoblast differentiation in normal and pre-eclamptic pregnancies--a review. Placenta *23 Suppl A*, S47–S57.

Caniggia, I., Winter, J., Lye, S.J., and Post, M. (2000). Oxygen and placental development during the first trimester: implications for the pathophysiology of pre-eclampsia. Placenta *21 Suppl A*, S25–S30.

Chakraborty, D., Rumi, M.A.K., Konno, T., and Soares, M.J. (2011). Natural killer cells direct hemochorial placentation by regulating hypoxia-inducible factor dependent trophoblast lineage decisions. Proc. Natl. Acad. Sci. U. S. A. *108*, 16295–16300.

Chen, A.E., Egli, D., Niakan, K., Deng, J., Akutsu, H., Yamaki, M., Cowan, C., Fitz-Gerald, C., Zhang, K., Melton, D.A., Eggan, K. (2009). Optimal timing of inner cell mass isolation increases the efficiency of human embryonic stem cell derivation and allows generation of sibling cell lines. Cell Stem Cell *4*, 103–106.

Chen, K.-F., Lai, Y.-Y., Sun, H.S., and Tsai, S.-J. (2005). Transcriptional repression of human cad gene by hypoxia inducible factor-1alpha. Nucleic Acids Res. *33*, 5190–5198.

Chen, Z.-Y., Wang, P.-W., Shieh, D.-B., Chiu, K.-Y., and Liou, Y.-M. (2015). Involvement of gelsolin in TGF-beta 1 induced epithelial to mesenchymal transition in breast cancer cells. J. Biomed. Sci. *22*, 90.

Cowden Dahl, K.D., Fryer, B.H., Mack, F.A., Compernolle, V., Maltepe, E., Adelman, D.M., Carmeliet, P., and Simon, M.C. (2005). Hypoxia-inducible factors 1alpha and 2alpha regulate trophoblast differentiation. Mol. Cell. Biol. *25*, 10479–10491.

Damsky, C.H., Fitzgerald, M.L., and Fisher, S.J. (1992). Distribution patterns of extracellular matrix components and adhesion receptors are intricately modulated during first trimester cytotrophoblast differentiation along the invasive pathway, in vivo. J. Clin. Invest. *89*, 210–222.

Das, P., Ezashi, T., Schulz, L.C., Westfall, S.D., Livingston, K.A., and Roberts, R.M. (2007). Effects of fgf2 and oxygen in the bmp4-driven differentiation of trophoblast from human embryonic stem cells. Stem Cell Res. *1*, 61–74.

DaSilva-Arnold, S., James, J.L., Al-Khan, A., Zamudio, S., and Illsley, N.P. (2015). Differentiation of first trimester cytotrophoblast to extravillous trophoblast involves an epithelial-mesenchymal transition. Placenta.

ten Dijke, P., and Hill, C.S. (2004). New insights into TGF-beta-Smad signalling. Trends Biochem. Sci. *29*, 265–273.

Erb, T.M., Schneider, C., Mucko, S.E., Sanfilippo, J.S., Lowry, N.C., Desai, M.N., Mangoubi, R.S., Leuba, S.H., and Sammak, P.J. (2011). Paracrine and epigenetic control of trophectoderm differentiation from human embryonic stem cells: the role of bone morphogenic protein 4 and histone deacetylases. Stem Cells Dev. *20*, 1601–1614.

Esterman, A., Finlay, T.H., and Dancis, J. (1996). The effect of hypoxia on term trophoblast: hormone synthesis and release. Placenta *17*, 217–222.

Ezashi, T., Matsuyama, H., Telugu, B.P.V.L., and Roberts, R.M. (2011). Generation of colonies of induced trophoblast cells during standard reprogramming of porcine fibroblasts to induced pluripotent stem cells. Biol. Reprod. *85*, 779–787.

Forbes, K., Westwood, M., Baker, P.N., and Aplin, J.D. (2008). Insulin-like growth factor I and II regulate the life cycle of trophoblast in the developing human placenta. Am. J. Physiol. Cell Physiol. *294*, C1313–C1322.

Fryer, B.H., and Simon, M.C. (2006). Hypoxia, HIF and the placenta. Cell Cycle Georget. Tex *5*, 495–498.

Genbacev, O., Zhou, Y., Ludlow, J.W., and Fisher, S.J. (1997). Regulation of human placental development by oxygen tension. Science *277*, 1669–1672.

Gerami-Naini, B., Dovzhenko, O.V., Durning, M., Wegner, F.H., Thomson, J.A., and Golos, T.G. (2004). Trophoblast differentiation in embryoid bodies derived from human embryonic stem cells. Endocrinology *145*, 1517–1524.

Graham, C.H., Hawley, T.S., Hawley, R.G., MacDougall, J.R., Kerbel, R.S., Khoo, N., and Lala, P.K. (1993). Establishment and characterization of first trimester human trophoblast cells with extended lifespan. Exp. Cell Res. *206*, 204–211.

Graham, C.H., Connelly, I., MacDougall, J.R., Kerbel, R.S., Stetler-Stevenson, W.G., and Lala, P.K. (1994). Resistance of malignant trophoblast cells to both the anti-proliferative and anti-invasive effects of transforming growth factor-beta. Exp. Cell Res. *214*, 93–99.

Graham, S.J.L., Wicher, K.B., Jedrusik, A., Guo, G., Herath, W., Robson, P., and Zernicka-Goetz, M. (2014). BMP signalling regulates the pre-implantation development of extra-embryonic cell lineages in the mouse embryo. Nat. Commun. *5*, 5667.

Guibourdenche, J., Handschuh, K., Tsatsaris, V., Gerbaud, P., Leguy, M.C., Muller, F., Brion, D.E., and Fournier, T. (2010). Hyperglycosylated hCG is a marker of early human trophoblast invasion. J. Clin. Endocrinol. Metab. *95*, E240–E244.

Hayashi, Y., Furue, M.K., Tanaka, S., Hirose, M., Wakisaka, N., Danno, H., Ohnuma, K., Oeda, S., Aihara, Y., Shiota, K., Ogura, A., Ishiura, S., Asashima, M. (2010). BMP4 induction of trophoblast from mouse embryonic stem cells in defined culture conditions on laminin. In Vitro Cell. Dev. Biol. Anim. *46*, 416–430.

Hemberger, M., Hughes, M., and Cross, J.C. (2004). Trophoblast stem cells differentiate in vitro into invasive trophoblast giant cells. Dev. Biol. *271*, 362–371.

Hohn, H.P., Linke, M., Ugele, B., and Denker, H.W. (1998). Differentiation markers and invasiveness: discordant regulation in normal trophoblast and choriocarcinoma cells. Exp. Cell Res. *244*, 249–258.

Hunkapiller, N.M., and Fisher, S.J. (2008). Chapter 12. Placental remodeling of the uterine vasculature. Methods Enzymol. *445*, 281–302.

Ietta, F., Wu, Y., Winter, J., Xu, J., Wang, J., Post, M., and Caniggia, I. (2006). Dynamic HIF1A regulation during human placental development. Biol. Reprod. *75*, 112–121.

Ilić, D., Genbacev, O., Jin, F., Caceres, E., Almeida, E.A., Bellingard-Dubouchaud, V., Schaefer, E.M., Damsky, C.H., and Fisher, S.J. (2001). Plasma membrane-associated pY397FAK is a marker of cytotrophoblast invasion in vivo and in vitro. Am. J. Pathol. *159*, 93–108.

Iyer, N.V., Kotch, L.E., Agani, F., Leung, S.W., Laughner, E., Wenger, R.H., Gassmann, M., Gearhart, J.D., Lawler, A.M., Yu, A.Y., Semenza, G.L. (1998). Cellular and developmental control of O2 homeostasis by hypoxia-inducible factor 1 alpha. Genes Dev. *12*, 149–162.

Janatpour, M.J., McMaster, M.T., Genbacev, O., Zhou, Y., Dong, J., Cross, J.C., Israel, M.A., and Fisher, S.J. (2000). Id-2 regulates critical aspects of human cytotrophoblast differentiation, invasion and migration. Dev. Camb. Engl. *127*, 549–558.

Jauniaux, E., Hempstock, J., Greenwold, N., and Burton, G.J. (2003). Trophoblastic oxidative stress in relation to temporal and regional differences in maternal placental blood flow in normal and abnormal early pregnancies. Am. J. Pathol. *162*, 115–125.

King, A., Thomas, L., and Bischof, P. (2000). Cell culture models of trophoblast II: trophoblast cell lines--a workshop report. Placenta *21 Suppl A*, S113–S119.

Kingdom, J., Huppertz, B., Seaward, G., and Kaufmann, P. (2000). Development of the placental villous tree and its consequences for fetal growth. Eur. J. Obstet. Gynecol. Reprod. Biol. *92*, 35–43.

Koumenis, C., and Wouters, B.G. (2006). “Translating” tumor hypoxia: unfolded protein response (UPR)-dependent and UPR-independent pathways. Mol. Cancer Res. MCR *4*, 423–436.

Kozak, K.R., Abbott, B., and Hankinson, O. (1997). ARNT-deficient mice and placental differentiation. Dev. Biol. *191*, 297–305.

Kulshreshtha, R., Ferracin, M., Negrini, M., Calin, G.A., Davuluri, R.V., and Ivan, M. (2007). Regulation of microRNA expression: the hypoxic component. Cell Cycle Georget. Tex *6*, 1426–1431.

Lee, Y., Kim, K.-R., McKeon, F., Yang, A., Boyd, T.K., Crum, C.P., and Parast, M.M. (2007). A unifying concept of trophoblastic differentiation and malignancy defined by biomarker expression. Hum. Pathol. *38*, 1003–1013.

Li, Y., Moretto-Zita, M., Soncin, F., Wakeland, A., Wolfe, L., Leon-Garcia, S., Pandian, R., Pizzo, D., Cui, L., Nazor, K., Loring, J.F., Crum, C.P., Laurent, L.C., Parast, M.M. (2013). BMP4-directed trophoblast differentiation of human embryonic stem cells is mediated through a ΔNp63+ cytotrophoblast stem cell state. Dev. Camb. Engl. *140*, 3965–3976.

MacPhee, D.J., Mostachfi, H., Han, R., Lye, S.J., Post, M., and Caniggia, I. (2001). Focal adhesion kinase is a key mediator of human trophoblast development. Lab. Investig. J. Tech. Methods Pathol. *81*, 1469–1483.

Maltepe, E., Krampitz, G.W., Okazaki, K.M., Red-Horse, K., Mak, W., Simon, M.C., and Fisher, S.J. (2005). Hypoxia-inducible factor-dependent histone deacetylase activity determines stem cell fate in the placenta. Dev. Camb. Engl. *132*, 3393–3403.

Marchand, M., Horcajadas, J.A., Esteban, F.J., McElroy, S.L., Fisher, S.J., and Giudice, L.C. (2011). Transcriptomic signature of trophoblast differentiation in a human embryonic stem cell model. Biol. Reprod. *84*, 1258–1271.

McMaster, M.T., Librach, C.L., Zhou, Y., Lim, K.H., Janatpour, M.J., DeMars, R., Kovats, S., Damsky, C., and Fisher, S.J. (1995). Human placental HLA-G expression is restricted to differentiated cytotrophoblasts. J. Immunol. Baltim. Md 1950 *154*, 3771–3778.

Mehler, M.F., Mabie, P.C., Zhang, D., and Kessler, J.A. (1997). Bone morphogenetic proteins in the nervous system. Trends Neurosci. *20*, 309–317.

Mishina, Y., Suzuki, A., Ueno, N., and Behringer, R.R. (1995). Bmpr encodes a type I bone morphogenetic protein receptor that is essential for gastrulation during mouse embryogenesis. Genes Dev. *9*, 3027–3037.

Mole, D.R., Blancher, C., Copley, R.R., Pollard, P.J., Gleadle, J.M., Ragoussis, J., and Ratcliffe, P.J. (2009). Genome-wide association of hypoxia-inducible factor (HIF)-1alpha and HIF-2alpha DNA binding with expression profiling of hypoxia-inducible transcripts. J. Biol. Chem. *284*, 16767–16775.

Murohashi, M., Nakamura, T., Tanaka, S., Ichise, T., Yoshida, N., Yamamoto, T., Shibuya, M., Schlessinger, J., and Gotoh, N. (2010). An FGF4-FRS2alpha-Cdx2 axis in trophoblast stem cells induces Bmp4 to regulate proper growth of early mouse embryos. Stem Cells Dayt. Ohio *28*, 113–121.

Muyan, M., and Boime, I. (1997). Secretion of chorionic gonadotropin from human trophoblasts. Placenta *18*, 237–241.

Nagashima, T., Li, Q., Clementi, C., Lydon, J.P., DeMayo, F.J., and Matzuk, M.M. (2013). BMPR2 is required for postimplantation uterine function and pregnancy maintenance. J. Clin. Invest. *123*, 2539–2550.

Ortiz-Barahona, A., Villar, D., Pescador, N., Amigo, J., and del Peso, L. (2010). Genome-wide identification of hypoxia-inducible factor binding sites and target genes by a probabilistic model integrating transcription-profiling data and in silico binding site prediction. Nucleic Acids Res. *38*, 2332–2345.

Pollheimer, J., and Knöfler, M. (2005). Signalling pathways regulating the invasive differentiation of human trophoblasts: a review. Placenta *26 Suppl A*, S21–S30.

Pringle, K.G., Kind, K.L., Sferruzzi-Perri, A.N., Thompson, J.G., and Roberts, C.T. (2010). Beyond oxygen: complex regulation and activity of hypoxia inducible factors in pregnancy. Hum. Reprod. Update *16*, 415–431.

Rosario, G.X., Konno, T., and Soares, M.J. (2008). Maternal hypoxia activates endovascular trophoblast cell invasion. Dev. Biol. *314*, 362–375.

Rossant, J., and Cross, J.C. (2001). Placental development: lessons from mouse mutants. Nat. Rev. Genet. *2*, 538–548.

Ryu, K., Park, C., and Lee, Y. (2011). Hypoxia-inducible factor 1 alpha represses the transcription of the estrogen receptor alpha gene in human breast cancer cells. Biochem. Biophys. Res. Commun. *407*, 831–836.

Shiverick, K.T., King, A., Frank, H., Whitley, G.S., Cartwright, J.E., and Schneider, H. (2001). Cell culture models of human trophoblast II: trophoblast cell lines--a workshop report. Placenta *22 Suppl A*, S104–S106.

Simon, M.C., and Keith, B. (2008). The role of oxygen availability in embryonic development and stem cell function. Nat. Rev. Mol. Cell Biol. *9*, 285–296.

Soncin, F., Natale, D., and Parast, M.M. (2015). Signaling pathways in mouse and human trophoblast differentiation: a comparative review. Cell. Mol. Life Sci. CMLS *72*, 1291–1302.

Strohmer, H., Kiss, H., Mösl, B., Egarter, C., Husslein, P., and Knöfler, M. (1997). Hypoxia downregulates continuous and interleukin-1-induced expression of human chorionic gonadotropin in choriocarcinoma cells. Placenta *18*, 597–604.

Strumpf, D., Mao, C.-A., Yamanaka, Y., Ralston, A., Chawengsaksophak, K., Beck, F., and Rossant, J. (2005). Cdx2 is required for correct cell fate specification and differentiation of trophectoderm in the mouse blastocyst. Dev. Camb. Engl. *132*, 2093–2102.

Takahashi, Y., Dominici, M., Swift, J., Nagy, C., and Ihle, J.N. (2006). Trophoblast stem cells rescue placental defect in SOCS3-deficient mice. J. Biol. Chem. *281*, 11444–11445.

Tanaka, S., Kunath, T., Hadjantonakis, A.K., Nagy, A., and Rossant, J. (1998). Promotion of trophoblast stem cell proliferation by FGF4. Science *282*, 2072–2075.

Wang, R.N., Green, J., Wang, Z., Deng, Y., Qiao, M., Peabody, M., Zhang, Q., Ye, J., Yan, Z., Denduluri, S., Idowu, O., Li, M., Shen, C., Hu, A., Haydon, R.C., Kang, R., Mok, J., Lee, M.J., Luu, H.L., Shi, L.L. (2014). Bone Morphogenetic Protein (BMP) signaling in development and human diseases. Genes Dis. *1*, 87–105.

Winnier, G., Blessing, M., Labosky, P.A., and Hogan, B.L. (1995). Bone morphogenetic protein-4 is required for mesoderm formation and patterning in the mouse. Genes Dev. *9*, 2105–2116.

Wu, Z., Zhang, W., Chen, G., Cheng, L., Liao, J., Jia, N., Gao, Y., Dai, H., Yuan, J., Cheng, L., Xiao, L. (2008). Combinatorial signals of activin/nodal and bone morphogenic protein regulate the early lineage segregation of human embryonic stem cells. J. Biol. Chem. *283*, 24991–25002.

Xu, R.-H., Chen, X., Li, D.S., Li, R., Addicks, G.C., Glennon, C., Zwaka, T.P., and Thomson, J.A. (2002). BMP4 initiates human embryonic stem cell differentiation to trophoblast. Nat. Biotechnol. *20*, 1261–1264.

Yang, J., Ledaki, I., Turley, H., Gatter, K.C., Montero, J.-C.M., Li, J.-L., and Harris, A.L. (2009). Role of hypoxia-inducible factors in epigenetic regulation via histone demethylases. Ann. N. Y. Acad. Sci. *1177*, 185–197.

Yoon, B.S., Ovchinnikov, D.A., Yoshii, I., Mishina, Y., Behringer, R.R., and Lyons, K.M. (2005). Bmpr1a and Bmpr1b have overlapping functions and are essential for chondrogenesis in vivo. Proc. Natl. Acad. Sci. U. S. A. *102*, 5062–5067.

Yu, P., Pan, G., Yu, J., and Thomson, J.A. (2011). FGF2 sustains NANOG and switches the outcome of BMP4-induced human embryonic stem cell differentiation. Cell Stem Cell *8*, 326–334.

Zhang, J., Cao, Y.-J., Zhao, Y.-G., Sang, Q.-X.A., and Duan, E.-K. (2002). Expression of matrix metalloproteinase-26 and tissue inhibitor of metalloproteinase-4 in human normal cytotrophoblast cells and a choriocarcinoma cell line, JEG-3. Mol. Hum. Reprod. *8*, 659–666.

Zhou, Y., Yuge, A., Rajah, A.M., Unek, G., Rinaudo, P.F., and Maltepe, E. (2014). LIMK1 regulates human trophoblast invasion/differentiation and is down-regulated in preeclampsia. Am. J. Pathol. *184*, 3321–3331.